

Sevim ÜNÜGÜR ÇELİK

PhD. Thesis In Chemistry

**NOVEL ION CONDUCTING POLYMER MATRICES: SYNTHESIS,
CHARACTERIZATIONS AND APPLICATIONS**

June - 2012

by

Sevim ÜNÜGÜR ÇELİK

June 2012

**NOVEL ION CONDUCTING POLYMER MATRICES: SYNTHESIS,
CHARACTERIZATIONS AND APPLICATIONS**

by

Sevim ÜNÜGÜR ÇELİK

A thesis submitted to

the Graduate Institute of Sciences and Engineering

of

Fatih University

in partial fulfillment of the requirements for the degree of

Doctor of Philosophy

in

Chemistry

June 2012
Istanbul, Turkey

APPROVAL PAGE

This is to certify that I have read this thesis and that in my opinion it is fully adequate, in scope and quality, as a thesis for the degree of Doctor of Philosophy.

Prof. Dr. Ayhan BOZKURT
Supervisor

I certify that this thesis satisfies all the requirements as a thesis for the degree of Doctor of Philosophy.

Assoc. Prof. Dr. Abdülhadi BAYKAL
Head of Department

Examining Committee Members

Prof. Dr. Ayhan BOZKURT

Prof. Dr. Turgay SEÇKİN

Assoc. Prof. Dr. Kurtuluş GÖLCÜK

Assist. Prof. Dr. Ali Ekrem MÜFTÜOĞLU

Assist. Prof. Dr. Burak ESAT

It is approved that this thesis has been written in compliance with the formatting rules laid down by the Graduate Institute of Sciences and Engineering.

Assoc. Prof. Dr. Nurullah ARSLAN
Director

Date
June 2012

NOVEL ION CONDUCTING POLYMER MATRICES: SYNTHESIS, CHARACTERIZATIONS AND APPLICATIONS

Sevim ÜNÜGÜR ÇELİK

Ph.D. Thesis - Chemistry
June 2012

Supervisor: Prof. Dr. Ayhan BOZKURT

ABSTRACT

Fuel cells are gaining increasing attention as a clean and promising technology for energy conversion. One of the key benefits of fuel cells compared to other methods is the direct energy conversion that enables the achievement of high efficiency. The electrolyte membrane is the most essential part of a fuel cell unit, and consequently has been the subject of considerable research and development. Among the various types of proton conducting electrolytes examined for fuel cell applications, polymer electrolyte membranes are regarded as viable candidates since they enable operation of the cells at desirably low temperatures. As novel proton conductive membranes siloxane based membranes were prepared via tethering of azole units into siloxane monomer and sol-gel polymerization. Cross-linked, transparent and high proton conductive membranes were obtained. In addition novel copolymers were produced using vinyl triazole, vinyl phosphonic acid, vinyl benzene boronic acid and vinyl benzyl phosphonic acid. Triazole containing copolymers were doped with phosphonic acid and this resulted in a maximum proton conductivity of 6×10^{-3} S/cm at 150 °C in anhydrous state.

Keywords: Fuel cell, proton conductivity, triazole, tetrazole, vinyl phosphonic acid, vinyl benzene boronic acid, vinyl benzyl phosphonic acid, copolymer, siloxane, sol-gel.

YENİ İYON İLETKEN POLİMER MATRİSLER: SENTEZİ, KARAKTERİZASYONU VE UYGULAMASI

Sevim ÜNÜGÜR ÇELİK

Doktora Tezi – Kimya
Haziran 2012

Tez Danışmanı: Prof. Dr. Ayhan BOZKURT

ÖZ

Yakıt pilleri enerji dönüşümü için temiz ve gelecek vaadeden bir teknoloji olarak dikkat çekmektedir. Diğer metotlarla karşılaştırıldığında yakıt pillerinin en önemli ayrıcalığı yüksek verimi sağlayan direk enerji dönüşümüdür. Elektrolit membran, yakıt pili hücrelerinin en önemli kısmıdır ve bu nedenle araştırma geliştirme faaliyetlerinin yoğunluğunu oluşturur. Yakıt pillerinde kullanılan proton iletken elektrolitlerden polimer elektrolit membranlar en uygulanabilir adaydır çünkü yakıt pillerini istenildiği gibi düşük sıcaklıklarda çalıştırabilir. Bu tez çalışması kapsamında, yeni proton iletken membranlar olarak azol birimleri siloksan monomerlere bağlandı ve sol-jel yöntemiyle siloksan bazlı membranlar sentezlendi. Çapraz bağlı, şeffaf ve yüksek proton iletken membranlar elde edildi. Ayrıca vinil triazol, vinil fosfonik asit, vinil benzen boronik asit ve vinil benzil fosfonik asit kullanılarak yeni kopolimerler sentezlendi. Triazol içeren kopolimerler fosforik asit ile katkılındı ve en yüksek iletkenlik nemsiz ortamda ve 150 °C'de 6×10^{-3} S/cm olarak elde edildi.

Anahtar Kelimeler: Yakıt pili, proton iletkenlik, triazol, tetrazol, vinil fosfonik asit, vinil benzen boronik asit, vinil benzil fosfonik asit, kopolimer, siloksan, sol-jel.

To my parents

ACKNOWLEDGEMENT

I express sincere appreciation to Prof. Dr. Ayhan BOZKURT for his guidance and insight throughout the research.

I express my thanks and appreciation to my family for their understanding, motivation and patience. In addition, I am thankful to Hamide, Funda and her friends for all their supports during my PhD education.

TABLE OF CONTENTS

ABSTRACT.....	iii
ÖZ.....	iv
DEDICATION.....	v
ACKNOWLEDGEMENT	vi
TABLE OF CONTENTS.....	vii
LIST OF TABLES	x
LIST OF FIGURES	xi
LIST OF SYMBOLS AND ABBREVIATIONS	xvi
CHAPTER 1 INTRODUCTION	1
1.1 Introduction	1
1.2 Fuel cells.....	3
1.2.1 Polymer electrolyte membrane fuel cell (PEMFC)	4
1.2.2 Solid oxide fuel cell (SOFC)	5
1.2.3 Alkaline fuel cell (AFC)	5
1.2.4 Molten-carbonate fuel cell (MCFC)	5
1.2.5 Phosphoric-acid fuel cell (PAFC).....	5
1.2.6 Direct-methanol fuel cell (DMFC)	6
1.3 Polymer electrolyte membrane (PEM) for fuel cells.....	6
1.3.1 Perfluorosulfonic acid membranes.....	6
1.3.2 Mechanisms of proton transport.....	8
1.3.3 Anhydrous proton conductive membranes.....	8
1.3.3.1 Azole-based heterocyclic compounds as proton solvents.....	11
1.3.3.2 Siloxane Based Proton Conductive Membranes.....	17
1.3.3.3 Proton Conductive Copolymer Membranes.....	20
CHAPTER 2 EXPERIMENTAL.....	25
2.1 Synthesis of triazole functional silane networks.....	25
2.2 Synthesis of tetrazole functional silane networks.....	27

2.3	Synthesis of copolymers based on 4-vinyl benzene boronic acid and 1-vinyl-1,2,4-triazole.....	28
2.4	Synthesis of copolymers based on 4-vinyl benzene boronic acid and vinyl phosphonic acid.....	29
2.5	Synthesis of diisopropyl-p-vinylbenzyl phosphonate (VBP) monomer and poly(vinyl benzyl phosphonic acid).....	31
2.6	Synthesis of poly(vinyl triazole-co-vinyl benzyl phosphonic acid) (P(VTri-co-VBPA) copolymer.....	33
2.7	Synthesis of poly(vinyl benzene boronic acid-co-vinyl benzyl phosphonic acid) (P(VBBA-co-VBPA) copolymer.....	34
2.8	Characterizations.....	36
CHAPTER 3 RESULTS AND DISCUSSION.....		40
3.1	Triazole functional silane networks.....	40
3.1.1	FTIR studies.....	40
3.1.2	Thermal analysis.....	42
3.1.3	Morphology.....	45
3.1.4	Proton conductivity.....	45
3.2	Tetrazole functional silane networks.....	49
3.2.1	FTIR studies.....	49
3.2.2	Thermal analysis.....	50
3.2.3	Proton conductivity.....	52
3.3	Copolymers based on 4-vinyl benzene boronic acid and 1-vinyl-1,2,4-triazole... ..	55
3.3.1	FT-IR study.....	56
3.3.2	Thermal Analysis.....	57
3.3.3	Conductivity Measurement.....	58
3.3.4	Cyclic Voltammetry.....	61
3.4	Copolymers based on 4-vinyl benzene boronic acid and vinyl phosphonic acid.....	62
3.4.1	Characterizations.....	62

3.4.2	Thermal Properties.....	63
3.4.3	Ion Exchange Capacity (IEC).....	65
3.4.4	Proton Conductivity.....	65
3.4.5	Cyclic Voltammetry.....	69
3.5	Diisopropyl-p-vinylbenzyl phosphonate (VBP) monomer and poly(vinyl benzyl phosphonic acid).....	70
3.5.1	Characterizations.....	70
3.5.2	Thermal properties.....	73
3.6	Poly(vinyl triazole-co-vinyl benzyl phosphonic acid), P(VTri-co-VBPA) copolymer.....	73
3.6.1	Characterizations.....	73
3.6.2	Thermal properties.....	76
3.6.3	Proton Conductivity.....	77
3.6.4	Cyclic Voltammetry.....	80
3.7	Poly(vinyl benzene boronic acid-co-vinyl benzyl phosphonic acid) (P(VBBA-co-VBPA) copolymer.....	81
3.7.1	Characterizations.....	81
3.7.2	Thermal Analysis.....	83
3.7.3	Ion Exchange Capacity (IEC).....	85
3.7.4	Proton Conductivity.....	85
3.7.5	Cyclic Voltammetry.....	88
3.8	Fuel Cell Test.....	89
CHAPTER 4	CONCLUSIONS	92
REFERENCES...	96
APPENDIX A	Curriculum Vitae.....	102

LIST OF TABLES

TABLE

1.1	Melting points, boiling points and pKa of the heterocycles.....	12
1.2	The chemical structures and maximum proton conductivity values of several siloxane based polymer matrices	19
2.1	The synthesis of P(VBBA-co-VPA) copolymers.....	29
3.1	Tg values, maximum proton conductivities and VTF parameters of the membranes....	48
3.2	Maximum proton conductivity, Tg and VTF parameters of the samples.	55
3.3	Composition of poly(vinyl benzene boronic acid-co-vinyl triazole) copolymers.....	55
3.4	IEC and maximum proton conductivity values for P(VBBA-co-VPA) copolymers.....	68
3.5	Composition of P(VTri-co-VBPA) copolymers.....	74
4.1	Composition, T _d and maximum proton conductivities of the copolymers.....	93
4.2	T _d , IEC and maximum proton conductivities of the copolymers.....	94
4.3	Composition, T _d and maximum proton conductivities of the copolymers.....	94
4.5	T _d , IEC and maximum proton conductivities of the copolymers.....	95

LIST OF FIGURES

FIGURE

1.1	Polymer Electrolyte Membrane Fuel Cell (PEMFC).....	4
1.2	Chemical structures of perfluorinated polymer electrolyte membranes.....	7
1.3	The Yeager 3 Phase Model of Nafion® Clusters.....	7
1.4	Proton conduction in imidazole through the Grotthuss mechanism, schematically showing the reorientation of the Im moiety.....	12
1.5	The structures of (a) 1-methyl imidazole, (b) benzimidazole, BnIm and (c) pyrazole, Py.....	13
1.6	Proton conduction in pyrazole through Grotthuss mechanism.....	14
1.7	The molecular structures of (a) 1H-1,2,4-triazole (b) 1H-1,2,3-triazole (c) 3-amino-1,2,4-triazole.....	15
1.8	The molecular structure of (a) 1H-tetrazole (b) 5-aminotetrazole.....	17
1.9	Structure of prepared co- and terpolymers.....	21
1.10	Structure of prepared copolymers.....	22
1.11	Structure of poly(VPA-co-4-VIm) copolymers.....	22
1.12	Structure of poly(VPA-co-VTri) copolymer.....	23
1.13	Structure of P(VTri-co-AMPS) copolymers.....	24
1.14	The structure of poly(vinyl benzene boronic acid-co-vinyl imidazole) copolymer.....	24
2.1	The synthesis of azole functional silane networks (Si-Tri and Si-ATri).....	26
2.2	Transparent and free standing film of Si-ATriTA0.5 sample.....	26
2.3	The synthesis of tetrazole functional silane networks (Si-ATet).....	27
2.4	Transparent and free standing film of Si-ATet.....	28
2.5	The synthesis of P(VBBA-co-VTri) copolymers.....	29
2.6	The synthesis of P(VBBA-co-VPA) copolymers.....	30
2.7	The synthesis of P(VBBA-co-VPA)-PEGME graft copolymers.....	30
2.8	The synthesis of diisopropyl-p-vinylbenzyl phosphonate.....	31

2.9	The synthesis of poly(diisopropyl-p-vinylbenzyl phosphonate), PVBP homopolymer..	32
2.10	The synthesis of poly(vinyl benzyl phosphonic acid) PVBPA homopolymer.....	32
2.11	The synthesis of poly(vinyl triazole-co-diisopropyl-p-vinylbenzyl phosphonate) (P(VTri-co-VBP) copolymer.....	33
2.12	The synthesis of poly(vinyl triazole-co-vinyl benzyl phosphonic acid) (P(VTri-co-VBPA) copolymer.....	34
2.13	The synthesis of poly(vinyl benzene boronic acid-co-diisopropyl-p-vinylbenzyl phosphonate) (P(VBBA-co-VBP) copolymer.....	35
2.14	The synthesis of poly(vinyl benzene boronic acid-co-vinyl benzyl phosphonic acid) (P(VBBA-co-VBPA) copolymer.....	35
2.15	The synthesis of P(VBB -co-VBPA)-PEGME graft copolymers.....	36
3.1	FT-IR spectra of PGPTMS and triazole functional materials.....	41
3.2	FT-IR spectra of aminotriazole functional materials.....	41
3.3	TG thermograms of triazole functional materials recorded at a heating rate of 10 °C/min under a nitrogen atmosphere.....	42
3.4	TG thermograms of aminotriazole functional materials recorded at a heating rate of 10 °C/min under a nitrogen atmosphere.....	43
3.5	DSC traces of triazole functional materials recorded at a heating rate of 10 °C/min under a nitrogen atmosphere.....	44
3.6	DSC traces of aminotriazole functional materials recorded at a heating rate of 10 °C/min under a nitrogen atmosphere.....	44
3.7	Scanning Electron Microscopy (SEM) images of (a-b) SiTri and (c-d) SiTriTA0.5.....	45
3.8	The σ_{ac} vs. frequency (Hz) for Si-TriTA0.5 and Si-TriTA1 at various temperatures....	46
3.9	The σ_{ac} vs. frequency (Hz) for Si-ATriTA0.5 at various temperatures.....	47
3.10	DC conductivities of pure and doped samples as a function of reciprocal temperature	47
3.11	FT-IR spectra of pure ATet, GPTMS and the polymer electrolytes.....	50
3.12	TG thermograms of the polymer electrolytes recorded at a heating rate of 10 °C/min under a nitrogen atmosphere.....	51

3.13	DSC traces of the polymer electrolytes recorded at a heating rate of 10 °C/min under a nitrogen atmosphere.....	52
3.14	The σ_{ac} vs. frequency (Hz) for Si-ATet, Si-ATetTA0.5 and Si-ATetTA1 at various temperatures.....	54
3.15	DC conductivities of pure and doped samples as a function of reciprocal temperature.....	54
3.16	FT-IR spectra of P(VBBA-co-VTri) copolymers.....	56
3.17	FT-IR spectra of H ₃ PO ₄ doped P(VBBA-co-VTri) copolymers.....	57
3.18	TG thermograms of pure and H ₃ PO ₄ doped P(VBBA-co-VTri) copolymers at a heating rate of 10 °C/min in inert atmosphere.....	58
3.19	AC conductivity versus frequency of the membranes at several temperatures.....	60
3.20	Variation of the proton conductivity of H ₃ PO ₄ doped P(VBBA-co-VTri) copolymers as a function of reciprocal temperature.....	60
3.21	Cyclic voltammograms of P(VBBA-co-VTri)1:1x=2 in 0.1 M TBATFB/acetonitrile. Curves with a scan rate of 50 mV/s.....	61
3.22	FTIR spectra of P(VBBA-VPA) copolymers.....	62
3.23	FTIR spectra of P(VBBA-VPA)-PEGME copolymers.....	63
3.24	TG thermograms of P(VBBA-VPA) and P(VBBA-VPA)-PEGME copolymers at a heating rate of 10 °C/min in inert atmosphere.....	64
3.25	DSC curves of P(VBBA-VPA)-PEGME copolymers at a heating rate of 10 °C/min in inert atmosphere.....	65
3.26	AC conductivity versus frequency for P(VBBA-co-VPA)-PEGME copolymers at different temperatures.....	67
3.27	Variation of the proton conductivity of P(VBBA-co-VPA)-PEGME copolymers as a function of reciprocal temperature.....	67
3.28	Variation of the proton conductivity of P(VBBA-co-VPA) copolymers as a function of reciprocal temperature at 50 % RH.....	68
3.29	Cyclic voltammograms of S3-PEGME in 0.1 M TBATFB/acetonitrile. Curves with a scan rate of 50 mV/s.....	69
3.30	¹ H NMR spectrum of diisopropyl-p-vinylbenzyl phosphonate (VBP) monomer.....	70
3.31	¹³ C NMR spectrum of diisopropyl-p-vinylbenzyl phosphonate (VBP) monomer.....	71

3.32	FTIR spectra of VBP and PVBP.....	72
3.33	FTIR spectrum of PVBPA.....	72
3.34	TG thermograms of PVBPA homopolymer recorded at a heating rate of 10 °C/min in inert atmosphere.....	73
3.35	FTIR spectra of P(VTri-co-VBP) copolymers.....	74
3.36	FTIR spectra of P(VTri-co-VBPA) copolymers.....	75
3.37	FTIR spectra of H ₃ PO ₄ doped P(VTri-co-VBPA) copolymers.....	75
3.38	TG thermograms of P(VTri-co-VBPA) copolymers at a heating rate of 10 °C/min in inert atmosphere.....	76
3.39	TG thermograms of H ₃ PO ₄ doped P(VTri-co-VBPA) copolymers at a heating rate of 10 °C/min in inert atmosphere.....	77
3.40	AC conductivity versus frequency for H ₃ PO ₄ doped P(VTri-co-VBPA) copolymer electrolytes.....	79
3.41	DC conductivity of H ₃ PO ₄ doped P(VTri-co-VBPA) copolymer electrolytes at different temperatures.....	80
3.42	Cyclic voltammograms of P(VTri-co-VBPA) _{1:0.5x=2} in 0.1 M TBATFB/acetonitrile. Curves with a scan rate of 50 mV/s.....	81
3.43a	FTIR spectra of P(VBBA-co-VBP) copolymers.....	82
3.43b	FTIR spectra of P(VBBA-co-VBPA) copolymers.....	82
3.44	FTIR spectra of P(VBBA-co-VBPA)-PEGME copolymers.....	83
3.45	TG thermograms of P(VBBA-co-VBPA) copolymers at a heating rate of 10 °C/min in inert atmosphere.....	84
3.46	TG thermograms of P(VBBA-co-VBPA)-PEGME copolymers at a heating rate of 10 °C/min in inert atmosphere.....	84
3.47	DSC curves of P(VBBA-co-VBPA)-PEGME copolymers at a heating rate of 10 °C/min in inert atmosphere.....	85
3.48	AC conductivity vs frequency for P(VBBA-co-VBPA)-PEGME copolymers at different temperatures.....	87
3.49	DC conductivity of P(VBBA-co-VBPA)-PEGME copolymers at different temperatures.....	87

3.50	Cyclic voltammograms of P(VBBA-co-VBPA)1:0.5-PEGME in 0.1 M TBATFB/ acetonitrile. Curves with a scan rate of 50 mV/s.....	88
3.51	Characteristic graph for a PEMFC.....	89
3.52	Components of a PEMFC.....	90
3.53	Single PEMFC test unit and tested membrane, P(VBBA-co-VTri)1:2X=2.....	91
4.1	The images and chemical structure of Si-ATriTA0.5.....	92

LIST OF SYMSBOLS AND ABBREVIATIONS

SYMBOL/ABBREVIATION

ATet	5-Aminotetrazole
ATri	3-Amino-1,2,4-triazole
BnIm	Benzimidazole
DSC	Differential Scanning Calorimetry
FTIR	Fourier Transform Infrared Radiation
Im	Imidazole
MeIm	1-Methylimidazole
NMR	Nuclear Magnetic Radiation
P4VI	Poly(4-vinylimidazole)
PAMPSA	Poly(2-acrylamido-2-methyl-1-propane sulfonic acid)
PEGMEA	Poly(ethylene glycol)methyl ether acrylate
PEMFCs	Polymer electrolyte membrane fuel cells
PEMs	Polymer electrolyte membranes
PVBBA	Poly (vinyl benzene boronic acid)
PVBPA	Poly(vinyl benzyl phosphonic acid)
PVPA	Poly(vinyl phosphonic acid)
PVTri	Polyvinyl triazole
Py	Pyrazole
RH	Relative humidity
SEM	Scanning Electron Microscopy
TA	Triflic acid
Tet	Tetrazole
TGA	Thermogravimetric Analysis
Tri	Triazole

CHAPTER 1

INTRODUCTION

1.1 INTRODUCTION

Fuel cell systems are regarded as key components for exploitation of the energy stored in hydrogen molecules. In principle, fuel cells offer a number of key advantages over conventional energy conversion devices, including: high energy conversion efficiency (due to direct conversion of chemical energy into electricity), low emissions and noise, flexibility in fuel selection, cogeneration capability, economy of scale, and low maintenance requirements. These attractive features have led to numerous initiatives toward the realization of fuel cell technology for practical applications.

Proton conducting polymers have received increasing attention due to their potential applications in polymer electrolyte membrane fuel cells (PEMFCs). For proton conductive membranes perfluorosulfonic acid membranes such as Nafion were generally used. These materials have hydrophilic and hydrophobic regions and the proton transfer occurs via water molecules present in their hydrophilic channels.

In order to produce membranes that have similar properties with Nafion, sulfonic acid and phosphonic acid functional polymers were synthesized. For this purpose, polystyrene, polysulfone, polyphosphazene, siloxane and polyimide polymers were sulfonated (Lufrano et al., 2008; Yen et al., 2007).

In addition, polyvinyl phosphonic acid and many different phosphonated matrices such as siloxanes (Tripathi et al., 2008) and polyphosphazanes (Allcock et al., 2002) were used as proton conductive material. Although these acidic polymers have high water uptake and proton conductivity, their usage is limited to 100 °C and therefore

alternative systems should be prepared that have high proton conductivity at high temperature.

For this purpose heterogenic solvents such as benzimidazole, imidazole and triazole were intercalated in these acidic polymers to provide proton conduction at high temperature (Şen et al., 2008; Goktepe et al., 2008). In addition polyvinyl imidazole, polyvinyl triazole and polyvinyl tetrazole were used as proton conductive polymer after doping with phosphoric or triflic acid (Çelik et al., 2008a).

In another approach copolymers that have both azole and acid groups were prepared using vinyl imidazole and vinyl triazole with vinyl phosphonic acid (Çelik et al.; 2008b). High proton conductivity was obtained in these studies in anhydrous conditions and with no dopant.

Inorganic-organic hybrid materials are of increasing interest as PEM materials since they offer the prospect of combining the mechanical toughness and flexibility of the organic component with the hardness and thermal stability of the inorganic component. These membranes are generally prepared by incorporating inorganic particles into organic polymer electrolytes or anchoring functional groups onto stable inorganic-organic hybrid matrices via chemical bonds. Cross-linking is a powerful and simple method to suppress the methanol crossover and water swelling of PEMs. After a cross-linking treatment, the polymer matrix forms a network where the macromolecular chain of polyelectrolyte is immobilized and compacted (Lee et al., 2006; Yang et al., 2005).

In this study, inorganic-organic hybrid membranes were produced via immobilization of heterocyclic molecules into siloxane monomer and sol-gel polymerization. In addition novel copolymers were synthesized using 4-vinyl benzene boronic acid (VBBA), 1-vinyl-1,2,4-triazole (VTri), vinyl phosphonic acid (VPA) and vinyl benzyl phosphonic acid (VBPA). Some of these copolymers were grafted with polyethylene glycol methyl ether (PEGME) and the others were doped with phosphoric acid to facilitate the proton transport.

The samples were characterized with NMR, FT-IR and elemental analysis. The thermal properties of the samples were analyzed with TGA and DSC. Morphology of siloxane membranes was investigated with SEM. The proton conductivity of the membranes was studied using impedance spectrometer.

1.2 FUEL CELLS

A fuel cell is a device that converts the chemical energy from a fuel into electricity through a chemical reaction with oxygen or another oxidizing agent. Hydrogen is the most common fuel, but hydrocarbons such as natural gas and alcohols like methanol are sometimes used. Fuel cells are different from batteries in that they require a constant source of fuel and oxygen to run, but they can produce electricity continually for as long as these inputs are supplied.

Welsh Physicist William Grove developed the first crude fuel cells in 1839. The first commercial use of fuel cells was in NASA space programs to generate power for probes, satellites and space capsules. Since then, fuel cells have been used in many other applications. Fuel cells are used for primary and backup power for commercial, industrial and residential buildings and in remote or inaccessible areas. They are used to power fuel cell vehicles, including automobiles, buses, forklifts, airplanes, boats, motorcycles and submarines.

There are already over 85 hydrogen refueling stations in the U.S. The National Research Council estimated that creating the infrastructure to supply fuel for 10 million fuel cell vehicles through 2025 would cost the government US\$8 billion over 16 years. The first public hydrogen refueling station was opened in Reykjavík, Iceland in April 2003. As of June 2011 California had 22 hydrogen refueling stations in operation. In 2010, fuel cell industry revenues exceeded a \$750 million market value worldwide, although, as of 2010, no public company in the industry had yet become profitable. There were 140,000 fuel cell stacks shipped globally in 2010, up from 11 thousand shipments in 2007, and in 2010 worldwide fuel cell shipments had an annual growth rate of 115%. Approximately 50% of fuel cell shipments in 2010 were stationary fuel cells, up from about a third in 2009, and the four dominant producers in the Fuel Cell Industry remain the United States, Germany, Japan and South Korea. Bloom Energy, a

major fuel cell supplier, says its fuel cells will meet a return on investment in 3–5 years, as its fuel cells generate power at 9-11 cents per kilowatt-hour, including the price of fuel, maintenance, and hardware (Wesoff, 2011; Adamson and Clint, 2011; Faur-Ghenciu, 2003).

1.2.1 Polymer electrolyte membrane fuel cell (PEMFC)

PEMFC is the most useful type for transportation applications (Starz et al., 1999). The PEMFC has very high power density and a relatively low operating temperature (20 - 100 °C). Therefore PEMFC is self-starting without the need of external warm up and readily generating electricity which makes it particularly promising. A hydrogen-powered PEMFC consists of two electrodes and a separator polymer membrane as shown in Fig. 1.1.

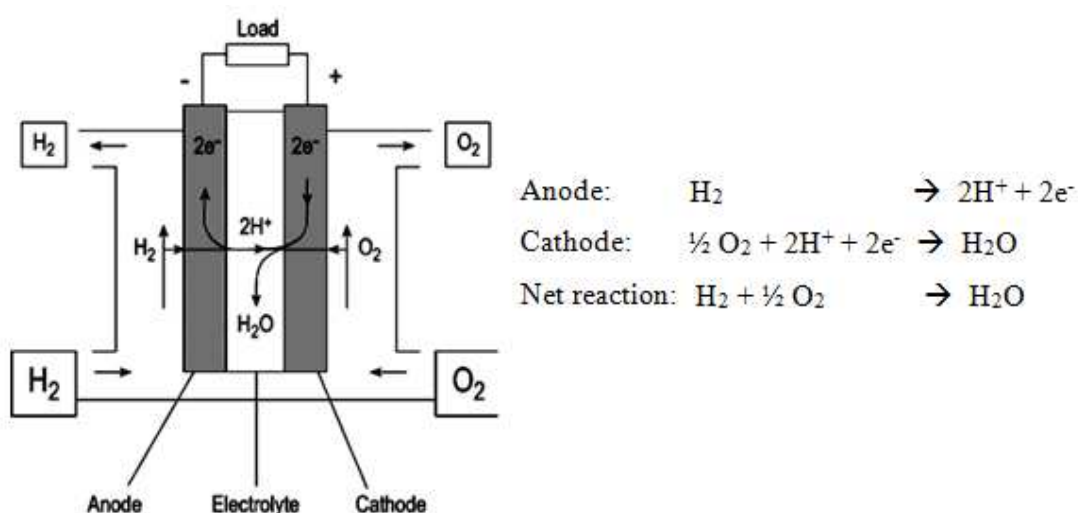


Figure 1.1. Polymer Electrolyte Membrane Fuel Cell (PEMFC).

Hydrogen is supplied to the anode and air is channeled to the cathode. At the anode, a platinum catalyst causes the hydrogen to split into positive hydrogen ions (protons) and negatively charged electrons. The polymer electrolyte membrane (PEM) permits only the transfer of proton to the cathode. The electrons travel along an external circuit to the cathode and create an electrical current. At the cathode, the electrons and protons combine with oxygen to form water which is the only waste product of hydrogen fueled PEMFCs.

1.2.2 Solid oxide fuel cell (SOFC)

Solid oxide fuel cells are considered as the best useful fuel cell for stationary power generators that could provide electricity and heat for houses, factories or towns (Singhal, 2008). The operation temperature is very high (700-1000 °C) for this type of fuel cell. This high temperature results a reliability problem, since parts of the fuel cell can break down after cycling on and off repeatedly. However, solid oxide fuel cells are very stable under continuous use. The SOFC has demonstrated the longest operating life of any fuel cell under certain operating conditions. The high temperature may also be an advantage: the steam produced by the fuel cell can be channeled into turbines to generate more electricity and the heat can be used for heating purposes. This process is called co-generation of heat and power and it improves the overall efficiency of the system.

1.2.3 Alkaline fuel cell (AFC)

Alkaline fuel cell is one of the oldest designs for fuel cells; the United States space program has used them since the 1960s (Van den Broeck, 1993). The AFC is very susceptible to contamination, so it requires pure hydrogen and oxygen. Alkaline fuel cells use an aqueous solution of potassium hydroxide in a porous stabilized matrix as an electrolyte. The operating temperature ranges from 65 to 200 °C. It is also very expensive, so this type of fuel cell is unlikely to be commercialized, but research has revisited this type of fuel cells recently again (Jiang, 2009).

1.2.4 Molten-carbonate fuel cell (MCFC)

Like the SOFC, molten-carbonate fuel cells are also useful for large stationary power generators (Bischoff, 2006). The fuel cells use molten alkaline carbonate (e.g., sodium bicarbonate NaHCO_3) as electrolyte. Since the operation temperature is 600 °C they can generate useful steam and improve the overall efficiency.

1.2.5 Phosphoric-acid fuel cell (PAFC)

The phosphoric-acid fuel cell has its potential use in small stationary power-generation systems (Kumura, 2004). Molten phosphoric acid (H_3PO_4) is used as

electrolyte. The optimum operating temperature range is 150-200 °C. It operates at a higher temperature than polymer electrolyte membrane fuel cells, so it has a longer warm-up time. Therefore, it is not possible to use them in cars.

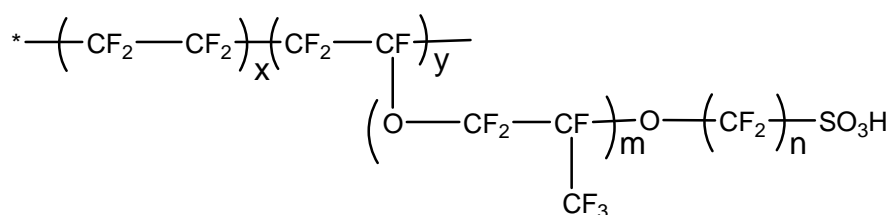
1.2.6 Direct-methanol fuel cell (DMFC)

Methanol fuel cells are comparable to a PEMFC in regards to its operating temperature (90-120 °C), but yet are not as efficient (Bolufer, 2008). They use a polymer membrane as electrolyte. Also, the DMFC requires a relatively large amount of platinum to act as a catalyst, which makes these fuel cells expensive. Methanol as fuel must be reformed to yield H₂ prior to the electrochemical processes. This is also true for the use of natural gas. Yet the PEMs are not sufficiently tight, methanol crossover is a problem (Jiang, 2009).

1.3 POLYMER ELECTROLYTE MEMBRANE (PEM) FOR FUEL CELLS

1.3.1 Perfluorosulfonic acid membranes

Development of PEMs for fuel cells has undergone a number of technological transformations since their inception. PEMFCs were originally introduced in early 1960's, based on using GE's sulfonated polystyrene as the electrolyte. Due to problems associated with the oxidative degradation of materials, this system was soon replaced by Du Pont's Nafion® ionomer, which proved to be superior in both performance and durability. Further progress in this field resulted in the development of perfluorosulfonic acid polymers such as Nafion® and Flemion® (Fig. 1.2). Several models have been proposed for the morphology of Nafion® (Heitner-Wirguin, 1996; Mauritz and Moore, 2004; Gierke et al., 1981; Schmidt-Rohrand Chen, 2008). For instance, Fig. 1.3 shows the Yeager 3-Phase Model, which is based on a three-phase clustered system with interconnecting channels within the polymer (Yeager and Eisenberg, 1982). The three regions consist of (A) a fluorocarbon backbone, some of which is microcrystalline, (B) an interfacial regions of relatively large fractional void volume containing some pendant side chains, some water, and those sulfate or carboxylic groups and counter ions which are not in clusters, and (C) clustered regions in which the majority of the ionic exchange sites, counter ions, and absorbed water exist (Brookman and Nicholson, 1986).



Nafion 117	$m \geq 1, n=2, x=5-13.5, y=1000$
Flemion	$m=0, n=1-5$
Aciplex	$m=0, n=2-5, x=1.5-14$
Dow membrane	$m=0, n=2, x=3.6-10$

Figure 1.2. Chemical structures of perfluorinated polymer electrolyte membranes (Rikukawa and Sanui, 2000).

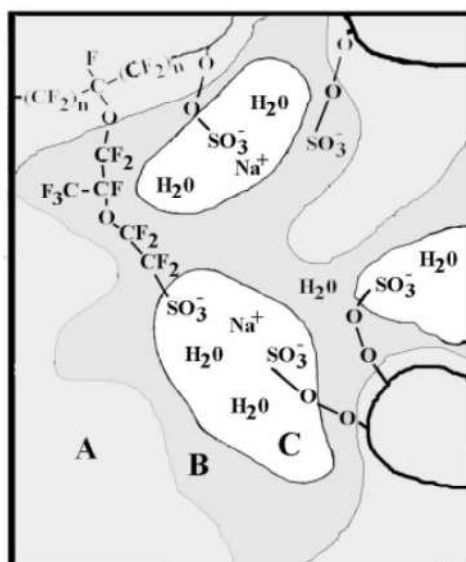


Figure 1.3. The Yeager 3 Phase Model of Nafion[®] Clusters (Yeager and Eisenberg, 1982).

Perfluorosulfonic acid-based materials are widely used as the PEM in fuel cell systems. The transport properties in these materials largely depend on the water content. Thus, in order to be practical, such systems must be operated at temperatures below the dew point of water (Kreuer et al., 1993). Other shortcomings and limitations, such as high cost, high susceptibility of proton conductivity to low humidity and temperatures above 80 °C have motivated research toward finding alternative PEMs with higher efficiency and performance at desired conditions.

1.3.2 Mechanisms of proton transport

The mechanism of proton transport in water molecules has been studied extensively (Eigen, 1964; Agmon, 1995; Agmon, 1996). The proton transport based on the “Grotthuss mechanism” (also called the “hopping mechanism”, “chain mechanism” or “structure diffusion”) comprises rapid intermolecular proton transfers (hopping) down a chain of hydrogen bonds, for which the transfer events are assumed to be highly correlated, with reorientation of water dipoles to produce a configuration which allows for the next hopping event (Grotthuss, 1806; Kreuer, 1997). The first process leads to a polarization of the hydrogen bond chain, i.e., to a local relative charge displacement, but not to DC conductivity. The second process causes the depolarization of the chain by reorientation of the water dipoles. A fast Grotthuss-type mechanism must enable the formation of protonic defects, and provide strongly fluctuating proton donor and acceptor functions in an otherwise non-polar environment. The latter avoids strong solvent effects that tend to suppress proton transfer reactions (Kreuer, 1996; Kreuer, 1997). However, this mechanism cannot explain all abnormal proton conductive systems. Based on NMR spectra and self-diffusion coefficients, Kreuer et al. proposed a “Vehicle mechanism”, also called molecular diffusion, for the interpretation of the conductivity of fast proton conductors, such as zeolites, Nafion etc (Kreuer et al., 1982). According to this model the proton does not migrate as H^+ but as H_3O^+ , NH_4^+ , etc., bonded to a “vehicle” such as H_2O , NH_3 , etc. The unloaded vehicles move in the opposite direction. Sequential hydrogen bonds are not necessary for proton transport with this model.

1.3.3 Anhydrous proton conductive membranes

Problems associated with the PEMs present major obstacles for widespread acceptance of PEMFCs. First, the existing PEMs are expensive and mechanically unstable, especially for operation at moderate and elevated temperatures. Second, these materials typically require the continuous presence of humidity in order to perform their function in electrode reactions and conducting protons, not only limiting the operating condition of fuel cells to temperatures below about 80 °C, but also with a negative impact on the performance of PEMFCs, through slowing the process kinetics in electrodes, combined with decrease in CO tolerance. In addition, existing membranes

are highly susceptible to degradation at elevated temperatures due to the shrinkage of electrolyte within the catalyst layer, which consequently reduces the electrochemical surface area in electrodes. Therefore, one of the key directions in development of PEMs is to implement novel designs in producing materials with sufficiently high chemical and mechanical stability with effective operation at intermediate temperatures (100-200 °C) and relatively low humidity (RH~25-30 %) levels (Kreuer, 2002).

Essentially, the development of PEMFCs capable of operating at temperatures approaching 200 °C can result in several key improvements in widespread use of fuel cells. For example, systems operating at elevated temperatures are more efficient and reduce the overall cell cost by decreasing the required platinum loading. In addition, the overall heat management of the device is simplified (Li et al., 2003; Lecolley et al., 2003). This also will eliminate some of the water management issues such as membrane swelling and water dynamics (Perrin et al., 2006). In addition, operating at high temperatures would play an important role in improving the overall performance of fuel cell operating with fuel containing impurities (e.g., carbon monoxide) and issues related to the efficiency of the heat rejection and water management (Li et al., 2009; Pu et al., 2005). Progresses on these criteria would have major contributions in cutting the costs associated with the PEMs.

A principal approaches for enabling operation of PEMs at higher temperature is the replacement of water with alternative proton solvents possessing higher boiling points. Investigations over the past few years have resulted in the development of several kinds of anhydrous proton conducting membranes. Preparation of polymer–acid blends was among the early trials in which basic or neutral polymers and copolymers (often containing functional groups such as imide, imine, ether, etc) were blended with strong acids (Alberti and Casciola, 2001; Bozkurt and Meyer, 2001; Kreuer, 2001). In these blend systems, acids such as H_3PO_4 or H_2SO_4 act as proton donor and plasticizer, and the transport is carried out mainly through the exchange of protons between the ions derived from the acid. A number of polymer electrolytes have been examined extensively, exhibiting high proton conductivity in the anhydrous state. However, one of the major drawbacks is that the acidic units are susceptible to self-condensation at high temperatures (Bozkurt and Meyer, 2001). Only a few systems, mainly those based on polybenzimidazole (PBI) membranes, have been reported demonstrating efficient

operation at temperatures above 100°C (Wei et al., 1995). Li et al. revealed that operation of acid-doped polymer electrolytes in fuel cell at temperatures below 100°C could result in washing the proton solvent away from the system. This indicates that special attention must be paid to the operation of such systems in a defined temperature range (Li et al., 2004). Schuster et al. provided a comprehensive review on the various types of protogenic groups as PEM separator materials for intermediate temperature and low humidity conditions) (Schuster et al., 2005).

Aiming to overcome the challenges faced in the exploitation of polymer-acid systems, an alternative kind of proton conducting electrolytes was introduced by Kreuer (Kreuer, 1997; Kreuer et al., 1998) operating with acidic polymers in combination with amphoteric nitrogen-containing heterocyclic structures as a proton solvent. As speculated, the performance of these systems did not depend on the humidity. In fact, heterocycles behave similar to water but are able to form hydrogen bond networks that undergo auto-protolysis at much higher extent leading to high proton conductivity (Kreuer et al., 1998). On the other hand, the host polymer improves the mechanical properties enabling fabrication of thin free-standing films with higher stability in the presence of electrode materials (Bermudez et al., 1992). In addition, the host polymer functions as a source of protons by supplying protons to heterocyclic protogenic solvents. This results in enhanced defect-type proton conductivity.

Despite progress made in the development of high temperature electrolytes and replacement of water with alternative protons solvents, the volatility of these low molecular weight solvents remains as one of the key shortcomings hampering their widespread acceptance. This has led to new research avenues in order to address this issue. For instance, researchers have tried to immobilize these heterocyclic compounds on the polymer structure. Based on the findings, this must be achieved carefully by using flexible spacers to avoid sacrificing the high local mobility of proton solvent molecules and protonic charge carriers. Due to the immobilization of the proton solvent molecules, proton transfer is anticipated to rely on the structural diffusion mechanism based on dynamic hydrogen bonds networks. The prevalence of this mechanism is well investigated in case of Im immobilized systems (Münch et al., 2001; Iannuzzi et al., 2004; Schuster et al., 2001). Simulation studies have shown that the structural diffusion is much more complex than the single jump of an excess proton from one molecule to

another. Also, the proton transfer requires extensive reorientation of adjacent heterocycles and reorganization of the hydrogen bond coordination sphere of the migrating protons. In this respect, an ideal tethering should be constructed of flexible and sufficiently long spacers to enable high local mobility. In addition, it must possess sufficiently high concentrations of proton solvents to maximize the charge carriers and enable sufficient percolation (Scharfenberger et al., 2006). Another approach in the development of proton conducting electrolytes is to combine the functions of the protogenic group and the proton solvent in a single molecule. Such molecules must be amphoteric in the sense that they behave as both a proton donor (acid) and proton acceptor (base) and they must form dynamical hydrogen bond networks.

1.3.3.1 Azole-based heterocyclic compounds as proton solvents

The concept of using heterocycles was first introduced by Kreuer et al. who suggested exploitation of nitrogen-containing heterocycles as protogenic solvents for proton conduction (Kreuer et al., 1998). Most heterocyclic groups have high boiling points which makes them attractive for the development of more temperature-tolerant proton conductive membranes. In addition, unlike water, they can be incorporated into the polymer structure to further reduce their volatility during operation.

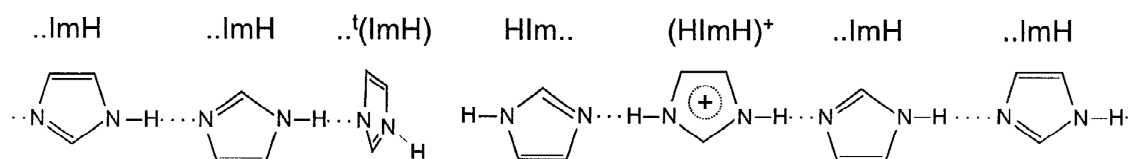
In these heterocycles, the basic nitrogen sites act as strong proton acceptors with respect to strong acid groups such as sulfonic acid and phosphonic acid group (Jannasch, 2003; Kreuer, 2007; Steininger et al., 2007). The rather isometric molecules are advantageous for extended local dynamics and their protonated and unprotonated nitrogen functions may act as donors and acceptors in proton transfer reactions while the ring itself is non-polar and avoids strong solvent effects. Furthermore, pure heterocycles in the liquid state show higher conductivity than pure water due to the high degree of self-dissociation indicating small solvent effects, which is also advantageous for high proton mobility. The pK_a values of various heterocycles are provided in Table 1.1.

Table 1.1. Melting points, boiling points and pK_a of the heterocycles.

Heterocycle	Melting point (°C)	Boiling point (°C)	pK _a
Imidazole	90	257	7.2
Benzimidazole	170	-	12.9
Methyl imidazole	-60	198	7.4
Pyrazole	68	187	2.5
1H-1,2,3-Triazole	23	203	1.17
1H-1,2,4-Triazole	120	256	2.39
1H-Tetrazole	157	220	4.89
5-Aminotetrazole	202	-	8.1

Imidazole (Im)

Imidazole (Im) is one of the most simple and widely used heterocycles (Fig. 1.4). Im has also found other applications such as in blends with ionic liquids (Sun et al., 2001; Noda et al., 2003). In physical aspects, Im is a solid material at standard condition with a boiling point of ~257 °C. Its proton conductivity at its melting point (90°C) is approximately 10⁻³ S/cm (Kreuer, 1997). The pK_a for Im is reported to be approximately 14.9 while the pK_a for imidazolium is about 7 (Münch et al., 2001).

**Figure 1.4.** Proton conduction in imidazole through the Grotthuss mechanism, schematically showing the reorientation of the Im moiety (Münch et al., 2001).

The proposed mechanism for the proton conduction in Im-based systems involves proton transfer between the neighboring protonated and unprotonated guest molecules (the Grotthuss mechanism) (Kreuer, 1997; Casciola et al., 1991). This occurs as a result of aggregation of Im moieties in hydrogen-bonded chains (Bozkurt et al., 2003; Yamada and Honma, 2005; Sevil and Bozkurt, 2004). Investigations using quantum chemical calculations on nitrogen atoms as mediator for proton conduction have indicated the possibility for hydrogen bond between nitrogen atoms and lower proton transfer barriers (Zhou et al., 2006; He et al., 2003). The schematic representation of the Grotthuss mechanism along the neighboring imidazole molecules is illustrated in Fig. 1.4. According to this schematic, the proton transfer between the adjacent Im molecules

involves reorientation of the Im moiety. While high proton mobility has been observed in Im-based materials, this reorientation step in Im molecules is regarded as a rate limiting factor for the long range proton transfer across membranes based on Im. As a result, the overall proton conductivity of Im-based membrane electrolytes, such as in ionic liquids, oligomers and polymers is relatively low. In addition, the electrochemical stability of Im appears to be inadequate for fuel cell applications, largely due to the high electronic density of the Im ring and also due to the diffusion and absorption of Im on the surface of the catalytic electrodes (Schuster et al., 2005; Noda et al., 2003; Yang et al., 2001; Li et al., 2005).

1-Methylimidazole (MeIm) (Fig. 1.5a) is a heterocycle from among the Im derivatives. Although the pK_{a1} value of MeIm molecule is much higher than that of Im, the conductivity of the complexes made from MeIm is not as high as those complexes made from Im (Schechter et al., 2002). This is attributed to the provision of strong interactions between the Im molecules that can form clusters of up to 20 molecules through hydrogen bonding (Acheson, 1976).

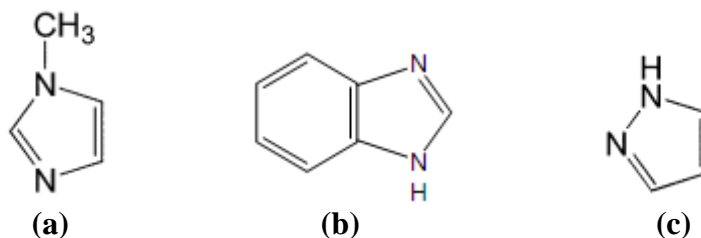


Figure 1.5. The structures of (a) 1-methyl imidazole, (b) benzimidazole, BnIm and (c) pyrazole, Py.

Benzimidazole (BnIm)

Benzimidazole (BnIm) (Fig. 1.5b) is a heterocyclic compound comprised of the fusion of benzene and Im with a melting point of 170°C. Similar to Im, the neighboring protonated and non-protonated nitrogens in BnIm act as donor and acceptor in proton transfer reactions. It should be noted that this is in contrast to acidic molecules such as phosphoric and sulfuric acids described as proton donors and acceptors with the formation of protonic defects (e.g., $H_2PO_4^-$; HSO_4^-) and intermolecular proton transfer reactions (Dippel et al., 1993). The reported pK_a for BnIm and benzimidazolium are

12.9 and 5.3, respectively (Münch et al., 2001). Although these values are slightly less than those for Im, benzimidazole can be used as a dopant in acidic polymers to facilitate the proton transfer via Grotthuss mechanism. In addition unlike Im, BnIm does not have electrochemical stability problem in fuel cell applications.

Pyrazole (Py)

According to Kreuer et al., molecular diffusion coefficients for pyrazole (Py) (Fig. 1.5c) are generally higher than those for Im. This is in accordance with the lower melting and boiling points (b.p.= 186 °C) of Py and also less tendency to form hydrogen bonded structures. On the other hand, Py possess a lower rate of proton conduction compared to Im. This is ascribed to the weaker tendency for molecular association by hydrogen bonding and also lower basicity of Py (Kreuer et al., 1998). The proton conductivity of Py is 1.4×10^{-6} S/cm (at 120 °C) (Casciola et al., 1991).

Based on the findings, proton diffusion for Py and Im is similar, occurring through a chain of suitably oriented molecules, without rotation of the protonated molecule (Casciola et al., 1991). This is attributed to the presence of the hydrogen bonded to the nitrogen in the neutral molecule. Once the proton has been transferred through the chain, the neutral molecules can rotate so as to be ready for a new proton transfer. Fig. 1.6 shows the proposed Grotthuss type transport mechanism in pyrazole. It is reported that pyrazole molecules possess low basicity ($pK_a=2.61$) and thus do not act as proton donor and acceptor in composite material largely due to the fact that non-protonated $-N=$ group of pyrazole ring cannot strongly interact with the free protons from the host material in complexes (Yamada and Honma, 2005). Therefore, pyrazole has not been preferred as a proton source in the composite membranes of polyacids in PEM synthesis.

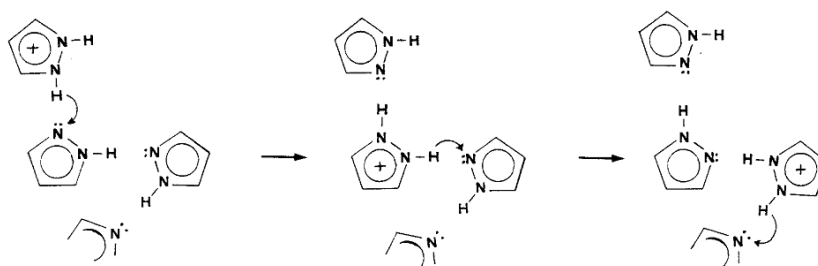


Figure 1.6. Proton conduction in pyrazole through Grotthuss mechanism (Casciola et al., 1991).

Triazole (Tri)

Triazoles are another class of heterocyclic protogenic solvents exhibiting promising results. Several triazoles are of interest: 1H-1,2,4-triazole (Fig. 1.7a) is a crystalline solid at standard condition with melting and boiling points of 120°C and 260°C, respectively; 1H-1,2,3-triazole (Fig. 1.7b) is a liquid at room temperature, with melting and boiling points of 23°C and 203°C, respectively (Zhou et al., 2005). As shown in Fig. 1.7, the molecular structure of Tri resembles that of other heterocyclic structures such as Im and Py, with the difference that Tri comprises three nitrogen atoms in the five-membered ring. In this regard, the prevalent proton conduction mechanism in Tri has been expected to be similar in nature to that of other heterocyclic compounds.

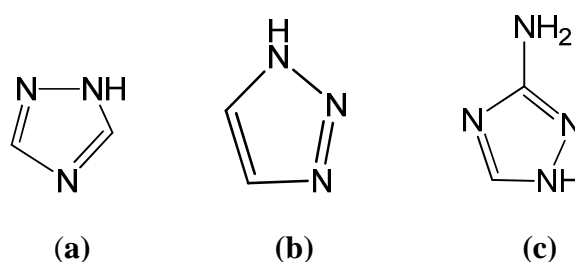


Figure 1.7. The molecular structures of (a) 1H-1,2,4-triazole (b) 1H-1,2,3-triazole (c) 3-amino-1,2,4-triazole.

Neutral Tri (Fig. 1.7b) has two tautomers, 1H-1,2,3-triazole and 2H-1,2,3-triazole, and so does protonated Tri, 1,3-diH-1,2,3-triazolium and 1,2-diH-1,2,3-triazolium cations (Zhou et al., 2006). These isomers inter-convert by tautomerisation, which may occur through intra- or inter-molecular proton transfer (Rauhut, 2003). Although 2H-1,2,3-triazole is more stable in the gas phase, 1H-1,2,3-triazole becomes more stable in solution because of its larger dipole moment (Minkin et al., 2000). The presence of these tautomers and their interactions has made a detailed study of the systems very complex. Zhou et al. employed quantum mechanical calculations and conducted a study on the intra- and intermolecular proton transfer in 1H(2H)-1,2,3-triazole based systems in order to gain an understanding on the interactions between the neutral Tri and triazolium cations, and its effect on the short and long range proton conduction (Zhou et al., 2006). Their findings indicated the formation of stable complexes between a -NH

group on the protonated Tri as the proton donor and a nitrogen atom on the neutral Tri as the proton acceptor. The ionic conductivity of pure 1H-1,2,3-triazole is 1.3×10^{-4} S/cm (at room temperature) which implies its considerable proton conductivity in liquid state and also produces protonic charge carriers upon self-dissociation of 1H-1,2,3-triazole molecules (Zhou et al., 2005).

The proton conductivity of pure 1H-1,2,4-triazole is reported to be 1.5×10^{-4} S/cm (at 115°C) and about 1.2×10^{-3} S/cm (at the melting point) (Li et al., 2005). This can be related to the low pK_{a1} where self dissociation of 1H-1,2,4-triazole produces highly mobile proton charge carriers (Li et al., 2005; Günday et al., 2006). Zhou et al. suggested the proton conduction for triazole-based systems to be different from that for Im largely due to the presence of several proton-carrying isomers for triazoles (Zhou et al., 2006). Therefore, Tri can be doped into acidic host polymers and may improve the anhydrous conductivity of the materials in the dry state. Based on the reports, in polyelectrolyte/Tri systems the heterocyclic groups form a hydrogen bonding networks and promote long-range proton transport that is far better than that with Im (Zhou et al., 2005). Results of an investigation using computational methods on the reactions paths for different proton transfer reactions in 1,2,3-triazole suggested that Tri forms clusters that favor intermolecular proton transfer reactions (Rauhut, 2003). Therefore, blending of Tri with an acidic polyelectrolyte can be useful for the development of high temperature resistive free-standing films due to the possibility of long-range proton transport via structural diffusion.

Tetrazole (Tet)

Tetrazoles are a class of heterocyclic molecules with four nitrogen atoms in the ring (Fig. 1.8). 1H-tetrazole is solid at room temperature and has melting and boiling points of 157°C (Mihina et al., 1950) and 220°C, respectively. It has a pK_a of 4.9 and several forms such as 5-aminotetrazole (Fig. 1.8b), 1-methyl 5-aminotetrazole and 1,5-diaminotetrazole (Satchell and Smith, 2002). Tetrazoles are thermally stable compounds and 5-aminotetrazole shows tautomerization as imino and amino forms (Lesnikovich et al., 2002; Levchik et al., 1992). Since it has higher nitrogen units in its ring, Tet is expected to perform easier proton transfer when used as a proton solvent in PEM materials.

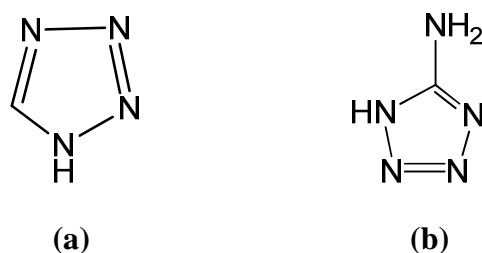


Figure 1.8. The molecular structure of (a) 1H-tetrazole (b) 5-aminotetrazole.

1.3.3.2 Siloxane Based Proton Conductive Membranes

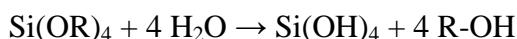
Siloxane based polymers are commonly produced via sol-gel method. The sol-gel process is a wet-chemical technique used for the fabrication of both glassy and ceramic materials. In this process, the sol (or solution) evolves gradually towards the formation of a gel-like network containing both a liquid phase and a solid phase. Typical precursors are metal alkoxides and metal chlorides, which undergo hydrolysis and polycondensation reactions to form a colloid. The basic structure or morphology of the solid phase can range anywhere from discrete colloidal particles to continuous chain-like polymer networks (Klein and Garvey, 1980; Brinker et al., 1982).

Under certain chemical conditions (typically in acid-catalyzed sols), the interparticle forces have sufficient strength to cause considerable aggregation and/or flocculation prior to their growth. The formation of a more open continuous network of low density polymers exhibits certain advantages with regard to physical properties in the formation of high performance glass and glass/ceramic components in 2 and 3 dimensions (Sakka et al., 1982).

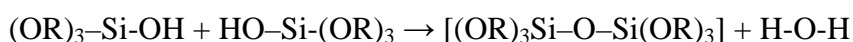
A well-studied alkoxide is silicon tetraethoxide, or tetraethyl orthosilicate (TEOS). The chemical formula for TEOS is given by: $\text{Si}(\text{OC}_2\text{H}_5)_4$, or $\text{Si}(\text{OR})_4$ where the alkyl group $\text{R} = \text{C}_2\text{H}_5$. Alkoxides are ideal chemical precursors for sol-gel synthesis because they react readily with water. The reaction is called hydrolysis, because a hydroxyl ion becomes attached to the silicon atom as follows:



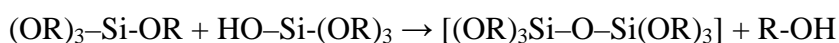
Depending on the amount of water and catalyst present, hydrolysis may proceed to completion, so that all of the OR groups are replaced by OH groups, as follows:



Any intermediate species $[(\text{OR})_2\text{-Si-(OH)}_2]$ or $[(\text{OR})_3\text{-Si-(OH)}]$ would be considered the result of partial hydrolysis. In addition, two partially hydrolyzed molecules can link together in a condensation reaction to form a siloxane $[\text{Si-O-Si}]$ bond:



or



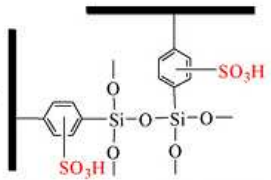
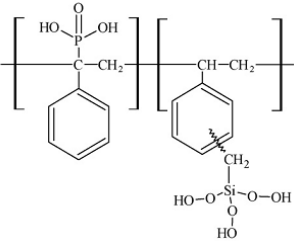
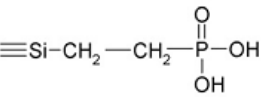
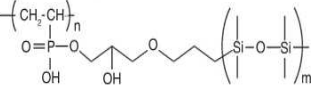
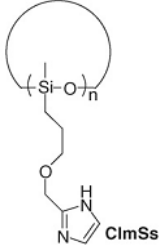
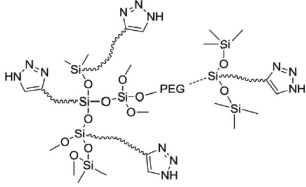
Thus, polymerization is associated with the formation of a 1, 2, or 3- dimensional network of siloxane $[\text{Si-O-Si}]$ bonds accompanied by the production of H-O-H and R-O-H species.

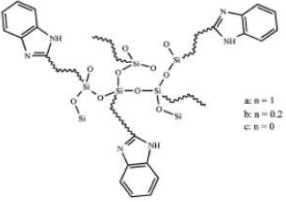
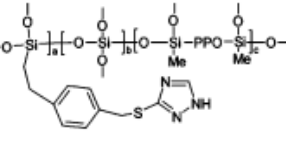
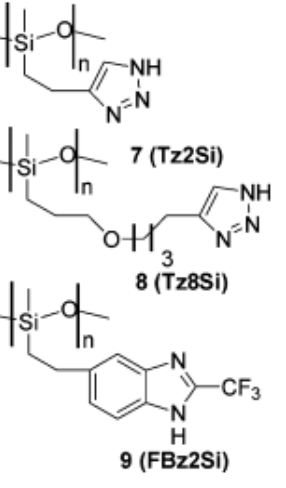
By definition, condensation liberates a small molecule, such as water or alcohol. This type of reaction can continue to build larger and larger silicon-containing molecules by the process of polymerization. Thus, a polymer is a huge molecule (or macromolecule) formed from hundreds or thousands of units called monomers. The number of bonds that a monomer can form is called its functionality. Polymerization of silicon alkoxide, for instance, can lead to complex branching of the polymer, because a fully hydrolyzed monomer Si(OH)_4 is tetrafunctional (can branch or bond in 4 different directions) (Matijevic, 1986; Brinker and Mukherjee, 1981; Sakka and Kamiya, 1980).

There are several proton conducting polymer systems prepared via sol-gel of silane groups in different polymers such as sulfonated poly(arylene ether ether ketone), Nafion and polyvinyl phosphonic acid. However in these studies the proton transport is performed by the humidity and the sulfonic acid groups of the polymer. Previously, in order to obtain siloxane based anhydrous proton conducting systems, imidazole (Lee et al, 2006), benzimidazole (Herz et al., 2003) and triazole (Li et al., 2005; Granados-Focil et al., 2007) were immobilized into silane matrices. In these studies triazole containing materials were reported to have better proton conductivity (5×10^{-3}) comparing to

imidazole based membranes. In addition the presence of flexible chains also affects the proton conduction where azoles are attached to this side chains and the segmental motions have high contribution on the proton conduction. The chemical structures and maximum proton conductivity values of several siloxane based polymer matrices are illustrated in Table 1.2.

Table 1.2. The chemical structures and maximum proton conductivity values of several siloxane based polymer matrices.

Material	Max. Cond. (S/cm)	Ref.
	0.015 at 25 °C, 56.7 % RH	Chen et al., 2007)
	0.01 at >80 °C, 100% RH	(Kato et al., 2007)
	0.142 at 120 °C, 100% RH (contains 40% polysilsesquioxane and 80% phosphonated SPEEK)	(Pezzin et al., 2008)
	0.037 at 80 °C, % 100 RH	(Yazawa et al., 2008)
	10 ⁻⁴ at 160 °C, anhydrous state	(Lee et al, 2006)
	10 ^{-3.5} at 160 °C, anhydrous state (contains 2.5 mol H ₃ PO ₄ /Tri)	(Sanghi et al., 2010)

	7×10^{-5} at 150 °C, anhydrous state	(Herz et al., 2003)
	5×10^{-3} at 140 °C, anhydrous state	(Li et al., 2005)
	5×10^{-3} at 170 °C, (contains %75 triflic acid) 10^{-3} at 180 °C, (contains %75 triflic acid) 5×10^{-4} at 190 °C, (contains %15 triflic acid)	(Granados-Focil et al., 2007)

1.3.3.3 Proton Conductive Copolymer Membranes

The development of copolymer membranes is among the latest areas of research on PEMFCs. This is largely driven by limitations in the capabilities of conventional materials and the need to design and fabricate engineered membranes through adoption of appropriate molecular architecture strategies.

Martwiset et al. synthesized random copolymer and terpolymers of 1,2,3-triazole-containing acrylates and poly(ethylene glycol)methyl ether acrylate (PEGMEA) with composition of 0 to 52 % of PEGMEA (Martwiset et al., 2007). A typical structure of the polymers is shown in Fig. 1.9. The proton conductivity of membranes changed from 0.5 to 1.5 orders of magnitude upon addition of trifluoro acetic acid at various levels. The authors examined the effect of the charge carrier density on the proton conductivity by doping the Tri rings with a strong acid, and also by substitution of the Tri groups with low molecular weight poly(ethylene glycol). It was found that substitution of BnIm by 1,2,3-triazole in polyacrylate containing 30 % PEGMEA resulted in higher proton

conductivity and weaker dependence on temperature. This was attributed to the possible effects of the lower pK_a , smaller size and lower melting point of Tri. Incorporation of PEGMEA up to levels of 30 % mol in 1,2,3-triazole systems resulted in improved conductivity. In contrast, the reduction in proton conductivity of terpolymers by addition of PEGMEA was attributed to the pronounced effect of decreasing charge carrier concentration rather than the effect of increased backbone mobility.

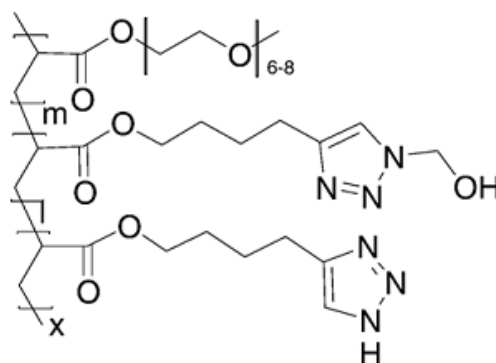


Figure 1.9. Structure of prepared co- and terpolymers (Martwiset et al., 2007).

Woudenberg et al. conducted a systematic study to investigate the effect of backbone mobility on the proton conductivity of the polymer and copolymer electrolyte membranes (Woudenberg et al., 2007). They immobilized BnIm units to several ether acrylate polymer backbones (Fig. 1.10). Monomers were prepared containing BnIm moieties attached to the respective functional group, resulting in polymers with T_g values ranging from 88 °C to 113 °C. The increase in T_g over expected values was attributed to the decreased mobility induced by aggregation, hydrogen bonding, and π - π interactions of the BnIm side chains. The acrylate polymer B5A showed conductivity of 0.015 mS/cm at 200 °C, nearly an order of magnitude larger than both B5NB and B5MA, 0.0024 mS/cm and 0.0048 mS/cm, respectively. The conductivity curves of the electrolytes showed VTF behavior. The positive effect on the conductivity by increasing mobility and the competing effect of charge carrier density reduction was observed in comparing B5A and B5MA. Similarly, heterocycle intercalated proton-conducting polysiloxanes have been synthesized via hydrosilylation of vinyl or allyl functionalized weakly basic heterocyclic motifs with a poly(methyl hydrosiloxane) precursor. The resulting polymers showed the highest reported proton conductivities of up to 0.1

mS/cm at temperatures below 80 °C and up to 5 mS/cm at 180 °C when doped with trifluoroacetic acid (Granados-Focil et al., 2007).

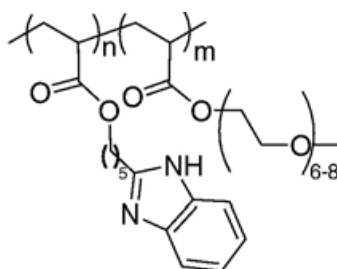


Figure 1.10. Structure of prepared copolymers (Woudenberg et al., 2007).

Bozkurt et al. (Bozkurt et al., 2003) synthesized proton-conducting polymers by free-radical copolymerization of vinylphosphonic acid (VPA) as a proton source with 4-vinylimidazole (4-VIm) as a proton solvent (Fig. 1.11). The copolymers were produced with 4-VIm/VPA mole ratio ranging from 4:1 to 1:2 in the feed. Thermogravimetric analysis revealed that copolymers were stable up to 200 °C, with no distinct glass transitions observed up to the onset of degradation. It was found from FTIR analysis that a donor–acceptor interaction between imidazolium ion and phosphonic acid, resulted in the formation of inter- and intramolecular complexation. DC conductivities of copolymer samples increased ranging from 10^{-6} to 10^{-12} S/cm within the measured temperature span, with increase in Im units immobilized in the chains. The overall low conductivity in poly(4-VIm-co-VPA) membranes was attributed to restrictions in the segmental motions of the polymer chains by ionic cross-linking.

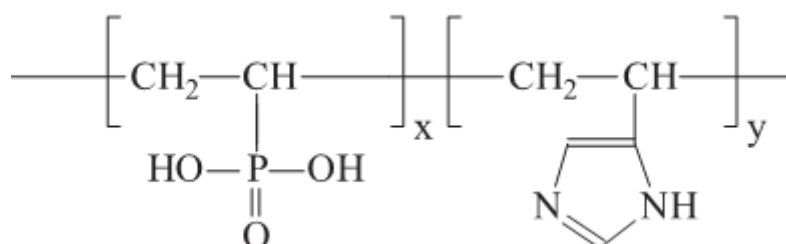


Figure 1.11. Structure of poly(VPA-co-4-VIm) copolymers (Bozkurt et al., 2003).

Novel proton-conducting copolymers based on VPA and 1-vinyl-1,2,4-triazole (VTri) were synthesized using conventional free radical polymerization of the corresponding monomers (Fig. 1.12). The molecular weight of the resultant copolymers was low and the presence of a glass transition in the copolymers indicated that ionic

interactions do not prevent segmental relaxations of the polymer chains (Çelik et al., 2008b). The proton conductivity increased with the content of phosphonic acid units in the polymer chain. In particular, poly(VPA-co-VTri), sample S2 (~70 % PVPA mole ratio) showed a conductivity of $\sim 10^{-3}$ S/cm at 120 °C in the anhydrous state. The proton transfer in this copolymer structure was analyzed with solid state NMR methods and hydrogen bonding formation was verified (Çelik et al., 2008b).

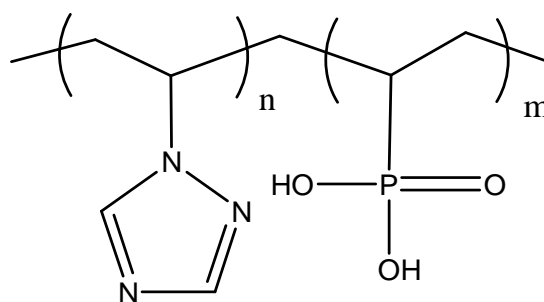


Figure 1.12. Structure of poly(VPA-co-VTri) copolymer (Çelik et al., 2008b).

In another study, Pu et al. employed normal free radical polymerization and click chemistry techniques to prepare a series of N-heterocycle side-chain copolymers, namely poly(1,2,4-vinyltriazole) (PVTri) and poly(1,2,4-vinyltriazole-co-5-vinyltetrazole-co-acrylonitrile) (P(VTr-VT-AN)) (Pu et al., 2007). The glass-transition temperatures of the polymers were between 70 and 85 °C. The proton conductivity of doped materials was about 10^{-5} S/cm at 60 °C under anhydrous condition, and showed Arrhenius behavior.

Proton conducting electrolyte membranes were prepared based on the free-radical copolymerization of 2-acrylamido-2-methyl-1-propanesulfonic acid (AMPS) and 1-vinyl-1,2,4-triazole (VTri) (Fig. 1.13) (Çelik and Bozkurt, 2010a). The AMPS content of copolymer was varied by the feed ratios from 36 % up to 62 %. The resultant copolymers were thermally stable up to approximately 250°C. In addition, the presence of a glass transition in the copolymers indicated that the presence of ionic interactions did not prevent cooperative relaxations of the copolymers. Based on the cyclic voltammetry results, the electrochemical stability domain extended to over 3 V. In addition, the temperature dependence of conductivity relaxation times indicated that the proton conductivity occurred by a hopping mechanism via structure diffusion.

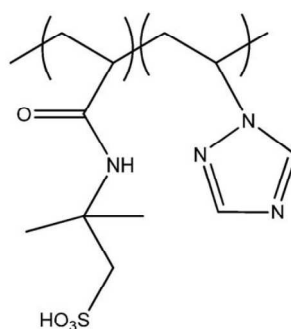


Figure 1.13. Structure of P(VTri-co-AMPS) copolymers (Çelik and Bozkurt, 2010a).

Pu and coworkers synthesized copolymers based on vinyl benzyl phosphonic acid and vinyl imidazole. They studied proton conducting properties of the membranes in 100 % humidified condition and obtained a proton conductivity of 0.1 S/cm at 30 °C. (Pu et al., 2009).

Sezgin et al. prepared copolymers based on vinyl benzene boronic acid and vinyl imidazole (Sezgin et al., 2009). In anhydrous condition the copolymers resulted a proton conductivity of 0.0027 S/cm.

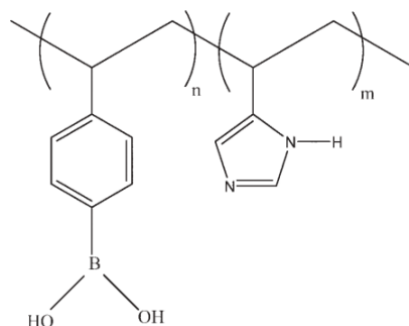


Figure 1.14. The structure of poly(vinyl benzene boronic acid-co-vinyl imidazole) copolymer (Sezgin et al., 2009).

CHAPTER 2

EXPERIMENTAL

2.1 SYNTHESIS OF TRIAZOLE FUNCTIONAL SILANE NETWORKS

3-Glycidoxypropyl trimethoxy silane (GPTMS) (>97%, Merck), 1H-1,2,4-triazole (>97%, Aldrich), 3-aminotriazole (>95%, Aldrich), trifluoromethane sulfonic acid (TA) (>98, Fluka), methanol (Merck) and hydrochloric acid (Merck) were used as received.

GPTMS was modified with 1H-1,2,4-triazole (Tri) and 3-aminotriazole (ATri) by ring opening of the epoxy group of GPTMS in methanol according to Fig. 2.1. 0.0085 mol of Tri or ATri was dissolved in 10 mL methanol and 0.0085 mol of GPTMS was added. The reaction mixture was purged with nitrogen and the modification reaction was performed at 80 °C for 24 h. Then polymerization of silane groups was performed using simple sol-gel process. The resulting pale yellow solution was poured on Teflon petri dish and for hydrolysis of methoxide groups 1 ml of 1 M HCl was added together with dopant (TA) and mixed. For condensation reaction the solution was kept on room temperature until evaporation of methanol and then heated stepwise until 100 °C (5 h) and dried in vacuum oven at 60 °C for 2 days. The resulting crosslinked material was transparent, mostly flexible and free standing membrane (Fig. 2.2). The addition of dopant acid (TA) softens the material and becomes more flexible.

Since the crosslinked material is not soluble in water and common organic solvents, doping of the triazole functional sample was done before sol-gel procedure. The ratio of trifluoromethane sulfonic acid was varied as $x=0.5$ and 1 with respect to azole unit. The resulting membranes were called as Si-TriTA $_x$ and Si-ATriTA $_x$. In order to confirm that all the triazole units are immobilized into the epoxy ring, Si-Tri membrane was grinded, washed with water and dried. Since there was no weight

difference with the initial sample, the tethering of the all triazole units into the epoxy ring was confirmed. In addition the filtrate was analyzed with ^1H NMR and there was no peak.

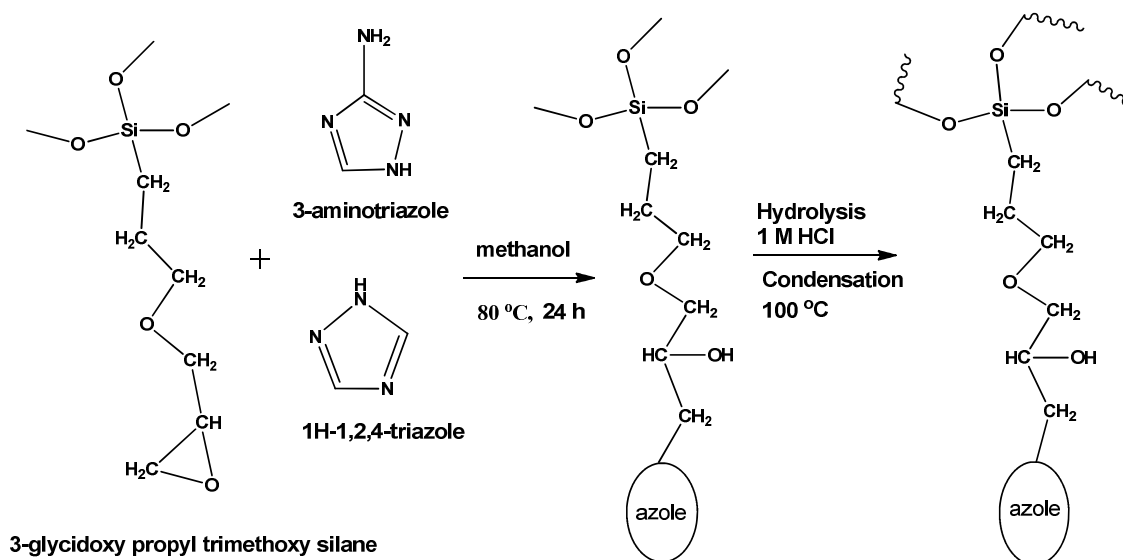


Figure 2.1. The synthesis of azole functional silane networks (Si-Tri and Si-ATri).



Figure 2.2. Transparent and free standing film of Si-ATriTA0.5 sample.

2.2 SYNTHESIS OF TETRAZOLE FUNCTIONAL SILANE NETWORKS

GPTMS was modified with 5-aminotetrazole (ATet) by ring opening of the epoxy group of GPTMS in methanol according to Fig. 2.3. 0.0085 mol of 5-aminotetrazole was dissolved in 10 mL methanol and 0.0085 mol of GPTMS was added. The reaction mixture was purged with nitrogen and the modification reaction was performed at 80 °C for 24 h. Then polymerization of silane groups was performed using simple sol–gel process. The resulting pale yellow solution was poured on Teflon petri dish and for hydrolysis of methoxide groups 1 mL of 1M HCl was added together with dopant (TA) and mixed. For condensation reaction the solution was kept on room temperature until evaporation of methanol and then heated stepwise until 100 °C (5 h) and dried in vacuum oven at 60 °C for 2 days. The resulting crosslinked material was transparent, flexible and free standing membrane with thickness of 300–500 μm (Fig. 2.4).

Since the crosslinked material is not soluble in water and common organic solvents, doping of the tetrazole functional sample was done before sol–gel procedure. The ratio of trifluoromethane sulfonic acid was varied as $x=0.5$ and 1 with respect to azole unit. The resulting membranes were called as Si-ATetTA0.5 and Si-ATetTA1. When the doping level is increased to $x=2$, the resulting material was not a free standing membrane which indicates low efficiency of sol–gel process. Therefore, $x=1$ was considered as the optimum doping level.

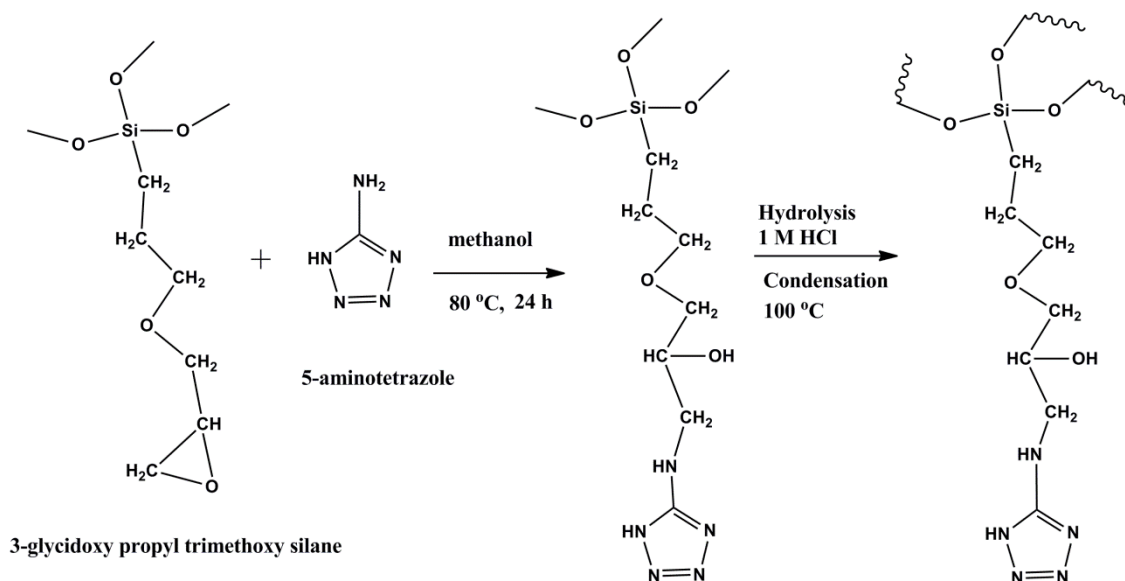


Figure 2.3. The synthesis of tetrazole functional silane networks (Si-ATet).



Figure 2.4. Transparent and free standing film of Si-ATet.

2.3 SYNTHESIS OF COPOLYMERS BASED ON 4-VINYL BENZENE BORONIC ACID AND 1-VINYL-1,2,4-TRIAZOLE

4-Vinyl benzene boronic acid (VBBA) was copolymerized with 1-vinyl-1,2,4-triazole (VTri) using free radical copolymerization in DMSO at 85 °C for 24 h (Fig. 2.5). Firstly 4-vinyl benzene boronic acid (0.0017 mol) was dissolved in DMSO (1 mL) and then VTri (0.00085, 0.0017 and 0.0034 mol) was added with different mol ratios. α,α' -Azodiisobutyramidine dihydrochloride (AIBADC) (0.5 % mol) was used as initiator. Copolymerization was not achieved with AIBN. The resulting products were washed with water and diethyl ether to remove PVTri homopolymer and unreacted monomers. VTri monomer and PVTri homopolymer are soluble in water and VBBA monomer is soluble in diethyl ether. Conversion: 100 %. The copolymers were called as P(VBBA-co-VTri)1:0.5, P(VBBA-co-VTri)1:1 and P(VBBA-co-VTri)1:2. After drying procedure the samples are not soluble in water and common organic solvents.

To obtain high proton conductive membranes the copolymers were dissolved in DMSO before drying process and then they were doped with H_3PO_4 at several molar

ratios ($x=1,2,3$) with respect to triazole units. The homogeneous solutions were poured on Teflon petri dishes and homogeneous, transparent membranes were obtained.

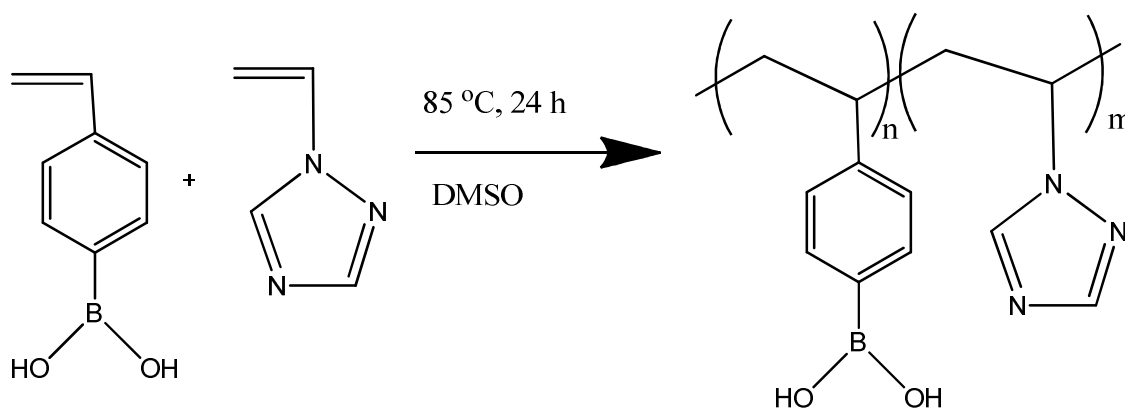


Figure 2.5. The synthesis of P(VBBA-co-VTri) copolymers.

2.4 SYNTHESIS OF COPOLYMERS BASED ON 4-VINYL BENZENE BORONIC ACID AND VINYL PHOSPHONIC ACID

4-Vinyl benzene boronic acid (VBBA) was copolymerized with vinyl phosphonic acid (VPA) using free radical copolymerization in DMSO at 85 °C for 24 h (Fig. 2.6). Firstly 4-vinyl benzene boronic acid was dissolved in DMSO (1 mL) and then VPA was added with different mol ratios (Table 2.1). α,α' -Azodiisobutyramidine dihydrochloride (AIBADC) (0.5% mol) was used as initiator. Copolymerization was not achieved with AIBN. The resulting products were washed with water and diethyl ether to remove PVPA homopolymer and unreacted monomers. The conversion was decreased with increasing VPA ratio which indicates that VPA has low reactivity ratio in this reaction conditions. After drying procedure the samples are not soluble in water and common organic solvents.

Table 2.1. The synthesis of P(VBBA-co-VPA) copolymers.

Sample	VBBA	VPA	Conversion
S1	1.00 g, 6.76 mmol	0.38 g, 3.52 mmol	1.30 g, 94 %
S2	1.00 g, 6.76 mmol	0.73 g, 6.76 mmol	0.91 g, 53 %
S3	1.00 g, 6.76 mmol	1.46 g, 13.5 mmol	1.1 g, 45 %

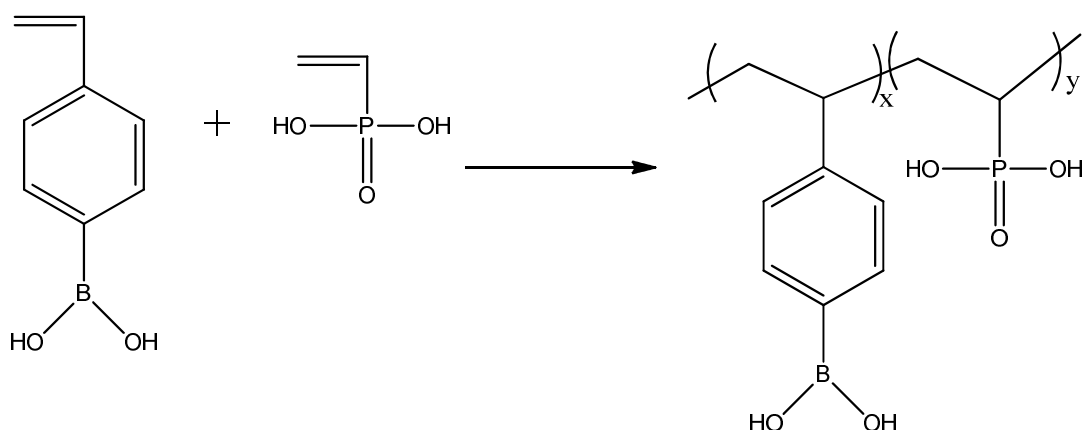


Figure 2.6. The synthesis of P(VBBA-co-VPA) copolymers.

The resulting P(VBBA-co-VPA) copolymers were grinded and the powder sample was reacted with polyethylene glycol monomethyl ether (PEGME, M_w :350) in THF (2-3 ml) at 90 °C for 48 h (Fig.2.7). Although the copolymers are not soluble in solvents it became homogeneous and soluble after reacting with PEGME. The resulting soft product was washed with diethyl ether to remove unreacted PEGME and dried in vacuum oven.

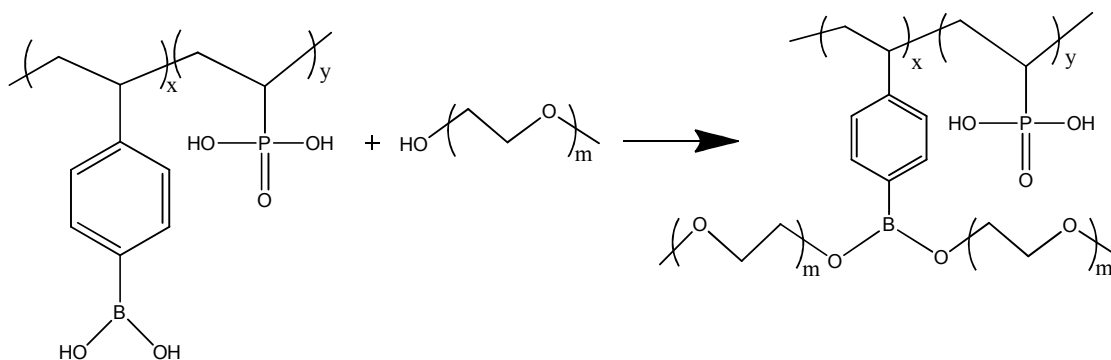


Figure 2.7. The synthesis of P(VBBA-co-VPA)-PEGME graft copolymers.

2.5 SYNTHESIS OF DIISOPROPYL-P-VINYLBENZYL PHOSPHONATE (VBP) MONOMER AND POLY(VINYL BENZYL PHOSPHONIC ACID)

Diisopropyl-p-vinylbenzyl phosphonate (Fig. 2.8) was synthesized in a similar method with the literature (Puel et al., 2009). Potassium tert-butoxide (8.16 g, 72.7 mmol) in dry THF (40 mL) was added dropwise into stirred solution of diisopropyl phosphite (14.19 g, 85.4 mmol) and p-vinylbenzyl chloride (10.72 g, 70.25 mmol) in THF within 2 h. And the reaction was maintained at room temperature throughout by occasional cooling with an ice bath. The mixture was kept stirring for another hour at room temperature and then filtered, diluted with diethyl ether (200 mL), and washed with water (100 mL) three times. The organic component was dried over sodium sulfate. The raw product was purified by flash column chromatography on silica. Residual vinylbenzyl chloride was eluted with toluene, and subsequently the product was washed off with ethyl acetate to yield colorless oil. Conversion: ~40 % of VBC was phosphonated.

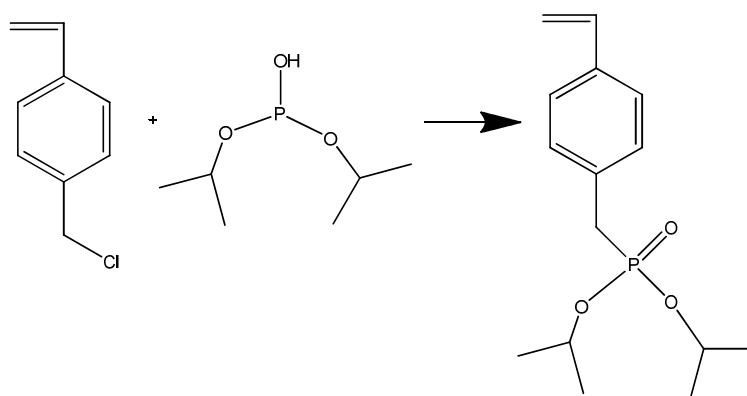


Figure 2.8. The synthesis of diisopropyl-p-vinylbenzyl phosphonate.

Diisopropyl-p-vinylbenzyl phosphonate (5.2 g, 0.0184 mol) was bulk homopolymerized by free radical polymerization using azobisisobutyronitrile (AIBN) (1 % mol) as initiator at 85 °C and 24 h (Fig. 2.9). The polymerization occurred just after the starting of the reaction as forming transparent rigid product. After 24 h the resulting rigid sticky product was washed with hexane to remove the unreacted monomer and dried in vacuum oven at 50 °C. Conversion: 94 %.

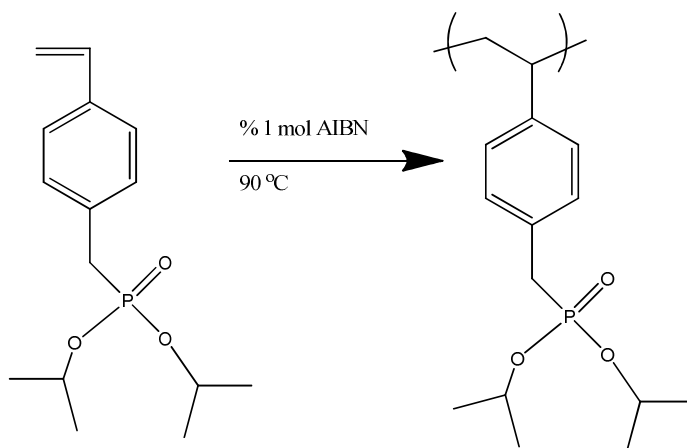


Figure 2.9. The synthesis of poly(diisopropyl-p-vinylbenzyl phosphonate), PVBP homopolymer.

The resulting poly(diisopropyl-p-vinylbenzyl phosphonate) (4.9 g) was placed in ethanol and waited for 2 days. The spherical rigid polymer was swelled in this period. The mixture was added into 10 M HCl and boiled at 100 °C for 24 h. Polymer did not dissolve in this period and then it was washed with distilled water several times to remove the free acids. After drying the product 3.5 g of PVBPA (Fig. 2.10) was obtained as rigid brittle material.

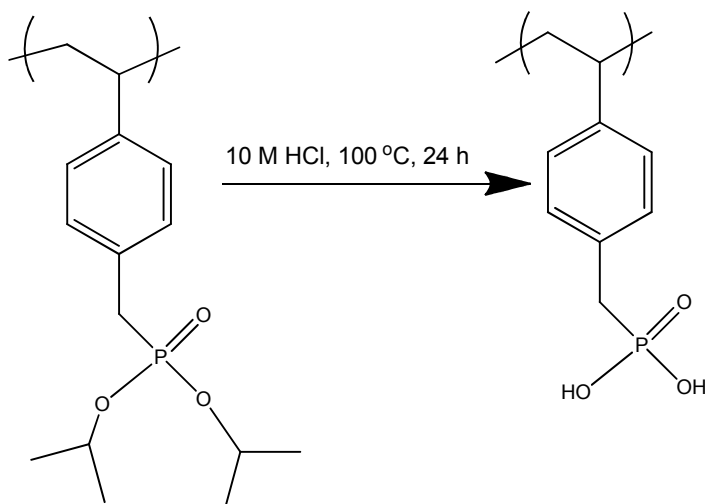


Figure 2.10. The synthesis of poly(vinyl benzyl phosphonic acid) PVBPA homopolymer.

2.6 SYNTHESIS OF POLY(VINYL TRIAZOLE-CO-VINYL BENZYL PHOSPHONIC ACID) (P(VTRI-CO-VBPA) COPOLYMER

Vinyl triazole (0.51 g, 0.0053 mol) was copolymerized with diisopropyl-p-vinylbenzyl phosphonate (0.00265, 0.0053 and 0.0106 mol) by free radical copolymerization in 2 mL toluene using AIBN (1 % mol) as initiator at 85 °C and 24 h (Fig. 2.11). The polymerization occurred just after the starting of the reaction as forming transparent, sticky, rigid product. After 24 h the resulting product was washed with diethyl ether and water to remove the unreacted monomers and then dried in vacuum oven at 50 °C.

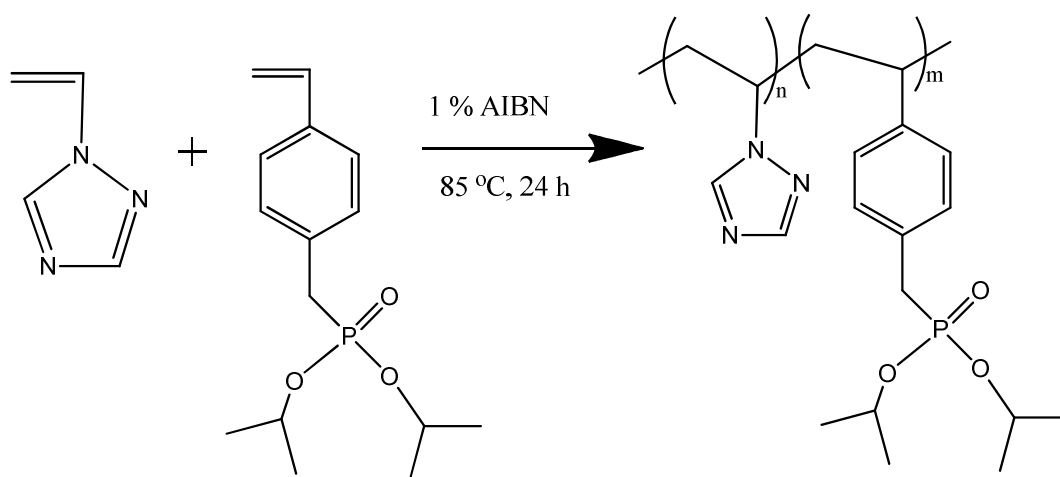


Figure 2.11. The synthesis of poly(vinyl triazole-co-diisopropyl-p-vinylbenzyl phosphonate) (P(VTri-co-VBP) copolymer.

The synthesized poly(vinyl triazole-co-diisopropyl-p-vinylbenzyl phosphonate) copolymers were swelled in ethanol and after adding 10 M HCl the mixture was boiled at 100 °C for 5 h. The copolymers did not dissolve in this period and then it was washed with distilled water several times to remove the free acids. The resulting phosphonic acid functional copolymers (Fig. 2.12) were dried at 50 °C in vacuum oven.

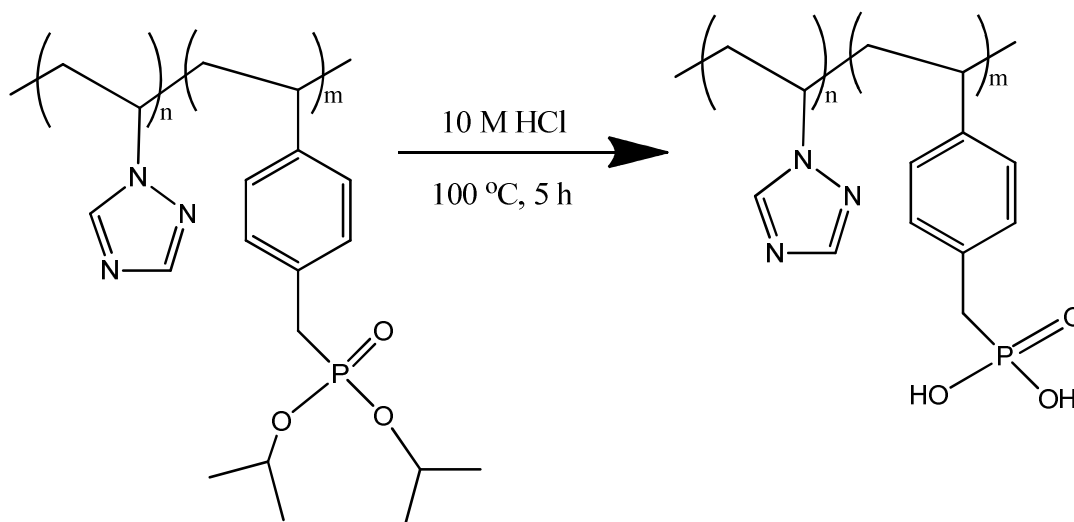


Figure 2.12. The synthesis of poly(vinyl triazole-co-vinyl benzyl phosphonic acid) (P(VTri-co-VBPA) copolymer).

2.7 SYNTHESIS OF POLY(VINYL BENZENE BORONIC ACID-CO-VINYL BENZYL PHOSPHONIC ACID) (P(VBBA-CO-VBPA) COPOLYMER

4-Vinyl benzene boronic acid (0.5 g, 0.00338 mol) was copolymerized with diisopropyl-p-vinylbenzyl phosphonate (0.00169, 0.00338 and 0.0676 mol) via free radical polymerization using DMSO (1.5 mL) as solvent at 85 °C and 24 h (Fig. 2.13). For high yield, the initiator was chosen as α,α' -azodiisobutyramidine dihydrochloride (AIBADC) (0.5% mol) for 1:0.5 and 1:1 composition and AIBN was chosen for 1:2 composition. Since polymerization of VBP prefers AIBN, it becomes impossible to obtain the copolymer using AIBADC for 1:2 composition. The polymerization occurred just after the starting of the reaction as forming pale pink viscous product. After 24 h the resulting viscous product was washed diethyl ether to remove the unreacted monomers.

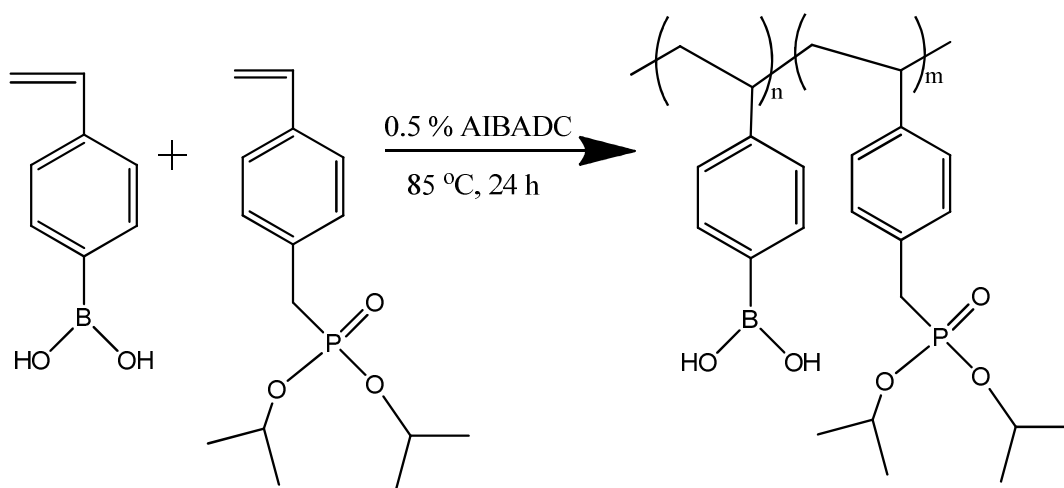


Figure 2.13. The synthesis of poly(vinyl benzene boronic acid-co-diisopropyl-p-vinylbenzyl phosphonate) (P(VBBA-co-VBP) copolymer).

The synthesized poly(vinyl benzene boronic acid-co-diisopropyl-p-vinylbenzyl phosphonate) copolymers were swelled in ethanol and after adding 10 M HCl the mixture was boiled at 100 °C for 5 h. The copolymers did not dissolve in this period and then it was washed with distilled water several times to remove the free acids. The resulting phosphonic acid functional copolymers (Fig. 2.14) were dried at 50 °C in vacuum oven.

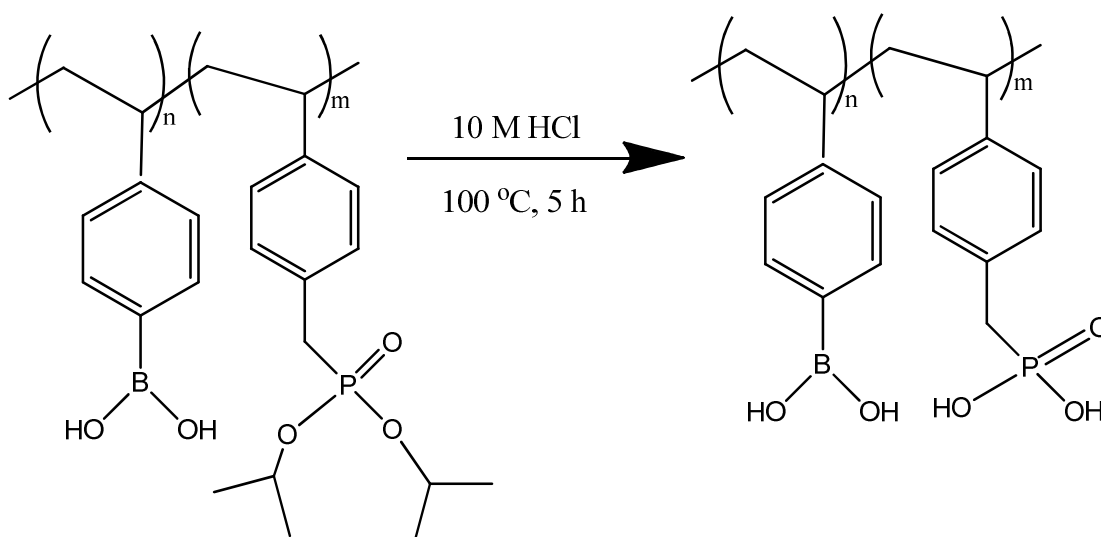


Figure 2.14. The synthesis of poly(vinyl benzene boronic acid-co-vinyl benzyl phosphonic acid) (P(VBBA-co-VBPA) copolymer).

The phosphonic acid functional P(VBBA-co-VBPA) copolymers were grinded and the powder sample was reacted with polyethylene glycol monomethyl ether (PEGME, Mw:350) using THF as solvent at 90 °C for 48 h (Fig. 2.15). Although the copolymers are not soluble in solvents it became homogeneous and soluble after reacting with PEGME. The resulting soft product was washed with diethyl ether to remove unreacted PEGME and dried in vacuum oven.

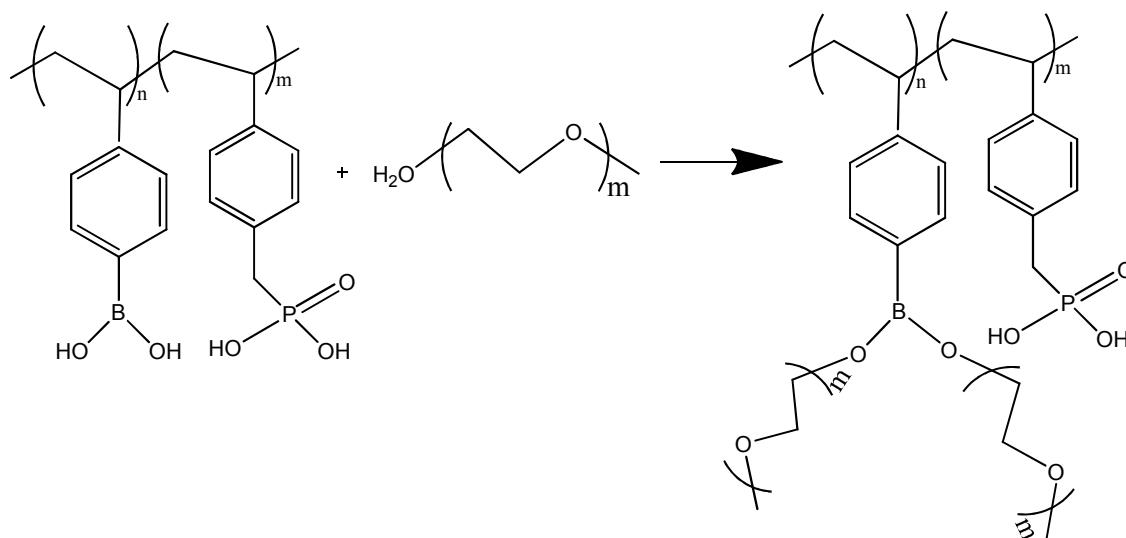


Figure 2.15. The synthesis of P(VBBA-co-VBPA)-PEGME graft copolymers.

2.8 CHARACTERIZATIONS

Nuclear magnetic resonance spectroscopy (NMR spectroscopy) is a research technique that exploits the magnetic properties of certain atomic nuclei to determine physical and chemical properties of atoms or the molecules in which they are contained. It relies on the phenomenon of nuclear magnetic resonance and can provide detailed information about the structure, dynamics, reaction state, and chemical environment of molecules. When placed in a magnetic field, NMR active nuclei (such as ¹H or ¹³C) absorb electromagnetic radiation at a frequency characteristic of the isotope. The resonant frequency, energy of the absorption, and the intensity of the signal are proportional to the strength of the magnetic field. ¹H NMR and ¹³C NMR measurements were performed with Bruker Avance 400 MHz in d-DMSO or d-chloroform.

Fourier-Transform IR (FTIR) is most useful for identifying chemicals that are either organic or inorganic. It can be utilized to quantitate some components of an unknown mixture. It can be applied to the analysis of solids, liquids, and gasses. The term Fourier Transform Infrared Spectroscopy (FTIR) refers to a fairly recent development in the manner in which the data is collected and converted from an interference pattern to a spectrum. FTIR can be used to identify chemicals from spills, paints, polymers, coatings, drugs, and contaminants. FTIR is perhaps the most powerful tool for identifying types of chemical bonds (functional groups). The wavelength of light absorbed is characteristic of the chemical bond as can be seen in this annotated spectrum. FT-IR spectra were recorded on a Bruker Alpha-P in ATR in range of 4000 cm^{-1} - 400 cm^{-1} .

The content of carbon, hydrogen, and nitrogen in the polymers was determined by elemental analysis using a LECO CHNS-932 instrument.

Thermogravimetry analysis (TGA) is based on the measurement of the weight loss of the material as a function of temperature, or isothermally as a function of time, in an atmosphere of nitrogen, helium, air, other gas, or in vacuum. TGA curve provides information concerning the thermal stability of the initial sample, intermediate compounds that may be formed and of the residue if any. In addition to thermal stability, the weight losses observed in TGA can be quantified to predict the pathway of degradation or to obtain compositional information. The ability to vary atmosphere during the TGA evaluation, particularly from an inert to a reactive gas, provides additional information about a material composition and its stability. The experimental data offer more sophisticated understanding of reactions occurring at materials heating. Thermal stabilities of the polymer electrolytes were examined by a Perkin Elmer STA 6000 Thermal Analyzer. The samples (~10 mg) were heated from room temperature to $750\text{ }^{\circ}\text{C}$ under N_2 atmosphere at a scanning rate of $10\text{ }^{\circ}\text{C}/\text{min}$.

DSC measures the temperatures and heat flow associated with transitions in materials as a function of time and temperature. It determines transition temperatures, melting and crystallization, and heat capacity. In heat flux instruments, the sample and reference are heated from the same source and the temperature difference is measured.

In amorphous polymers DSC shows the glass transition temperature (T_g) and presence of single T_g verifies the homogeneity of the polymer. DSC measurements were carried out on a Perkin Elmer Jade DSC under N_2 atmosphere and heating-cooling curves were recorded at a rate of $10\text{ }^\circ\text{C}/\text{min}$. The second heating curves were evaluated.

A scanning electron microscope (SEM) is a type of electron microscope that images a sample by scanning it with a beam of electrons in a raster scan pattern. The electrons interact with the atoms that make up the sample producing signals that contain information about the sample's surface topography, composition, and other properties such as electrical conductivity. For conventional imaging in the SEM, specimens must be electrically conductive, at least at the surface, and electrically grounded to prevent the accumulation of electrostatic charge at the surface. Nonconductive materials are therefore usually coated with an ultrathin coating of electrically conducting material (e.g. gold), deposited on the sample either by low-vacuum sputter coating or by high-vacuum evaporation. The morphology of the membranes was observed by scanning electron microscopy (SEM) type JEOL 7001 FESEM. The samples were previously coated with gold in a sputtering device.

Ion exchange capacity (IEC) of material can be expressed as the quantity of ions that can be taken up by a specific volume of the material. This would be expressed in quantity-per-unit volume, such as kilograms per cubic foot (Kg/ft^3) or milli-equivalents per milliliter (meq/mL), which also equals equivalents per liter (eq/L). IEC of proton conductive polymers was determined by volumetric titration. The samples were immersed and stirred in 20 mL of 0.10 M NaOH/1.0 M NaCl mixed aqueous solution (1/4 by volume) for 24 h at room temperature. Subsequently, 10 mL of 0.10 N HCl solution was added, and the excess amount of HCl was back titrated with 0.025 N NaOH aqueous solution in the presence of phenolphthalein indicator. The IEC value (mmol/g) of the samples was calculated using Eq. 2.1.

$$\text{IEC} = 0.025 \times (V_{\text{NaOH}} - V_{\text{B}}) / W_{\text{dry}} \quad (2.1)$$

where V_{NaOH} is volume of 0.025 N NaOH aqueous solutions for the volumetric titration, V_{B} is volume of the NaOH aqueous solution for blank titration (same procedure without sample), and W_{dry} is dry weight of the samples.

The proton conductivity studies of the samples were performed using a Novocontrol dielectric-impedance analyzer. The films were sandwiched between platinum blocking electrodes and the conductivities were measured in the frequency range 1 Hz-3 MHz at 10 °C intervals. The temperature was controlled with a Novocontrol cryosystem using liquid nitrogen, which is applicable between -150 and 250 °C.

The frequency-dependent AC conductivities, $\sigma_{ac}(\omega)$, of the polymer blends were calculated using Eq 2.2:

$$\sigma'(\omega) = \sigma_{ac}(\omega) = \epsilon''(\omega) \omega \epsilon_0 \quad (2.2)$$

Where $\sigma'(\omega)$ is the real part of conductivity, $\omega = 2\pi f$ is the angular frequency, ϵ_0 is the vacuum permittivity ($\epsilon_0 = 8.852 \times 10^{-14}$ F/cm), and ϵ'' is the imaginary part of complex dielectric permittivity (ϵ^*).

Cyclic voltammograms were obtained with a potentiostat CHI instrument Model 842B. Voltammograms of the samples were recorded in a three electrode CV system, using a polymer electrolyte modified Pt working electrode and a Pt counter electrode. The reference electrode was silver/silver chloride (Ag/AgCl) calibrated by a ferrocene/ferricinium redox system. Cyclic voltammetry studies were carried out in 0.1 M tetraethylammonium tetrafluoroborate (TBATFB)/acetonitrile.

CHAPTER 3

RESULTS AND DISCUSSION

3.1 TRIAZOLE FUNCTIONAL SILANE NETWORKS

3.1.1 FTIR studies

The FT-IR spectra of pure and doped azole functional samples are shown in Fig. 3.1 and 3.2. PGPTMS has epoxy peak at 906 cm^{-1} and it disappears when azole groups were tethered to GPTMS which verifies the ring opening reaction. For all the samples there is a double band between 1000-1100 region due to Si-O-Si groups (Guo et al., 2006). Si-Tri has peaks at 1514 and 1450 cm^{-1} due to triazole ring stretching (Krishnakumar and Xavier, 2004). After doping Si-Tri, the intensity of the peaks between $1450\text{-}1570\text{ cm}^{-1}$ changes which may be due to protonation of triazole rings. The strong bands formed at 1221 and 1160 cm^{-1} are attributed to SO_2 and a strong absorption peak at 1024 cm^{-1} most probably belongs to $-\text{SO}_3^-\text{[H}^+]$ (Bozkurt, 2005). In addition to these peaks Si-ATri samples also show a N-H bending vibration at 1635 cm^{-1} . For all the samples the aliphatic C-H stretchings were observed at $2850\text{-}2950\text{ cm}^{-1}$. After doping of the polymers the formation of a new peak around 3100 cm^{-1} indicates the protonation of the triazole rings and band broadening between $3500\text{-}2600\text{ cm}^{-1}$ proves hydrogen bond network formation (Günday et al., 2006).

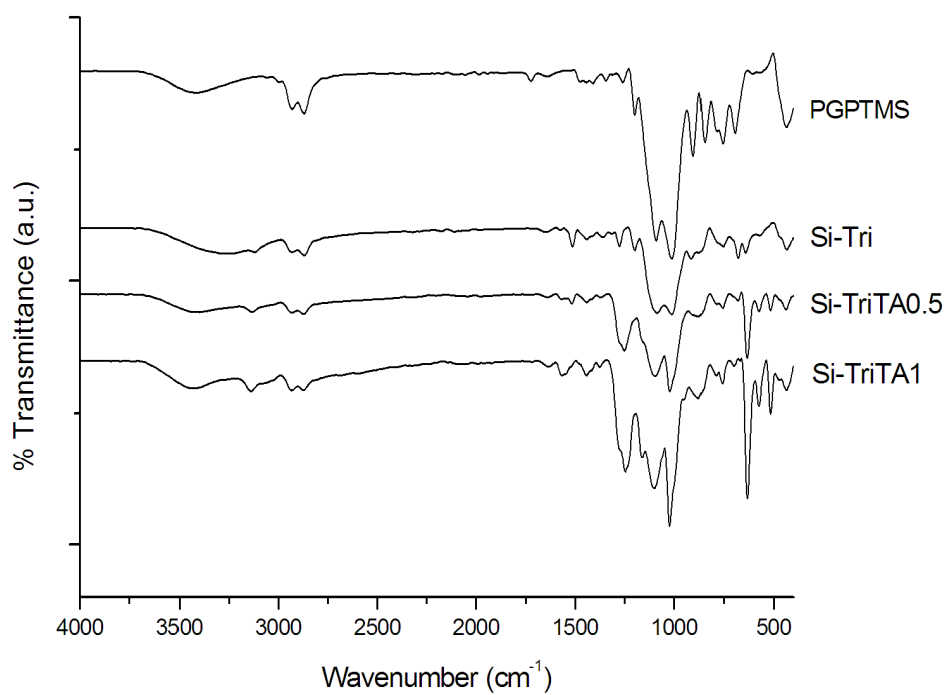


Figure 3.1. FT-IR spectra of PGPTMS and triazole functional materials.

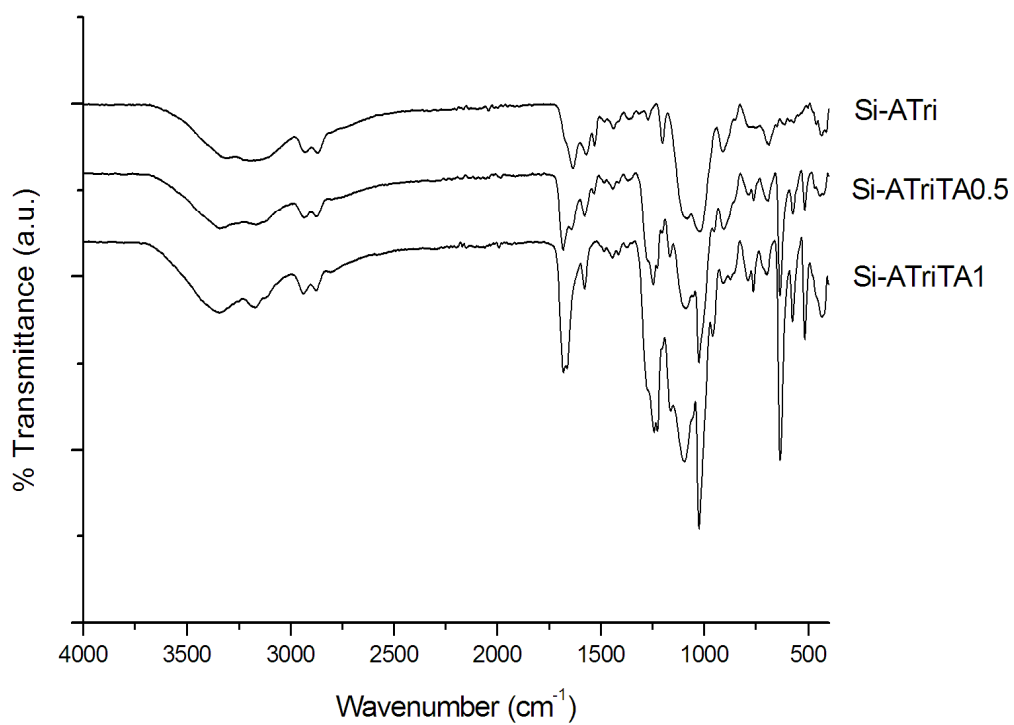


Figure 3.2. FT-IR spectra of aminotriazole functional materials.

3.1.2 Thermal analysis

The thermal stability of pure and doped Tri and ATri functional samples were studied by thermogravimetric analysis (TGA) and depicted in Fig. 3.3 and 3.4. Sol-gel derived polymer of pure GPTMS was thermally stable up to 300 °C. Triazole functional samples Si-Tri, Si-TriTA0.5 and Si-TriTA1 are thermally stable up to 250 °C. For aminotriazole functional samples the thermal stability decreased to 200 °C. For all the samples the major degradation occurs in single step up to 500 °C and acid doping has little effect on the thermal stability of the materials.

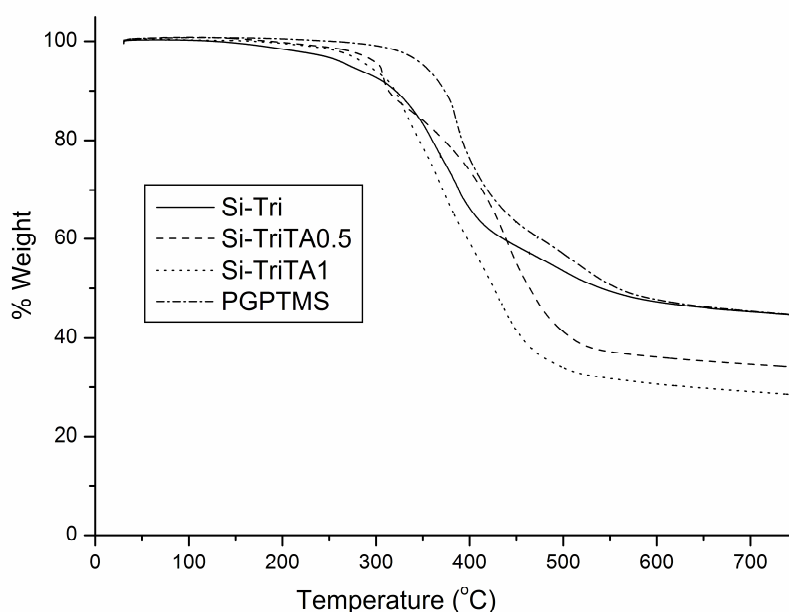


Figure 3.3. TG thermograms of triazole functional materials recorded at a heating rate of 10 °C/min under a nitrogen atmosphere.

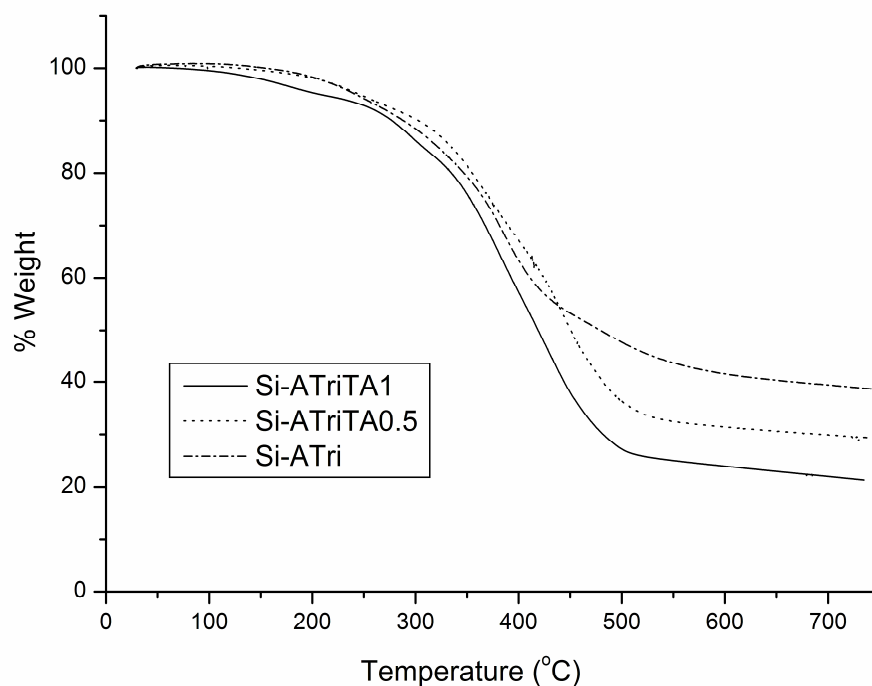


Figure 3.4. TG thermograms of aminotriazole functional materials recorded at a heating rate of 10 °C/min under a nitrogen atmosphere.

Fig. 3.5 and 3.6 show the DSC curves of pure and doped Tri and ATri functional samples under inert atmosphere at a scan rate of 10 °C/min. The second curves were evaluated. The melting points of pure Tri and ATri compounds are 120 and 157 °C, respectively. The T_g of PGPTMS is around 30 °C. As seen in the figures T_g points decreased with modification of PGPTMS with azole units. The T_g points of the polymer electrolytes are 4 °C for Si-Tri, 9 °C for Si-TriTA0.5, 7 °C for Si-TriTA1, 21 °C for Si-ATri, 13 °C for Si-ATriTA0.5 and 3 °C for Si-ATriTA1. Although the T_g points are close to each other it can be said that the T_g points slightly shifts to lower temperatures as the doping ratio increases due to softening effect of the dopant acid.

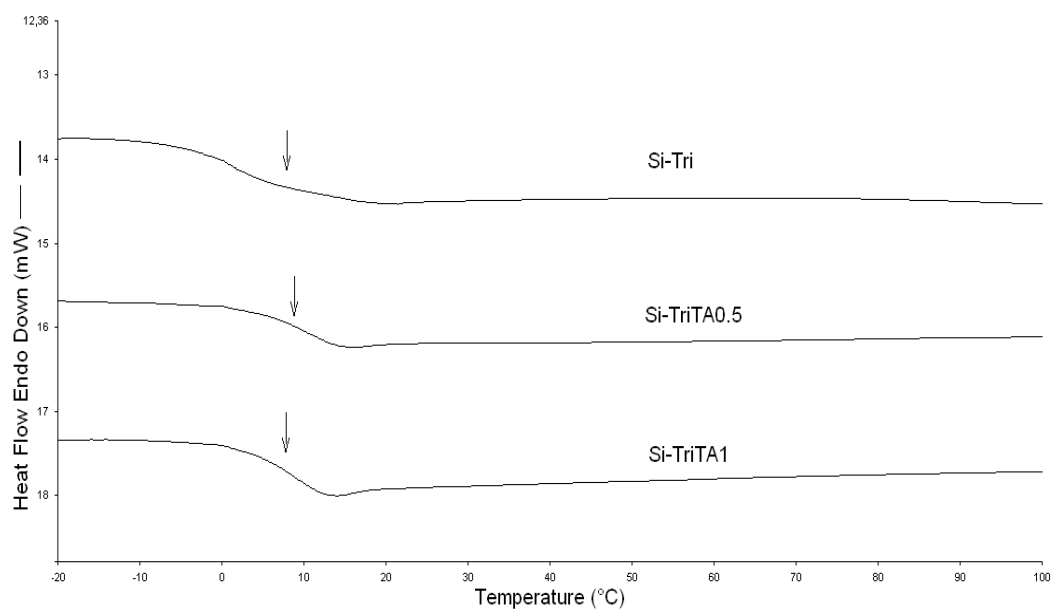


Figure 3.5. DSC traces of triazole functional materials recorded at a heating rate of 10 °C/min under a nitrogen atmosphere.

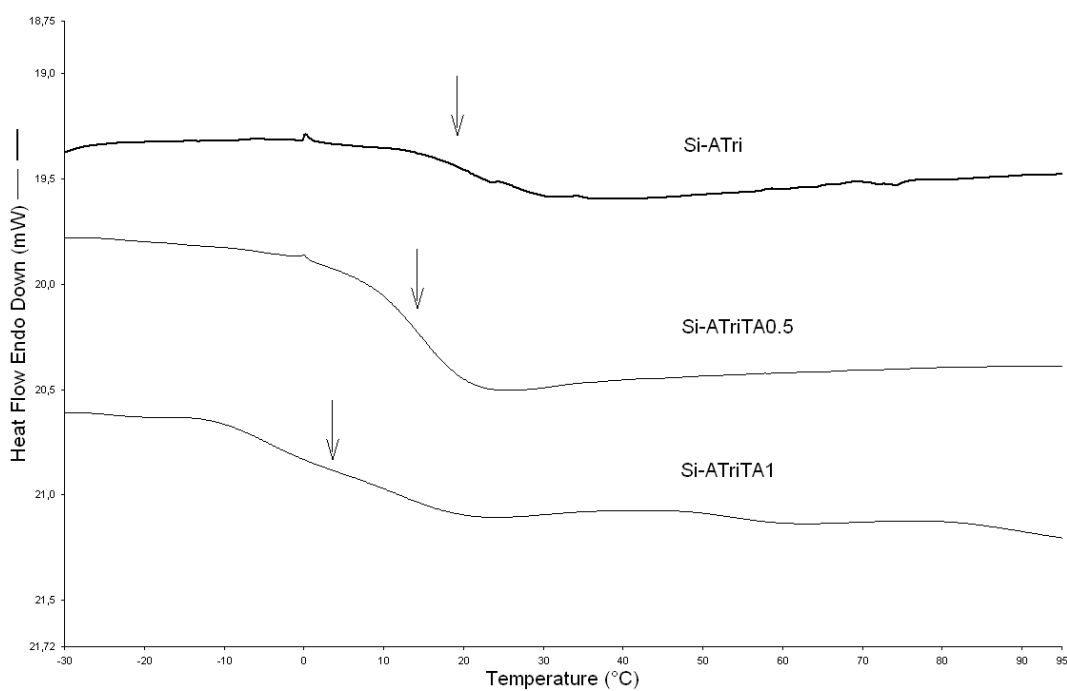


Figure 3.6. DSC traces of aminotriazole functional materials recorded at a heating rate of 10 °C/min under a nitrogen atmosphere.

3.1.3 Morphology

The morphology of the samples was analyzed with Scanning Electron Microscopy and depicted in Fig. 3.7. For all the samples the images exhibit single phase formation and the membranes seem homogeneous. There is no difference between the images of the doped sample and pure sample. This shows that the dopant acid uniformly distributed into the polysiloxane matrix and there is no agglomeration or phase separation at micrometer scale level.

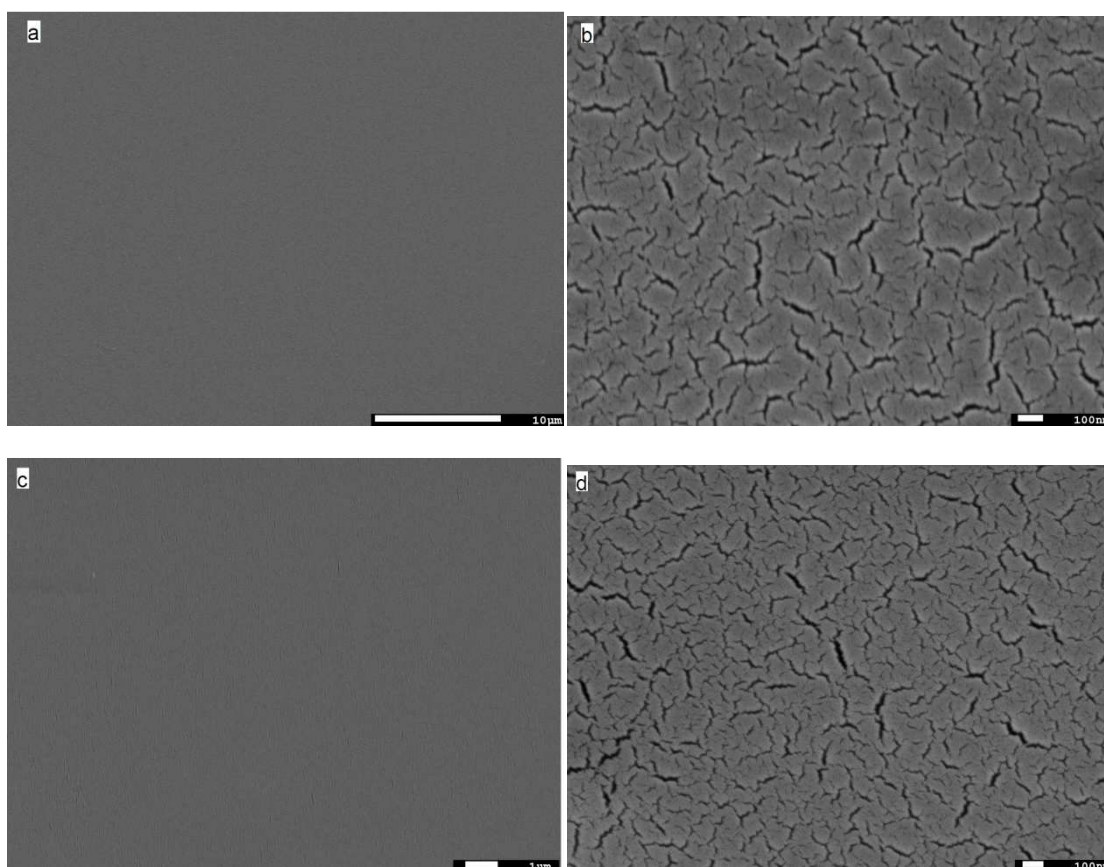


Figure 3.7. Scanning Electron Microscopy (SEM) images of (a-b) SiTri and (c-d) SiTriTA0.5.

3.1.4 Proton conductivity

Fig. 3.8 and Fig. 3.9 show the AC conductivity of the samples versus frequency at several temperatures. The σ_{ac} versus frequency curves change with the frequency where in the low frequency region, the reduction in the conductivity is due to polarization of the blocking electrodes. The proton conductivity increases as temperature increases.

The DC conductivity (σ_{dc}) of the samples was derived from the plateaus of $\log \sigma_{ac}$ versus $\log F$ by linear fitting of the data.

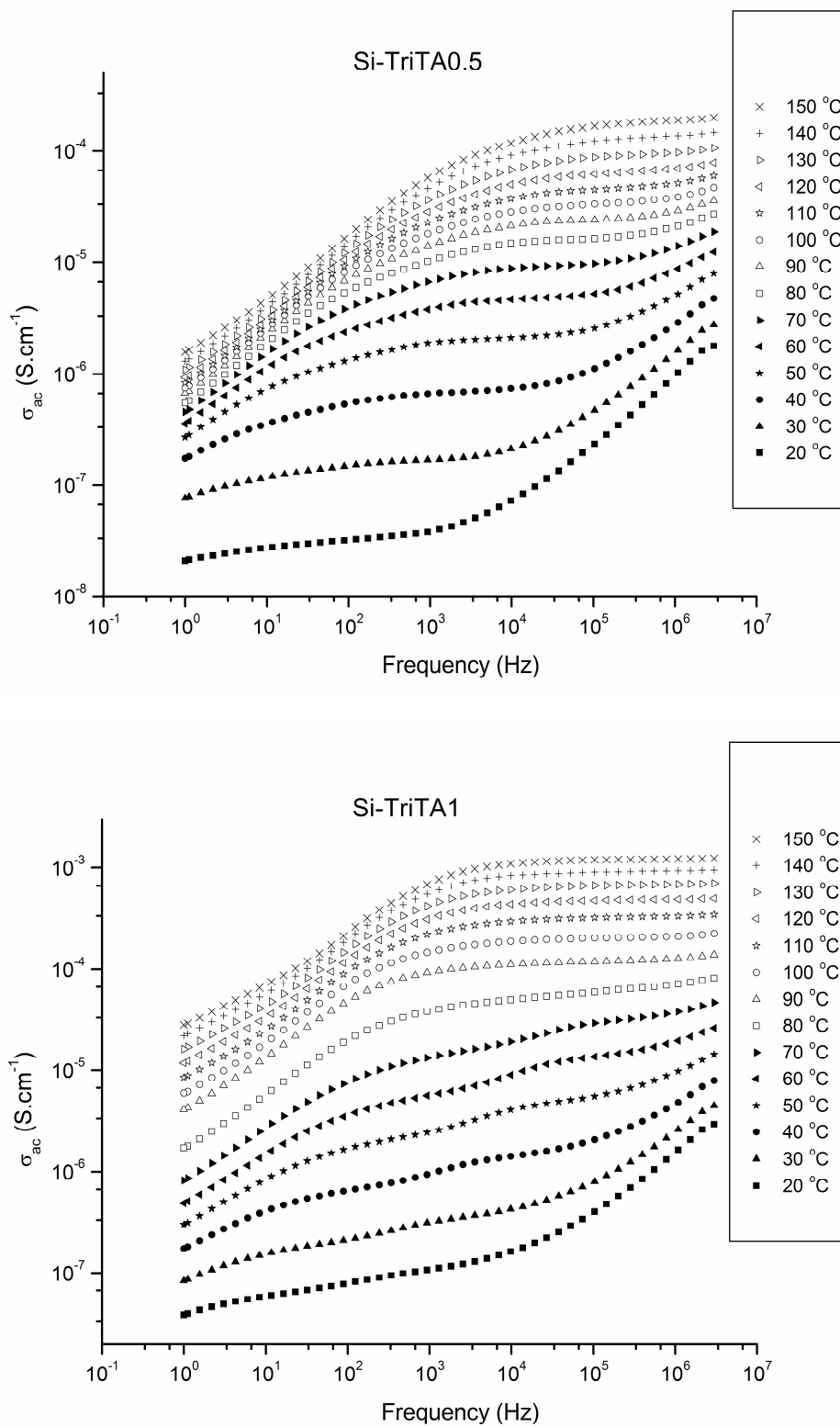


Figure 3.8. The σ_{ac} vs. frequency (Hz) for Si-TriTA0.5 and Si-TriTA1 at various temperatures.

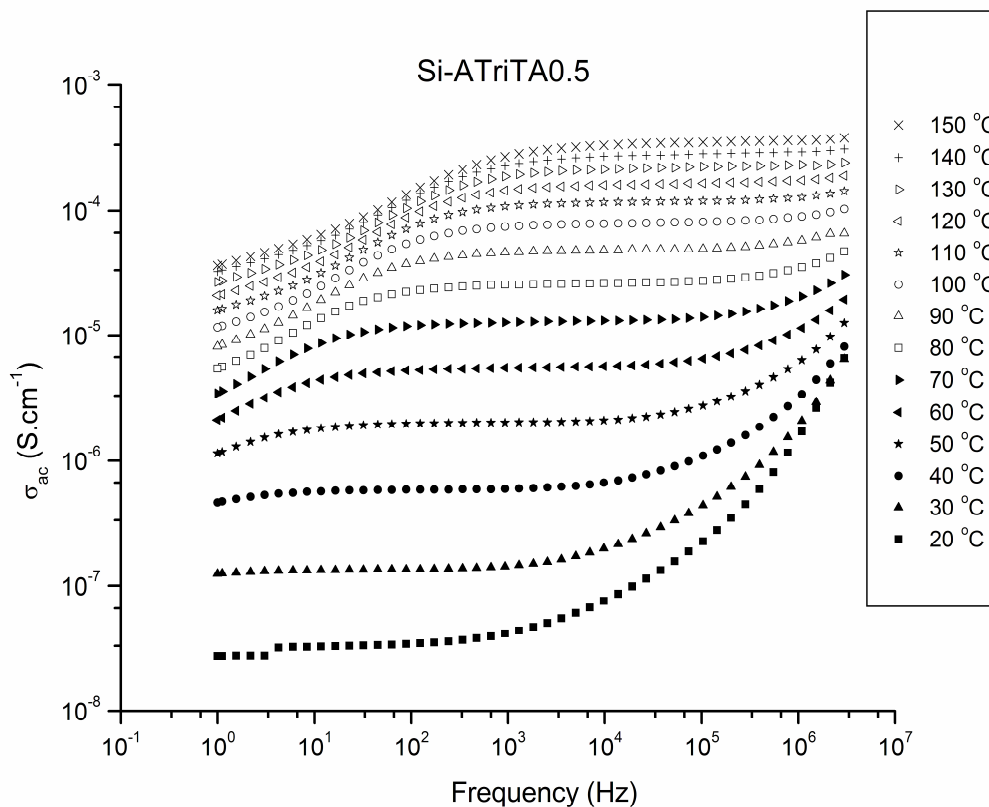


Figure 3.9. The σ_{ac} vs. frequency (Hz) for Si-ATriTA0.5 at various temperatures.

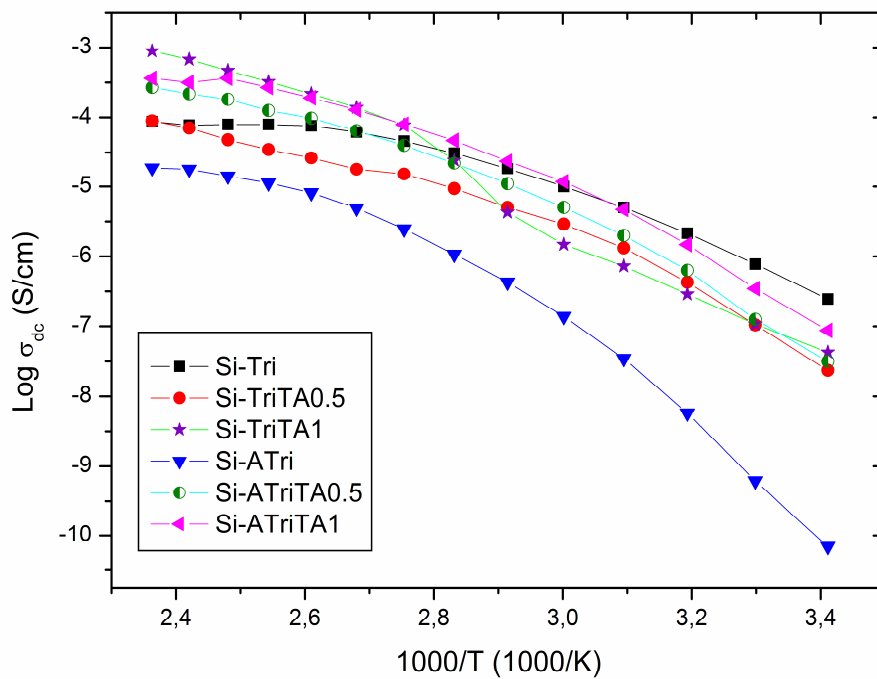


Figure 3.10. DC conductivities of pure and doped samples as a function of reciprocal temperature.

The DC conductivities of the samples were compared in Fig. 3.10. The conductivity isotherm illustrates that the DC conductivity strongly depends on the temperature and the doping ratio, x . The proton conductivity in this system is carried out by protons of the acid and azole compounds. Pure triazole functional samples (Si-Tri and Si-ATri) show high proton conductivity which confirms the high contribution of azole units in the transport mechanism. Although Si-Tri has higher proton conductivity than Si-ATri, there is no much difference for the doped samples. Temperature dependence of the conductivity in polymer electrolytes has often been taken as indicative of a particular type of conduction mechanism. A marked curvature is observed for all samples and the curves are interpreted with the Vogel–Tamman–Fulcher (VTF) equation (Eq. 3.1);

$$\log \sigma = \log \sigma_0 - E_v/[k(T-T_0)] \quad (3.1)$$

where σ_0 (S/cm) is the conductivity at infinite temperature, E_v is the Vogel activation energy (eV) and T_0 is the Vogel temperature which is the start of the segmental relaxations ($^{\circ}\text{C}$) (Table 3.1).

Table 3.1. T_g values, maximum proton conductivities and VTF parameters of the membranes.

Sample	T_g ($^{\circ}\text{C}$)	Max. Proton Conductivity (S/cm) (at 150 $^{\circ}\text{C}$)	T_0 ($^{\circ}\text{C}$)	$\text{Log}\sigma_0$	E_a (eV)
Si-Tri	4	8.7×10^{-5}	-30	-2.0	36
Si-TriTA0.5	9	8.9×10^{-5}	-40	-2.4	62
Si-TriTA1	7	8.9×10^{-4}	---	---	---
Si-ATri	21	1.8×10^{-5}	-53	-0.8	136
Si-ATriTA0.5	13	2.7×10^{-4}	-49	-1.3	86
Si-ATriTA1	3	3.6×10^{-4}	-43	-1.4	72

In anhydrous systems proton transfer is provided by two different mechanisms. The first is the structural diffusion (Grotthuss mechanism) in which the conductivity is mainly controlled by proton transport through ionized acidic groups, i.e. SO_3^- and the azole ring (Grotthuss mechanism). The second is the vehicle mechanism where the

protons travel through the material on a neutral or charged “vehicle” (Dippel et al., 1993).

Triflic acid (TA) is a strong acid with a conductivity of $\sim 10^{-5}$ S/cm at room temperature (Russell and Senior, 1980). Proton transfer of triflic acid to different azole derivatives was previously reported (Subbaraman et al., 2009) and the study indicated the effect of pKa of the azole molecules on proton conductivity of azole-TA systems. However later studies showed that proton conductivity of the azole immobilized systems depends mostly on the acid ratio and the segmental motions rather than the pKa values (Granados-Focil et al., 2007).

In the current system, the presence of SO_3^- anions implies that the proton diffusion occurs mainly by Grotthuss mechanism. It seems that the proton hopping from one N–H site to a free nitrogen contributes to the conductivity of the triazole functional systems as in the case of imidazole where the long range proton transfer occurs throughout the protonic defects, i.e., protons transport between protonated and unprotonated heterocyclic units (Kreuer et al., 1998). In addition, proton hopping from one N–H site to sulfate ions may also contribute to the conductivity. The presence of curvatures in Fig. 3.10 indicates the contribution of segmental motions on proton conductivity. Low T_g of the materials also verifies this contribution.

In this study, triazole compounds were immobilized into a silane structure and after doping with $\text{CF}_3\text{SO}_3\text{H}$, sol-gel method was used for the formation of a silane network. The preparation is simple and the matrix contains both an azole unit attached to a flexible side group and acid units interacting with the azole. In that system, the maximum proton conductivity was measured for Si-TriTA1 as 8.9×10^{-4} S/cm at 150 °C in the anhydrous state.

3.2 TETRAZOLE FUNCTIONAL SILANE NETWORKS

3.2.1 FTIR studies

The FT-IR spectra of pure ATet, GPTMS, Si-ATet and the doped samples are shown in Fig. 3.11. GPTMS has epoxide peak at 910 cm^{-1} and it disappears when ATet was tethered to CPTMS which verifies the ring opening reaction. The characteristic ring

stretchings of 5-aminotetrazole were observed at 1295, 1450 and 1640 cm^{-1} (Levchik et al., 1992). For Si-ATet there is a double band between 1000-1100 region due to Si-O-Si groups (Guo, 2006). For doped matrices the strong bands formed at 1230 and 1160 cm^{-1} are attributed to SO_2 and a strong absorption peak at 1016 cm^{-1} most probably belongs to $-\text{SO}_3^-[\text{H}^+]$ (Bozkurt, 2005). For all the samples the aliphatic C-H stretchings were observed at 2850-2950 cm^{-1} . After doping of the polymers the formation of a new peak around 3100 cm^{-1} indicates the protonation of the tetrazole rings and band broadening between 3500-2600 cm^{-1} proves hydrogen bond network formation (Günday et al., 2006).

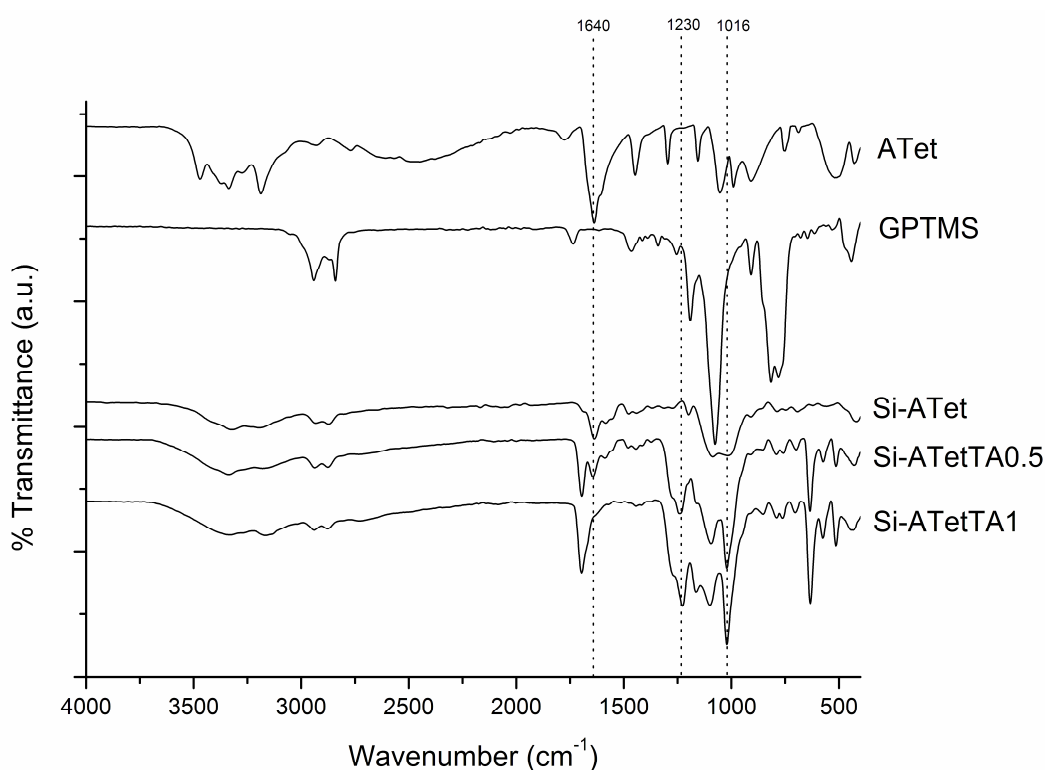


Figure 3.11. FT-IR spectra of pure ATet, GPTMS and the polymer electrolytes.

3.2.2 Thermal analysis

The thermal stability of pure and doped samples were studied by thermogravimetric analysis (TGA) and depicted in Fig. 3.12. ATet is reported to be thermally stable up to 200 °C (Lesnikovich et al., 2002). Si-ATet is thermally stable up to 200 °C and the degradation temperature shifts to lower values as the doping ratio increases. The weight loss between 150-250 °C may be attributed to condensation of C-

OH, Si-OH and sulfonic acid groups. All the samples can be said to be thermally stable up to 180 °C.

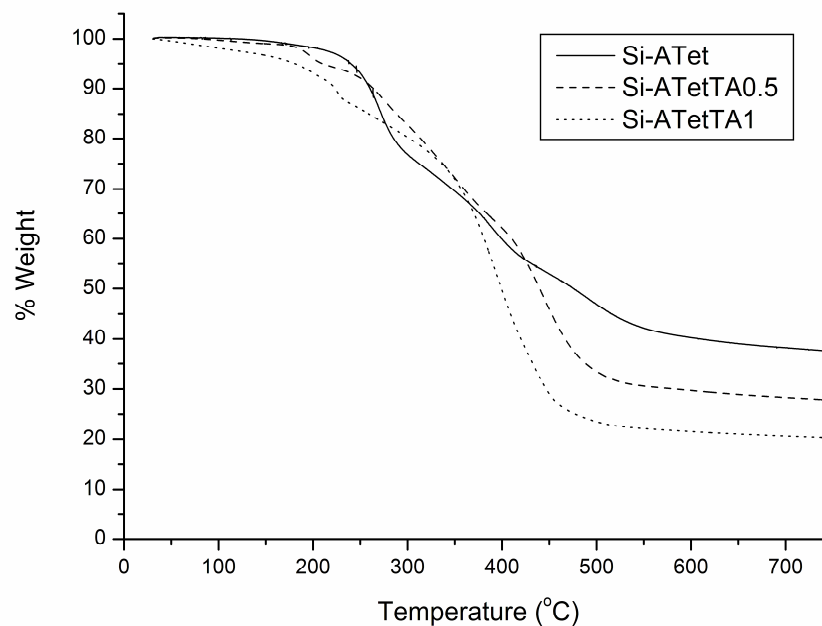


Figure 3.12. TG thermograms of the polymer electrolytes recorded at a heating rate of 10 °C/min under a nitrogen atmosphere.

Fig. 3.13 shows the DSC curves of pure and doped samples under inert atmosphere at a scan rate of 10 °C/min. The second heating curves were evaluated. The melting point of pure ATet is 203 °C. As seen in the Fig. 3.13 the Tg points of the polymer electrolytes are 25 °C for Si-ATet, 10 °C for Si-ATetTA0.5 and 6 °C for Si-ATetTA1. Although the Tg points are close to each other it can be said that the Tg points shifts to lower temperatures as the doping ratio increases due to softening effect of the dopant acid. The presence of single Tg confirms the homogeneity of the materials.

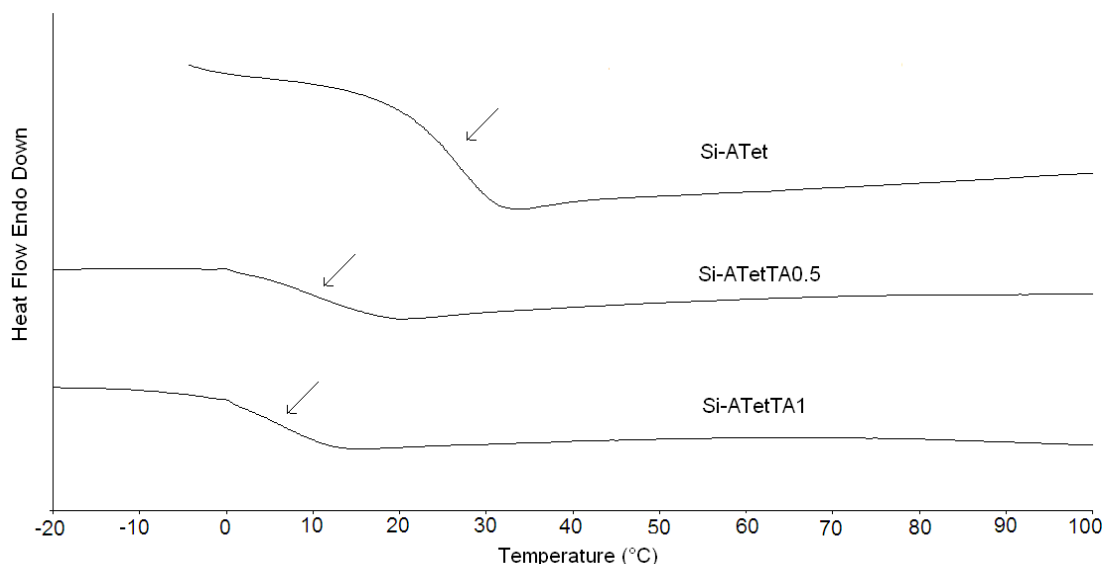
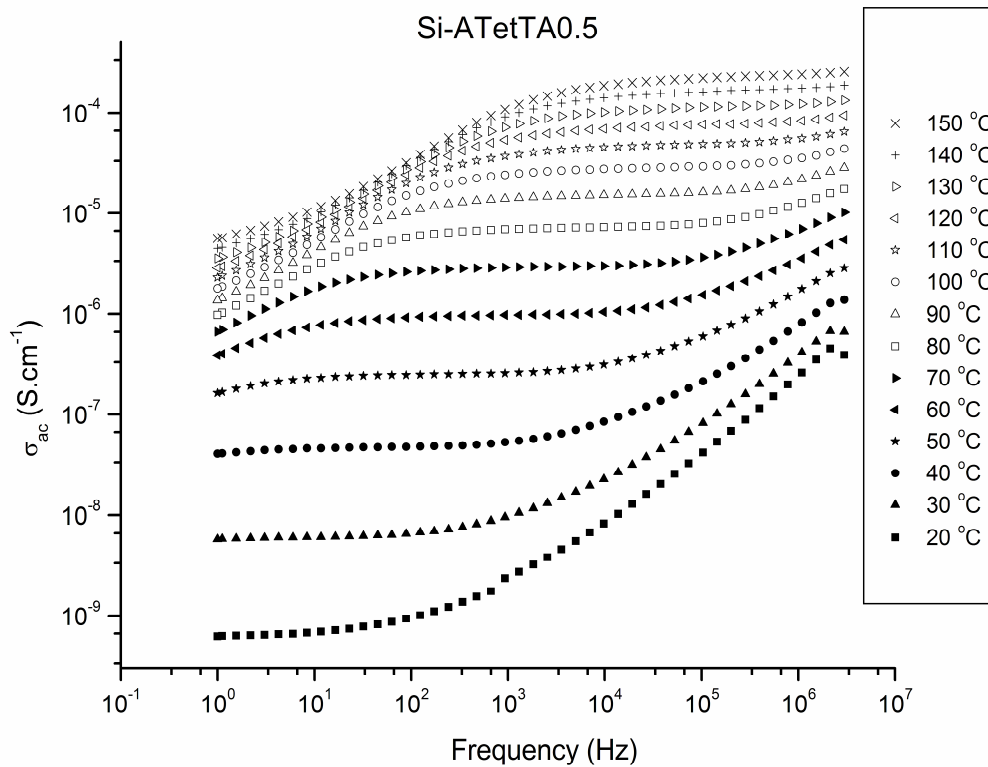
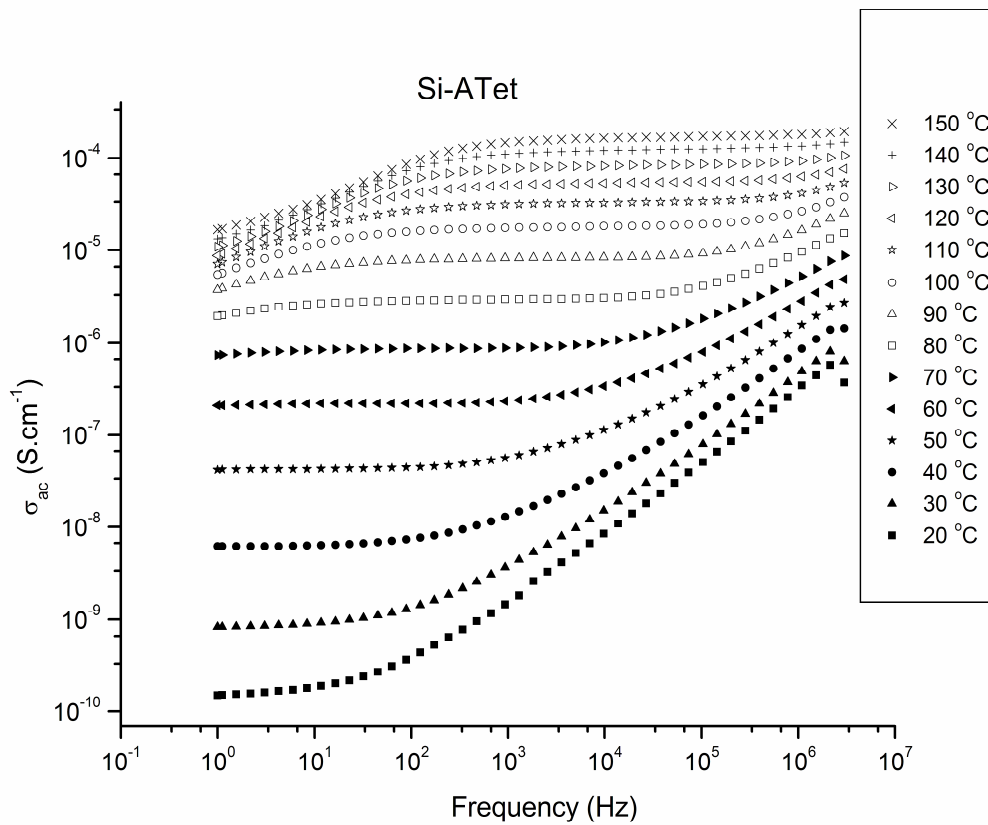


Figure 3.13. DSC traces of the polymer electrolytes recorded at a heating rate of 10 °C/min under a nitrogen atmosphere.

3.2.3 Proton conductivity

Fig. 3.14 shows the AC conductivity of the samples versus frequency at several temperatures. The σ_{ac} versus frequency curves change with the frequency where in the low frequency region, the reduction in the conductivity is due to polarization of the blocking electrodes. The conductivity increase at low temperature and high frequencies results from the regular dispersion in polymer electrolytes. The proton conductivity increases as temperature increases.

The DC conductivity (σ_{dc}) of the samples was derived from the plateaus of $\log \sigma_{ac}$ versus $\log F$ by linear fitting of the data. The DC conductivities of the samples were compared in Fig. 3.15. The conductivity isotherm illustrates that the DC conductivity strongly depends on the temperature and the doping ratio, x . The proton conductivity in this system is carried out by protons of the acid and azole compounds. Pure tetrazole functional sample (Si-ATet) shows high proton conductivity which confirms the high contribution of azole units in the transport mechanism. Temperature dependence of the conductivity in polymer electrolytes has often been taken as indicative of a particular type of conduction mechanism. A marked curvature is observed for all samples the curves are interpreted with the Vogel–Tamman–Fulcher (VTF) equation (Eq. 3.1) (Table 3.2).



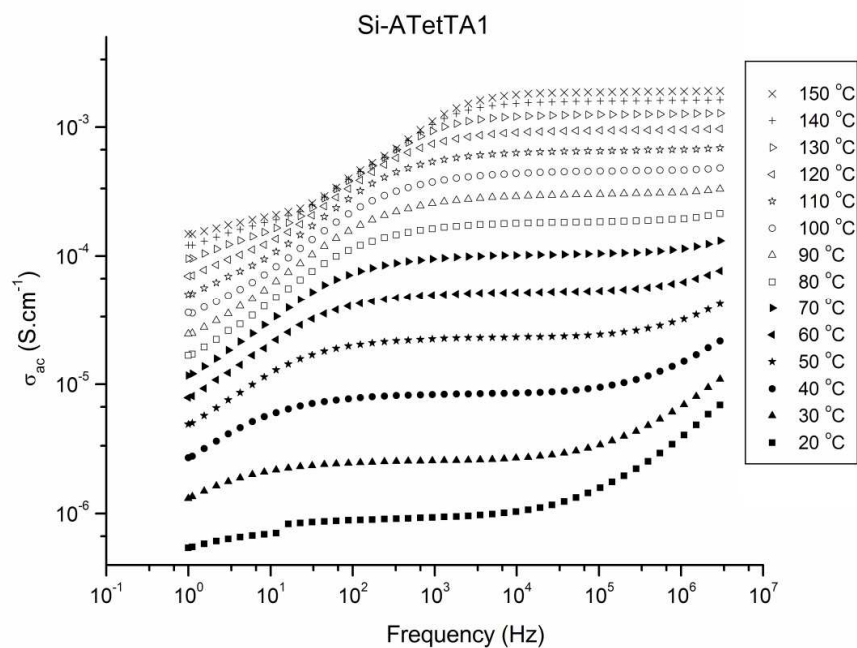


Figure 3.14. The σ_{ac} vs. frequency (Hz) for Si-ATet, Si-ATetTA0.5 and Si-ATetTA1 at various temperatures.

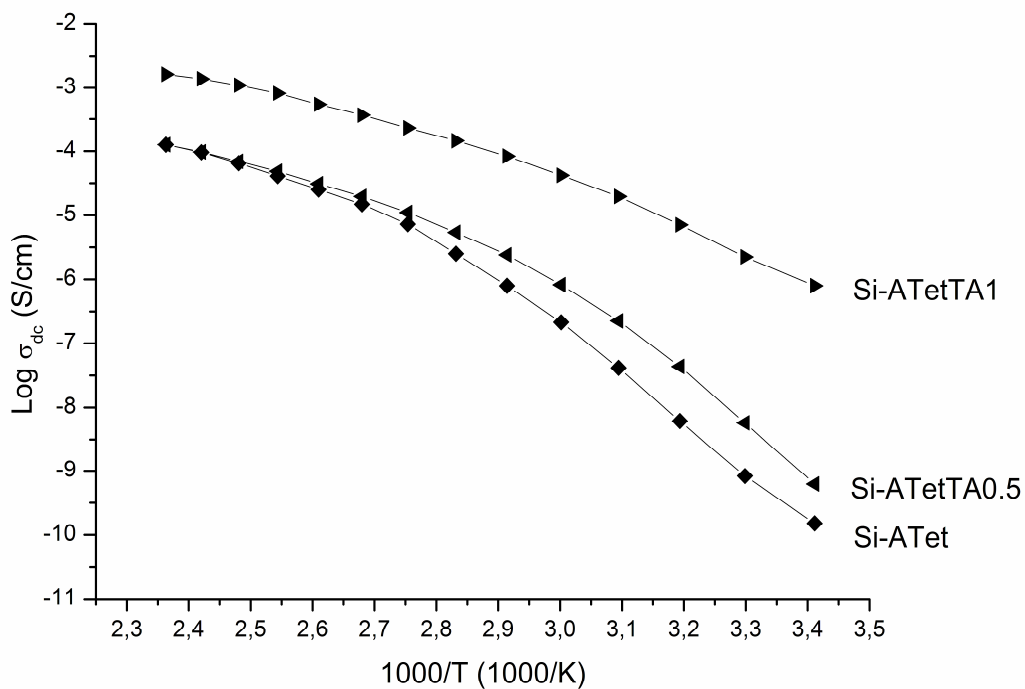


Figure 3.15. DC conductivities of pure and doped samples as a function of reciprocal temperature.

Table 3.2. Maximum proton conductivity, T_g and VTF parameters of the samples.

Sample	Max. Proton Cond. (S/cm) at 150 °C	Log σ_0 (S/cm)	T_g (°C)	T_o (°C)	E_v (eV)
Si-ATet	1.70×10^{-4}	-0.60	25	-46	0.126
Si-ATetTA0.5	2.00×10^{-4}	-1.35	10	-40	0.094
Si-ATetTA1	1.87×10^{-3}	0.32	6	-72	0.106

In this study, 5-aminotetrazole was immobilized into a silane structure and after doping with CF_3SO_3H , sol-gel method was used for the formation of a silane network. The preparation is simple and the matrix contains both an azole unit attached to a flexible side group and acid units interacting with the azole. In that system, the maximum proton conductivity was measured for Si-ATetTA1 as 0.0018 S/cm at 150 °C in the anhydrous state.

3.3 COPOLYMERS BASED ON 4-VINYL BENZENE BORONIC ACID AND 1-VINYL-1,2,4-TRIAZOLE

Copolymerizations of VBBA and VTri were conducted at several molar feed ratios and compositions of the copolymers are analyzed by elemental analysis (Table 3.3). The mol ratio (VBBA:VTri: 1:0.5, 1:1; 1:2) of the copolymers is calculated using the nitrogen contents. The results demonstrated that copolymer compositions are close to the monomer feed ratios as expected from 100 % conversion.

Table 3.3. Composition of poly(vinyl benzene boronic acid-co-vinyl triazole) copolymers.

Sample	Feed mol ratio, (VBBA:VTri)	Elemental Analysis			Copolymer mol ratio,(VBBA:VTri)
		C (%)	H (%)	N (%)	
P(VBBA-co-VTri) 1:0.5	1:0.5	58.93	6.06	10.13	1:0.46
P(VBBA-co-VTri) 1:1	1:1	56.91	5.81	15.34	1:0.83
P(VBBA-co-VTri) 1:2	1:2	54.45	5.62	22.47	1:1.61

3.3.1 FT-IR study

The FT-IR spectra of copolymers are shown in Fig. 3.16. The OH stretching of $-B(OH)_2$ group gives a broad peak at around 3390 cm^{-1} . The aromatic CH stretching is observed at 3080 cm^{-1} and the absorption bands at 2950 and 2870 cm^{-1} are attributed to the symmetric and asymmetric stretching vibration of aliphatic CH units. The OH deformation of $-B(OH)_2$ group is located at 1008 cm^{-1} (Kahraman et al., 2004). The peaks at 1564 and 1461 cm^{-1} are assigned to triazole ring C=N and C-N stretchings, respectively (Krishnakumar and Xavier, 2004). As seen in the figure the intensity of the peaks related to triazole ring increases as the ratio of VTri unit increases in the copolymers. After doping with H_3PO_4 , characteristic P-OH, P=O, and P-O $^-$ absorptions appear at $1200\text{--}950\text{ cm}^{-1}$ (Fig. 3.17). The broad peak about 3100 cm^{-1} may be attributed to N-H bond due to protonation of the triazole ring with phosphoric acid.

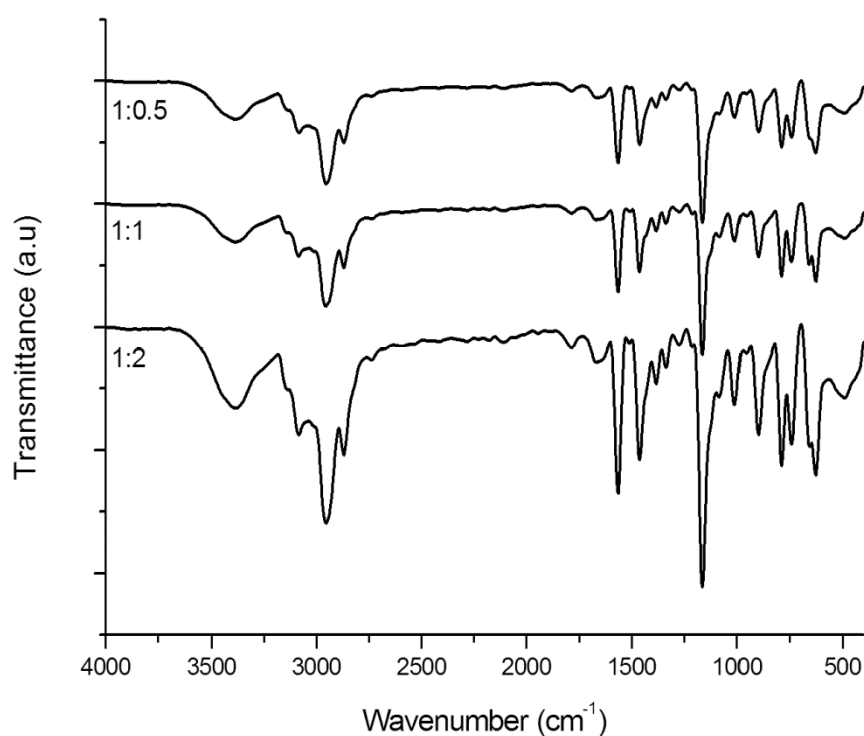


Figure 3.16. FT-IR spectra of P(VBBA-co-VTri) copolymers.

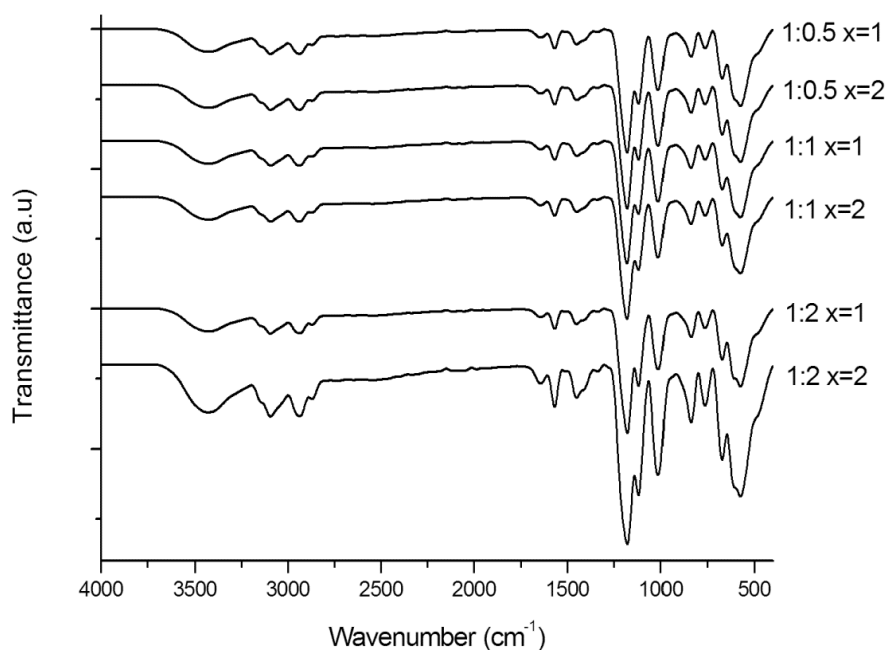


Figure 3.17. FT-IR spectra of H_3PO_4 doped P(VBBA-co-VTri) copolymers.

3.3.2 Thermal Analysis

The thermal properties of the copolymers were investigated with TGA and DSC. Pure PVTri was reported to be thermally stable up to 350 °C (Celik et al, 2008a). Fig. 3.18 shows the TGA curves of the copolymers and the doped samples. The little weight loss up to 100 °C may be attributed to absorbed humidity. There is a 15% weight loss between 100-200 °C due to condensation of boronic acid groups in VBBA units. The major degradation occurs after 350 °C. As the mol ratio of VTri increases in copolymers the thermal stability also increases. When the copolymers were doped with phosphoric acid thermal stability decreases a little, but both pure copolymers and the doped membranes can be said to be thermally stable up to at least 150 °C. For all samples there is a little decomposition up to 200 °C and then the major decomposition occurs above 350 °C.

The glass transition temperatures of the copolymers were investigated with DSC. The T_g of pure PVTri was reported as 165 °C (Celik et al, 2008a), however in these copolymers no T_g was observed in the measurement range of -50 to 250 °C.

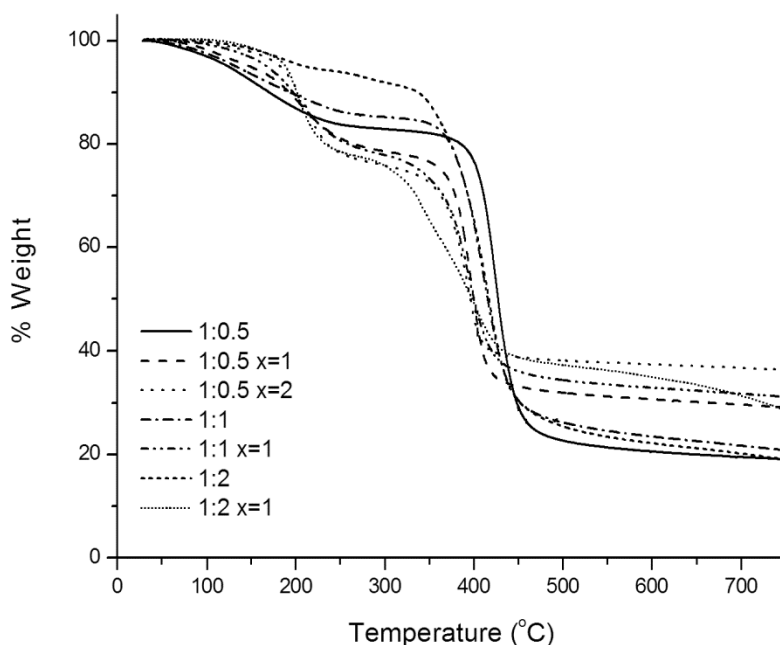


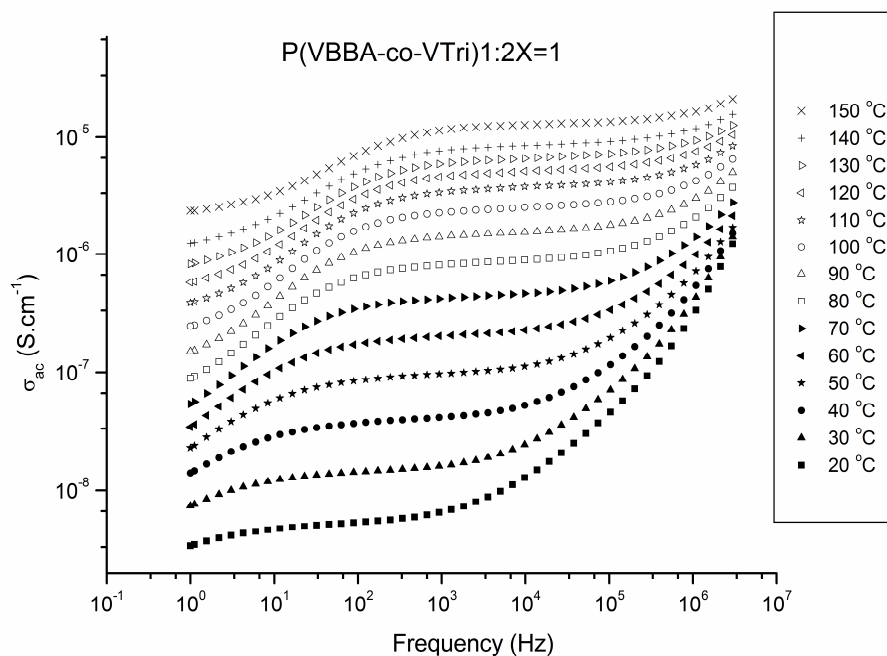
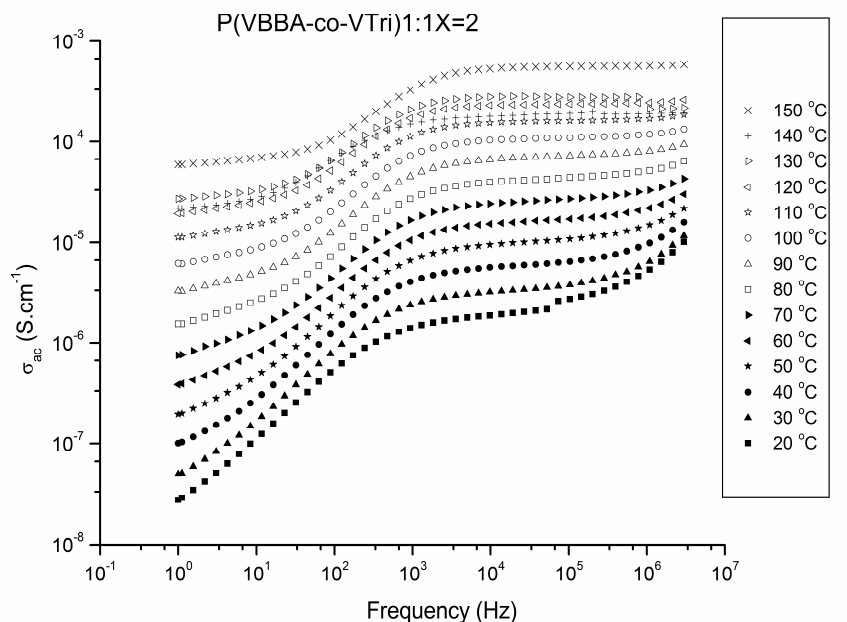
Figure 3.18. TG thermograms of pure and H_3PO_4 doped P(VBBA-co-VTri) copolymers at a heating rate of $10\text{ }^\circ\text{C}/\text{min}$ in inert atmosphere.

3.3.3 Conductivity Measurement

Fig. 3.19 shows the AC conductivity of the samples versus frequency at several temperatures. The σ_{ac} versus frequency curves change with the frequency where in the low frequency region, the reduction in the conductivity is due to polarization of the blocking electrodes. The conductivity increase at low temperature and high frequencies results from the regular dispersion in polymer electrolytes. The proton conductivity increases as temperature increases.

The DC conductivity (σ_{dc}) of the samples was derived from the plateaus of $\log \sigma_{ac}$ versus $\log F$ by linear fitting of the data. The DC conductivities of the samples were compared in Fig. 3.20. The conductivity isotherm illustrates that the DC conductivity strongly depends on the temperature and the doping ratio, x . The proton conductivity in this system is carried out by protons of the acid and triazole compounds. Pure copolymers have low proton conductivity since there is no proton defect formation and continuous path for conduction. After doping the copolymers triazole groups were

protonated and the proton conductivity occurs between protonated triazole and phosphoric acid units via Grotthuss mechanism. Maximum proton conductivity was obtained for the sample P(VBBA-co-VTri)1:2X=3 as 6×10^{-3} S/cm at 120 °C in anhydrous state.



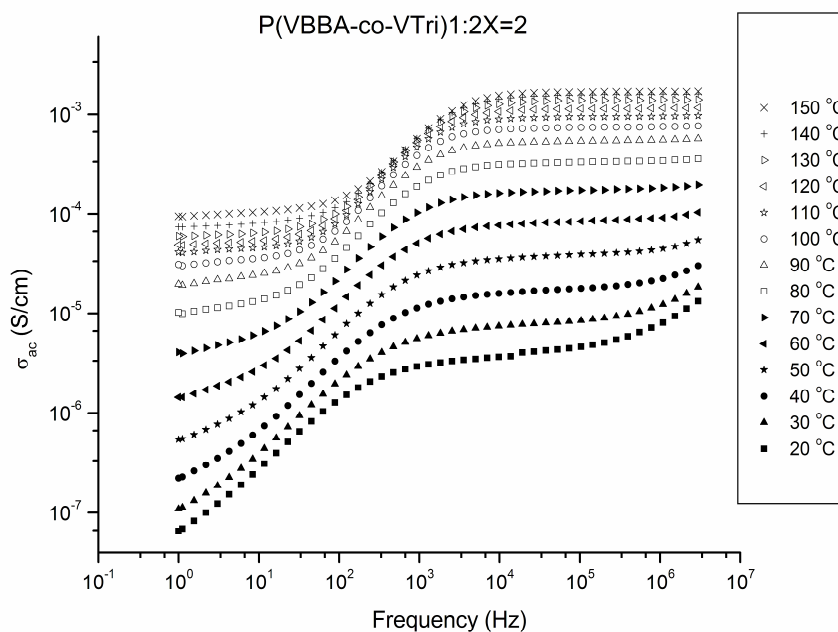


Figure 3.19. AC conductivity versus frequency of the membranes at several temperatures.

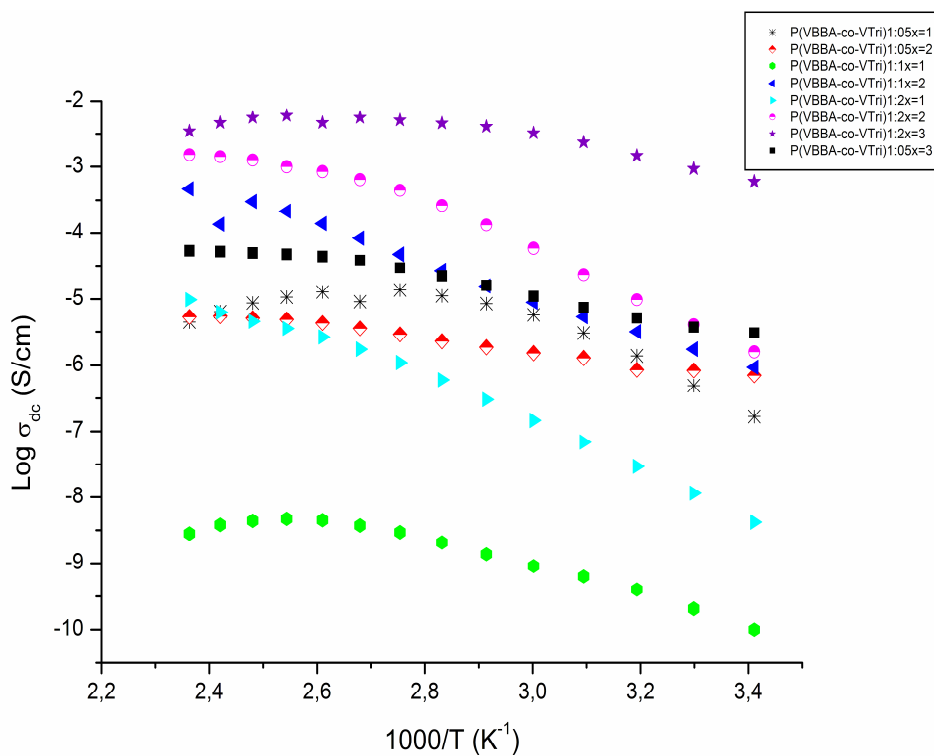


Figure 3.20. Variation of the proton conductivity of H_3PO_4 doped P(VBBA-co-VTri) copolymers as a function of reciprocal temperature.

3.3.4 Cyclic Voltammetry

Cyclic voltammogram of P(VBBA-co-VTri)1:1x=2 was given in Fig. 3.21. The measurement was performed in a typical three electrode cell containing 0.1 mol dm^{-3} CH_3CN solution of tetrabutylammonium hexafluorophosphate (TBAPF6) using a platinum work electrode, a platinum auxiliary electrode, and an Ag/Ag⁺ reference electrode. The figure shows that the CV of the copolymer comprises no peak within in the anodic and cathodic sweep (-2.0 – 2.0 V potential range). Thus the electrochemical stability window is about 4 V. These results imply that the copolymer has adequate electrochemical stability under fuel cell conditions.

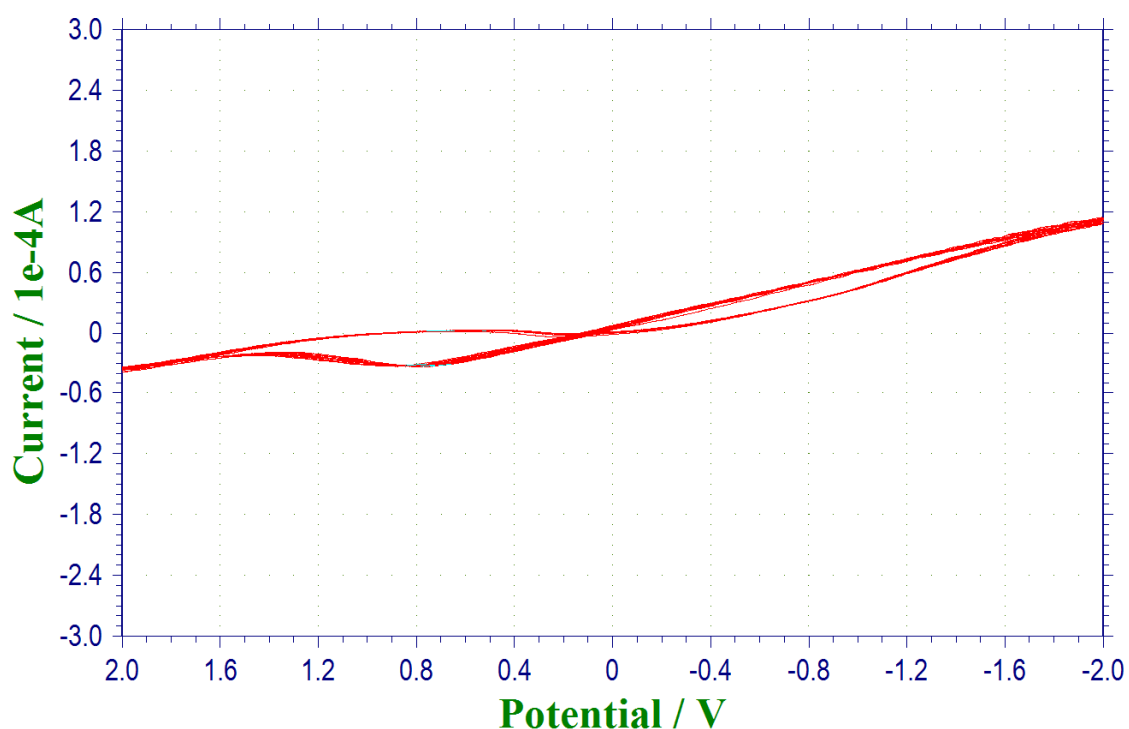


Figure 3.21. Cyclic voltammograms of P(VBBA-co-VTri)1:1x=2 in 0.1 M TBATFB/ acetonitrile. Curves with a scan rate of 50 mV/s.

3.4 COPOLYMERS BASED ON 4-VINYL BENZENE BORONIC ACID AND VINYL PHOSPHONIC ACID

3.4.1 Characterizations

FTIR spectra of the copolymers are given in Fig. 3.22. Aliphatic C-H bond gives symmetric and asymmetric vibrations at 2925 cm^{-1} . C=C bond of benzene ring shows absorption at 1606 cm^{-1} . C-H out of plane vibration is observed at 843 cm^{-1} . The band at 1343 cm^{-1} is attributed to B-O bond. The broad band at 3400 cm^{-1} is due to both -B-(OH) and phosphonic acid -OH groups. The symmetric and asymmetric vibrations of P-OH bond in VPA are seen between $1040\text{-}910\text{ cm}^{-1}$ (Brown et al., 1999). The peak at 1176 cm^{-1} belongs to P=O bond. In S3 the intensity of B-O peak at 1343 cm^{-1} is lower than S1 and there is an increase in P-OH peak at 910 cm^{-1} which verifies the increase in VPA content. After grafting the copolymers there are strong peaks at 1100 cm^{-1} and 2870 cm^{-1} due to C-O-C and aliphatic C-H bonds in PEGME (Fig. 3.23).

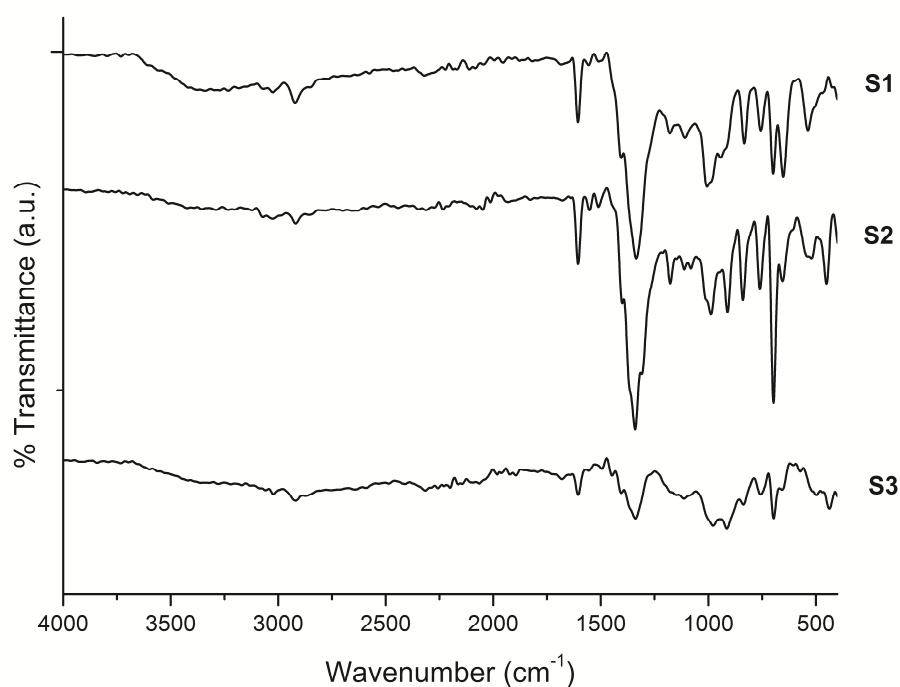


Figure 3.22. FTIR spectra of P(VBBA-VPA) copolymers.

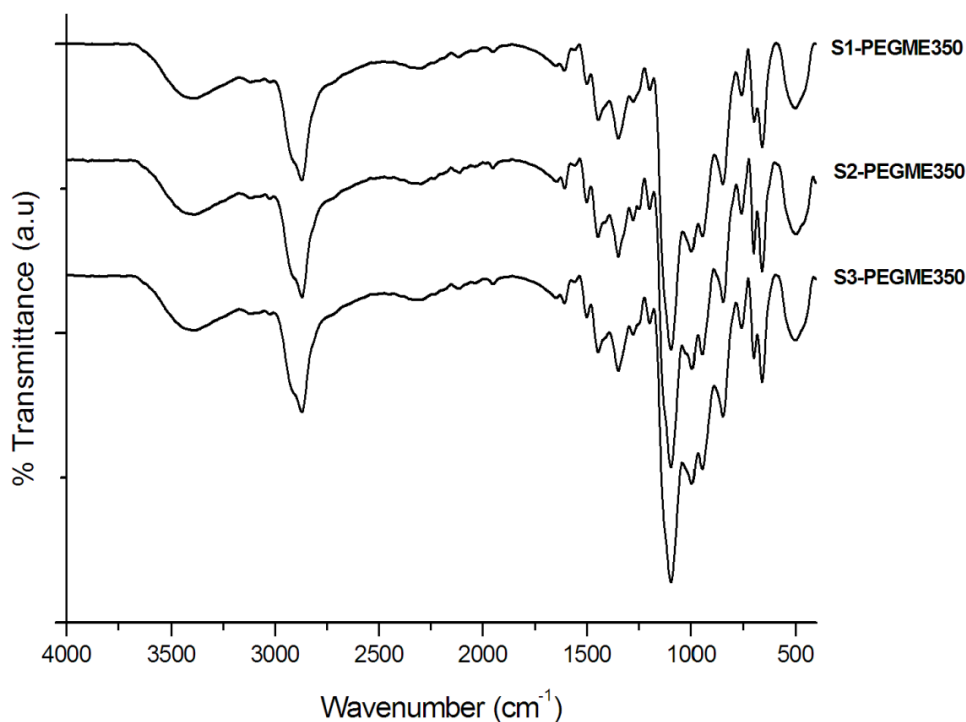


Figure 3.23. FTIR spectra of P(VBBA-VPA)-PEGME copolymers.

3.4.2 Thermal Properties

The thermal properties of the copolymers were analyzed with TGA and DSC. The thermal properties of pure poly(vinyl benzene boronic acid) and poly(vinyl phosphonic acid) were previously reported. PVBBA is thermally stable up to 400 °C but there is 15 % weight loss between 100-300 °C due to condensation of $B(OH)_2$ units (Çelik and Bozkurt, 2010b). PVPA is thermally stable up to 200 °C but there is a little weight loss between 100-200 °C due to condensation of phosphonic acid units (Jiang et al., 1999). Fig. 3.24 shows TGA curves of the copolymers and grafted samples. There is 15 % weight loss at 100-200 °C due to condensation of acid groups. The major decomposition occurs above 400 °C which is higher than decomposition temperature of pure PVPA. This indicates that the presence of VBBA unit in the material increases its thermal stability. When the copolymers were grafted with PEGME the thermal stability decreased to 250 °C.

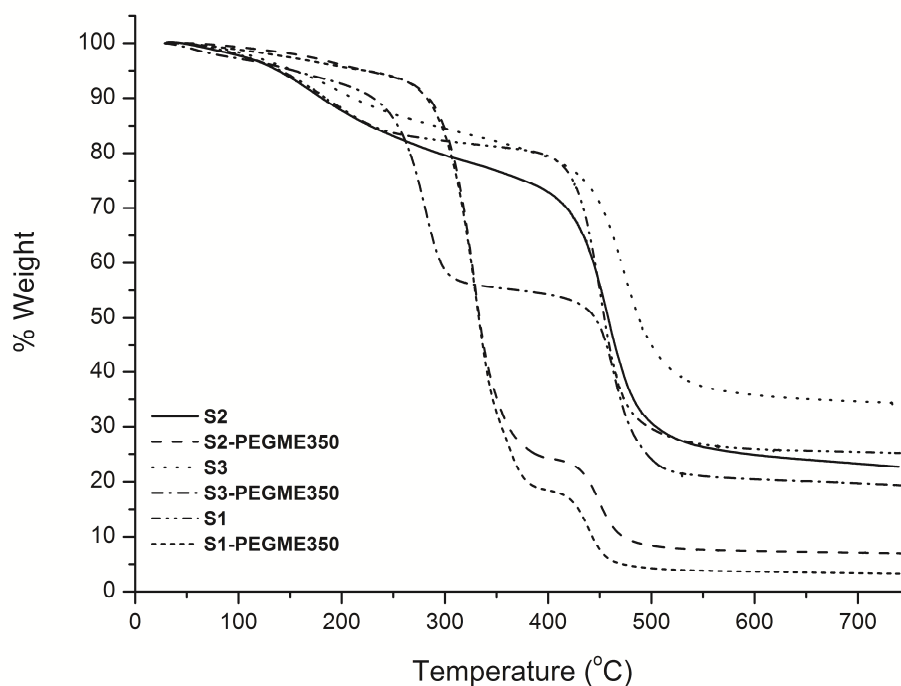


Figure 3.24. TG thermograms of P(VBBA-VPA) and P(VBBA-VPA)-PEGME copolymers at a heating rate of 10 °C/min in inert atmosphere.

The glass transition temperatures of the copolymers were analyzed with DSC but there is not a definite T_g between -50 and 200 °C. Pure PVPA has a T_g of -23 °C (Sevil and Bozkurt, 2004). Pure PVBBA has also no T_g. After grafting the copolymers with PEGME, there is a melting like behavior between -10 and 0 °C but the T_g points are not observable at the measurement range (Fig. 3.25).

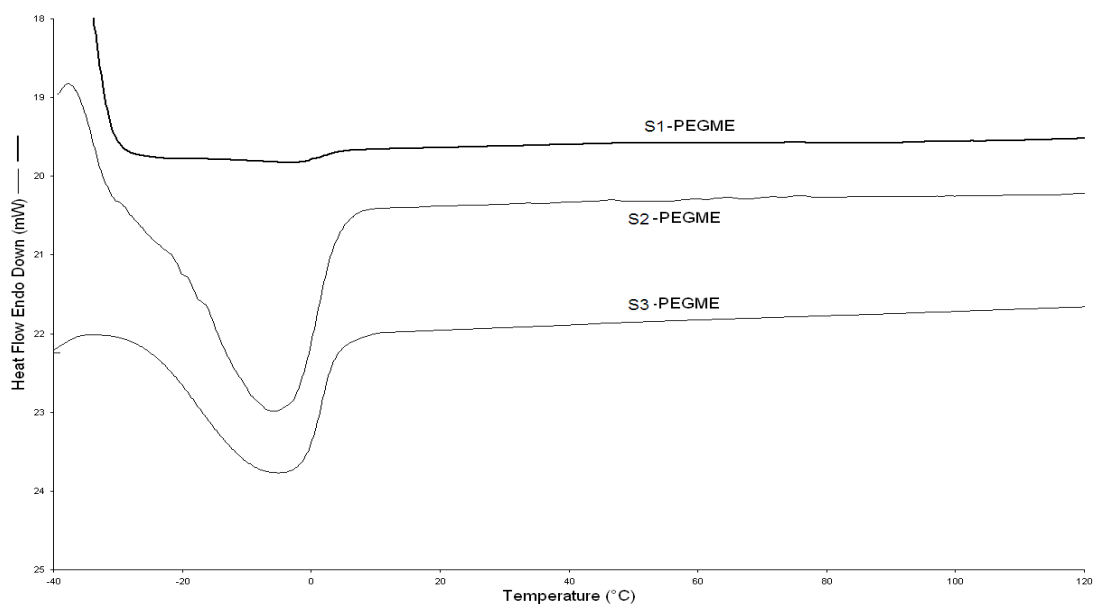


Figure 3.25. DSC curves of P(VBBA-VPA)-PEGME copolymers at a heating rate of 10 °C/min in inert atmosphere.

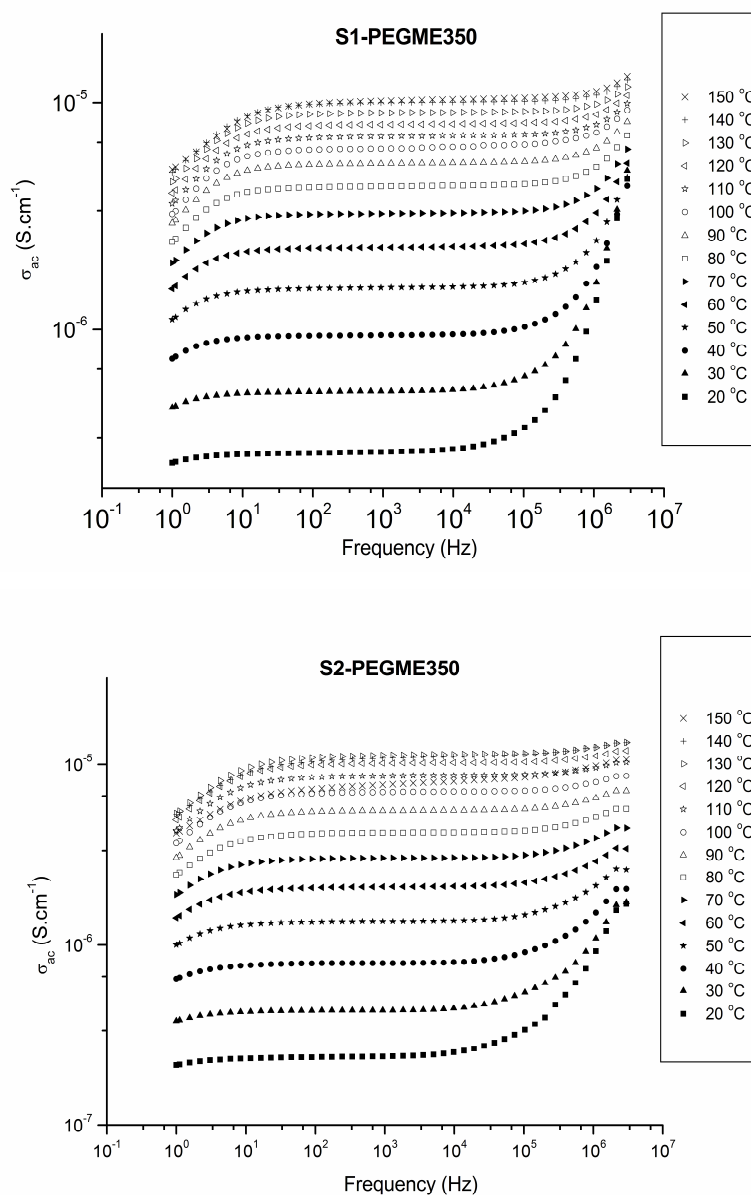
3.4.3 Ion Exchange Capacity (IEC)

IEC of the copolymers were calculated using Eq. 2.1 and summarized in Table 3.4. The ion exchange capacity of pure PVPA and PVBBA were also determined with the same method and obtained as 9.8 mmol/g and 5.5 mmol/g, respectively. As seen in the table, IEC values increase with VPA content. In these copolymers there may be little crosslink or anhydride formation due to condensation of both VBBA and VPA units during drying process. The insoluble behavior of the materials verifies this consideration. In this IEC determination method the samples were put in alkaline salt solution for 24 h to provide complete salt formation and cleavage of anhydrides. This is also important for the efficiency of back titration (Kim et al., 2007).

3.4.4 Proton Conductivity

Fig. 3.26 shows the AC conductivity of the grafted copolymers versus frequency at several temperatures. The σ_{ac} versus frequency curves change with the frequency where in the low frequency region, the reduction in the conductivity is due to polarization of the blocking electrodes. The conductivity increase at low temperature and high frequencies results from the regular dispersion in polymer electrolytes. The proton conductivity increases as temperature increases.

The DC conductivity (σ_{dc}) of the samples was derived from the plateaus of $\log \sigma_{ac}$ versus $\log F$ by linear fitting of the data. The DC conductivities of the samples were compared in Fig. 3.27. The conductivity isotherm illustrates that the DC conductivity depends on the temperature and VPA content. A marked curvature is observed for all samples and the curves are interpreted with the Vogel–Tamman–Fulcher (VTF) equation (Eq. 3.1). Pure copolymers have low proton conductivity and after grafting them the proton conductivity values reach to acceptable values. Grafted materials are soft materials which shows that the segmental motions have high contribution on the proton conductivity.



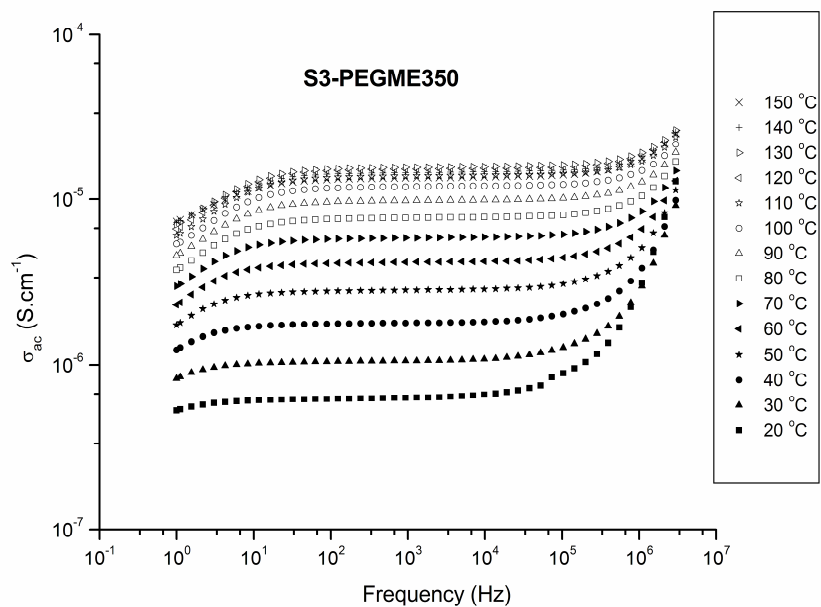


Figure 3.26. AC conductivity versus frequency for P(VBBA-co-VPA)-PEGME copolymers at different temperatures.

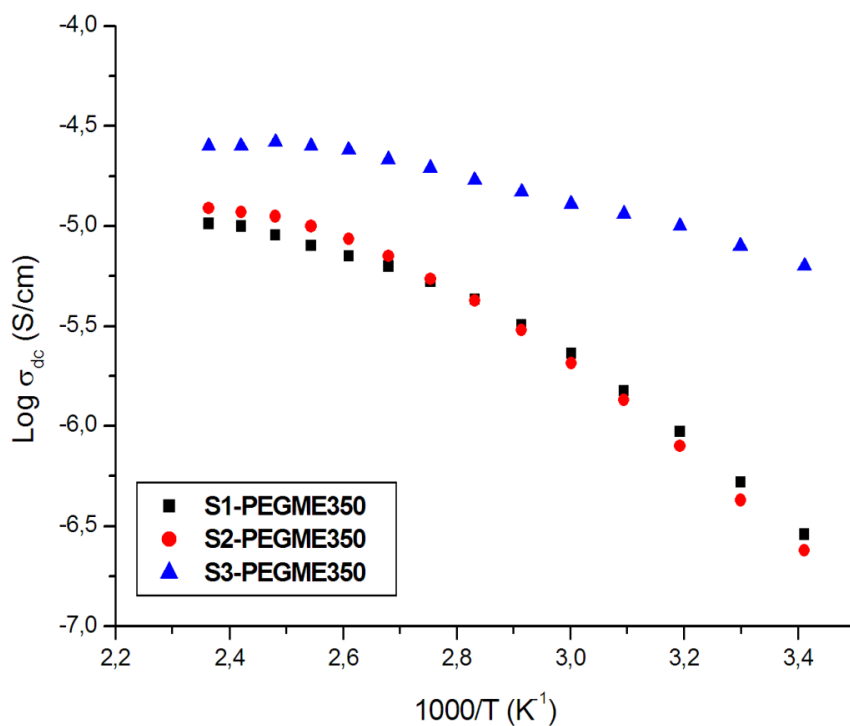


Figure 3.27. Variation of the proton conductivity of P(VBBA-co-VPA)-PEGME copolymers as a function of reciprocal temperature.

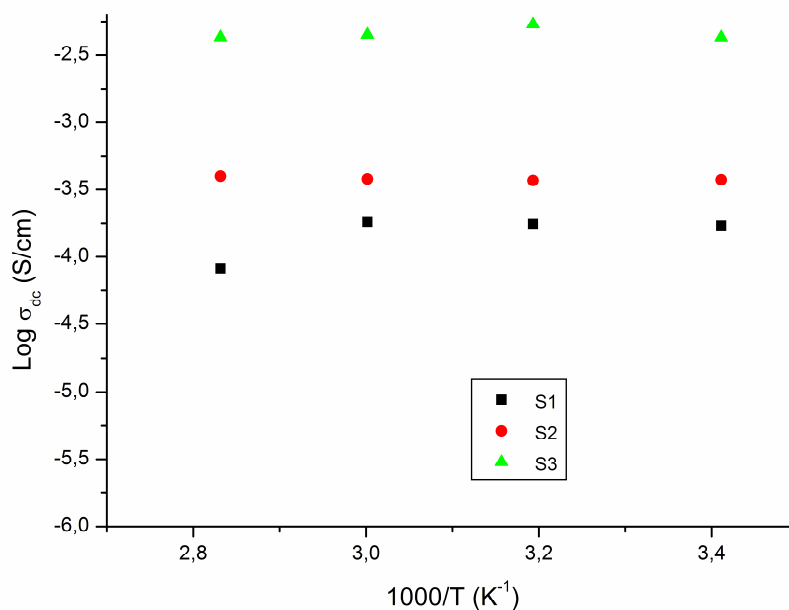


Figure 3.28. Variation of the proton conductivity of P(VBBA-co-VPA) copolymers as a function of reciprocal temperature at 50% RH.

The proton conductivity of copolymers was also investigated in humidified condition. The films of the copolymers were humidified as 50 % RH and the conductivity measurement was done at 20-100 °C (Fig. 3.28). As expected the proton conductivity increases with VPA content and reaches 4.3×10^{-3} S/cm at 30 °C.

Table 3.4. IEC and maximum proton conductivity values for P(VBBA-co-VPA) copolymers.

Sample	VBBA	VPA	Conv.	IEC	Max. Proton Cond.
S1	1.00 g , 6.76 mmol	0.38 g, 3.52 mmol	1.30 g, 94 %	6.70 mmol/g	1.8×10^{-4} S/cm at 30 °C, 50 % RH
S2	1.00 g, 6.76 mmol	0.73 g, 6.76 mmol	0.91 g, 53 %	7.05 mmol/g	3.7×10^{-4} S/cm at 30 °C, 50 % RH
S3	1.00 g, 6.76 mmol	1.46 g, 13.5 mmol	1.1 g, 45 %	7.55 mmol/g	4.3×10^{-3} S/cm at 30 °C, 50 % RH

3.4.5 Cyclic Voltammetry

Cyclic voltammogram of S3-PEGME was given in Fig. 3.29. The measurement was performed in a typical three electrode cell containing 0.1 mol dm^{-3} CH_3CN solution of tetrabutylammonium hexafluorophosphate (TBAPF6) using a platinum work electrode, a platinum auxiliary electrode, and an Ag/Ag⁺ reference electrode. The figure shows that the CV of the copolymer comprises no peak within in the anodic and cathodic sweep (-2.0 – 2.0 V potential range). Thus the electrochemical stability window is about 4 V. These results imply that the copolymer has adequate electrochemical stability under fuel cell conditions.

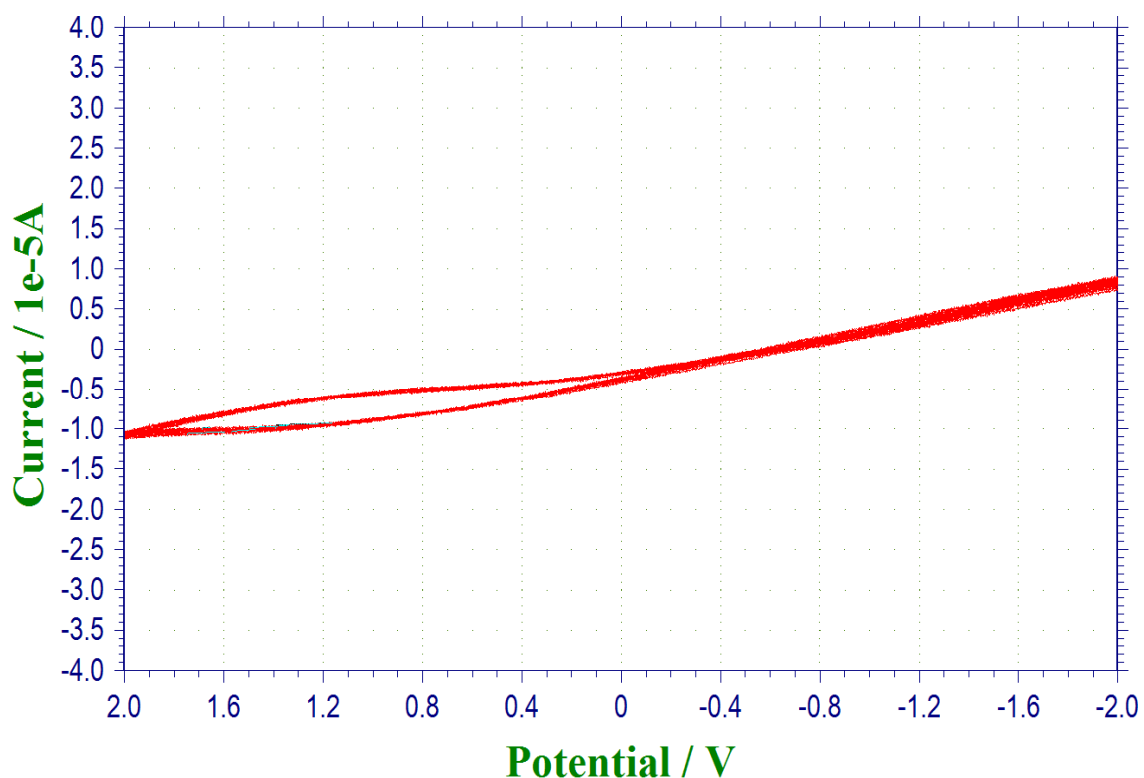


Figure 3.29. Cyclic voltammograms of S3-PEGME in 0.1 M TBATFB/acetonitrile.

Curves with a scan rate of 50 mV/s.

3.5 DIISOPROPYL-P-VINYLBENZYL PHOSPHONATE (VBP) MONOMER AND POLY(VINYL BENZYL PHOSPHONIC ACID)

3.5.1 Characterizations

The synthesis of VBP monomer and the purity of the resulting monomer was verified via ^1H and ^{13}C NMR. The spectra and the assignments of the peaks were illustrated in Fig. 3.30 and 3.31. It is clear that the benzyl chloride bonds were successfully phosphonated with diisopropyl phosphonate units.

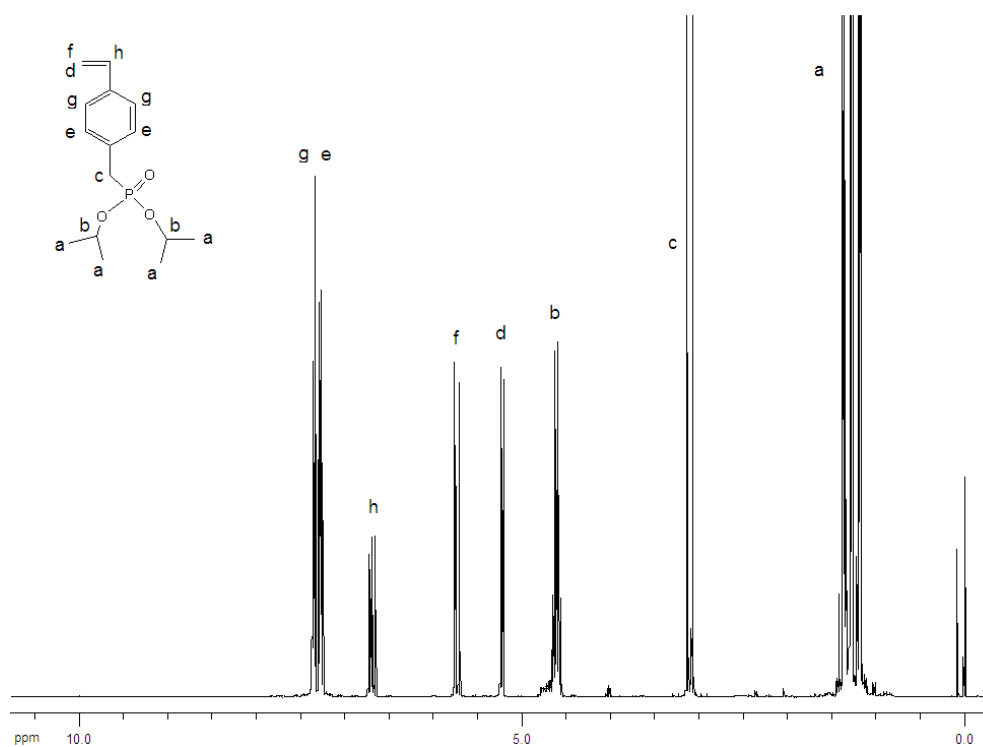


Figure 3.30. ^1H NMR spectrum of diisopropyl-p-vinylbenzyl phosphonate (VBP) monomer.

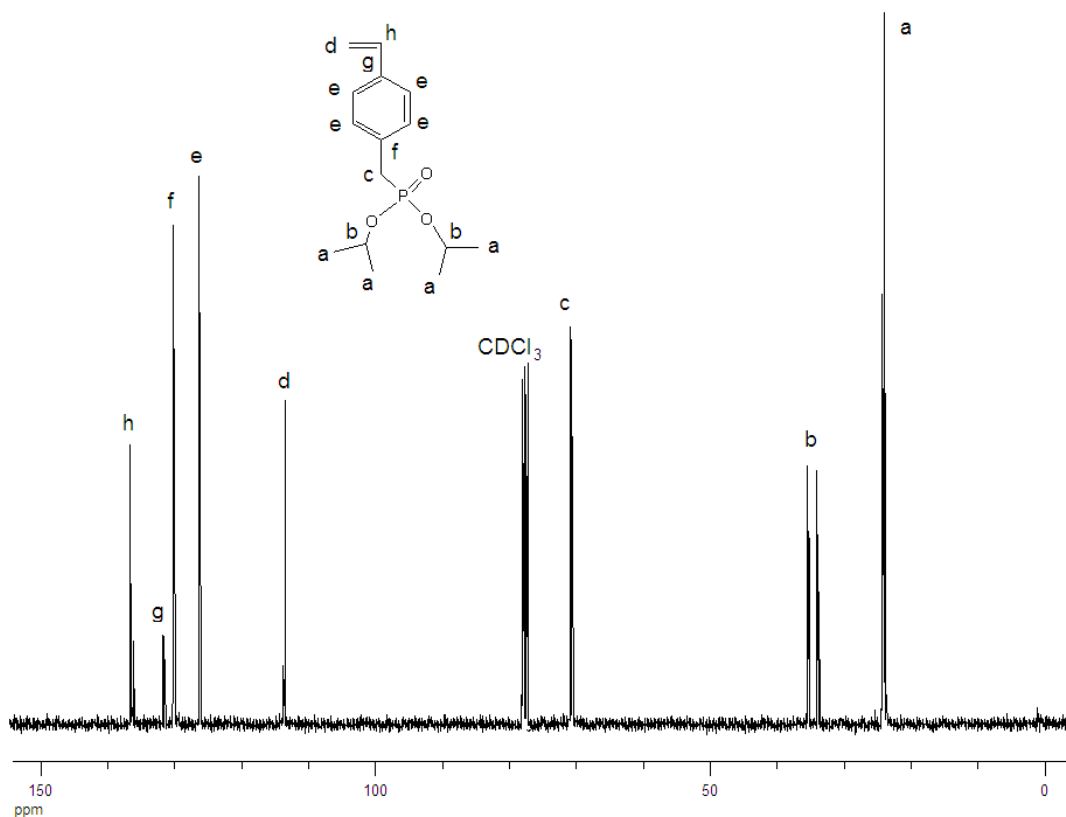


Figure 3.31. ^{13}C NMR spectrum of diisopropyl-p-vinylbenzyl phosphonate (VBP) monomer.

FTIR spectra of pure diisopropyl-p-vinylbenzyl phosphonate (VBP) monomer and its homopolymer (PVBP) were illustrated in Fig. 3.32. Aliphatic C-H vibrations gives peaks at 2925 and 2981 cm^{-1} . =C-H out-of-plane bending vibration of p-disubstituted benzene ring is seen at 840 cm^{-1} . The strong peak at 1240 cm^{-1} belongs to P=O bond. P-O-alkyl bonds have vibrations between 900-1150 cm^{-1} . Vinyl group has absorption at 1630 cm^{-1} and disappears after polymerization. After hydrolysis there is a broad band formation between 2500-3500 cm^{-1} and new peaks arise at 1637 cm^{-1} and 924 cm^{-1} due to phosphonic acid group formation (Fig. 3.33).

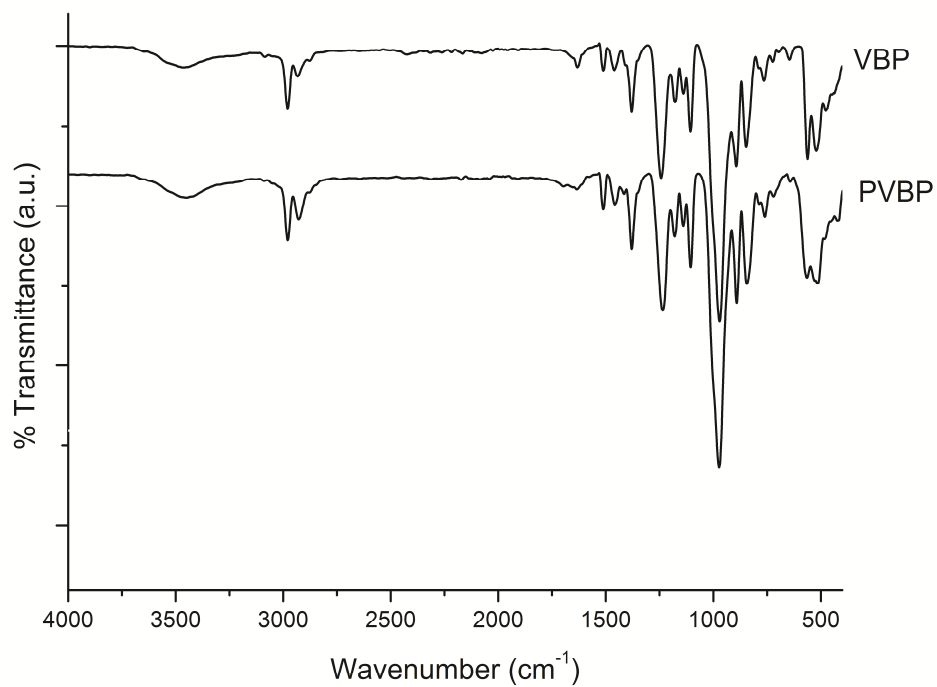


Figure 3.32. FTIR spectra of VBP and PVBP.

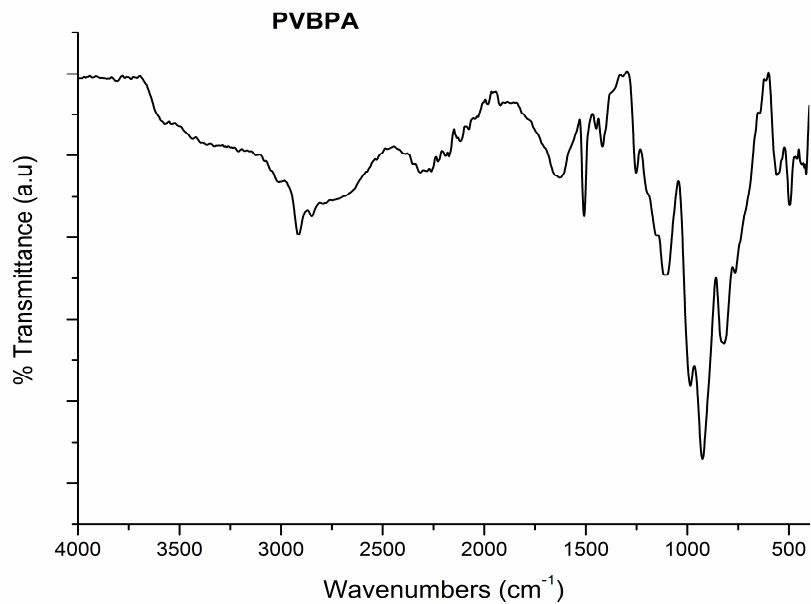


Figure 3.33. FTIR spectrum of PVBPA.

3.5.2 Thermal properties

Poly(vinyl benzyl phosphonic acid) homopolymer is thermally stable up to 430 °C (Fig. 3.34) but there is a little (10%) weight loss between 30-200 °C due to loss of absorbed water and also condensation of phosphonic acid units. The glass transition temperature of PVBPA homopolymer was analyzed with DSC and in second heating a Tg behavior was observed at 110 °C.

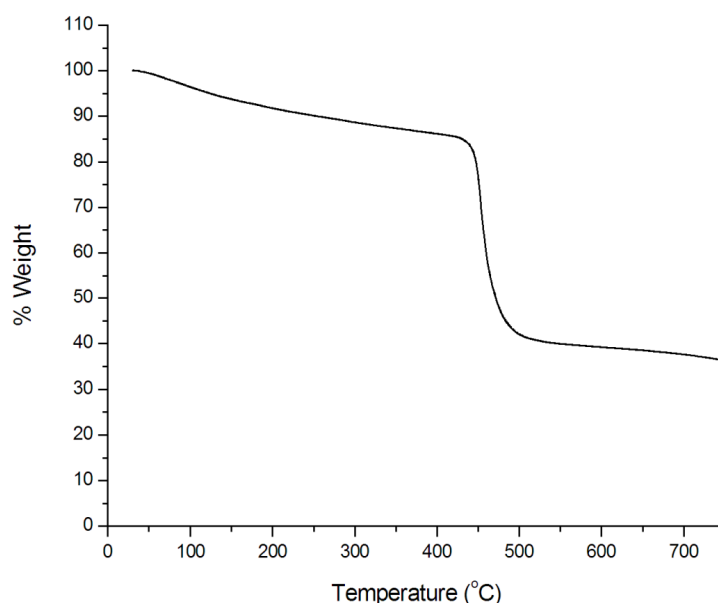


Figure 3.34. TG thermograms of PVBPA homopolymer recorded at a heating rate of 10 °C/min in inert atmosphere.

3.6 POLY(VINYL TRIAZOLE-CO-VINYL BENZYL PHOSPHONIC ACID), P(VTRI-CO-VBPA) COPOLYMER

3.6.1 Characterizations

Copolymerizations of VTri and VBP were conducted at several molar feed ratios and compositions of the final hydrolyzed copolymers were analyzed by elemental analysis (Table 3.5). The mol ratio (VTri:VBPA) of the copolymers is calculated using the nitrogen contents. The results demonstrated that copolymer compositions are a little

different from feed ratios but there is an increasing VBPA ratio and there different samples to compare the properties.

Table 3.5. Composition of P(VTri-co-VBPA) copolymers.

Sample	Feed mol ratio, (VTri:VBPA)	Elemental Analysis			Copolymer ratio, (VTri:VBPA)
		C (%)	H (%)	N (%)	
P(VTri-co-VBPA) 1:0.5	1:0.5	49.17	5.91	12.93	1: 1.16
P(VTri-co-VBPA) 1:1	1:1	50.03	5.78	11.34	1: 1.39
P(VTri-co-VBPA) 1:2	1:2	49.90	5.77	9.20	1: 1.82

FTIR spectra of P(VTri-co-VBP), P(VTri-co-VBPA) copolymers and H_3PO_4 doped samples are illustrated in Fig. 3.35, Fig. 3.36 and Fig. 3.37. The triazole ring stretching is observed at 1450-1650 cm^{-1} . Aliphatic C-H vibrations gives peaks at 2930 and 2980 cm^{-1} . =C-H out-of-plane bending vibration of p-disubstituted benzene ring is seen near 840 cm^{-1} . The strong peak at 1240 cm^{-1} belongs to P=O bond. P-O-alkyl bonds have vibrations between 950-1150 cm^{-1} . After hydrolysis there is a broad band formation between 2500-3500 cm^{-1} and new peaks arise at 1643 cm^{-1} and 930 cm^{-1} due to phosphonic acid group formation (Fig. 3.36). After doping the copolymers the characteristic absorptions of H_3PO_4 are observed at 2300 cm^{-1} , 1107 cm^{-1} and 925 cm^{-1} and their intensities increase with phosphonic acid content.

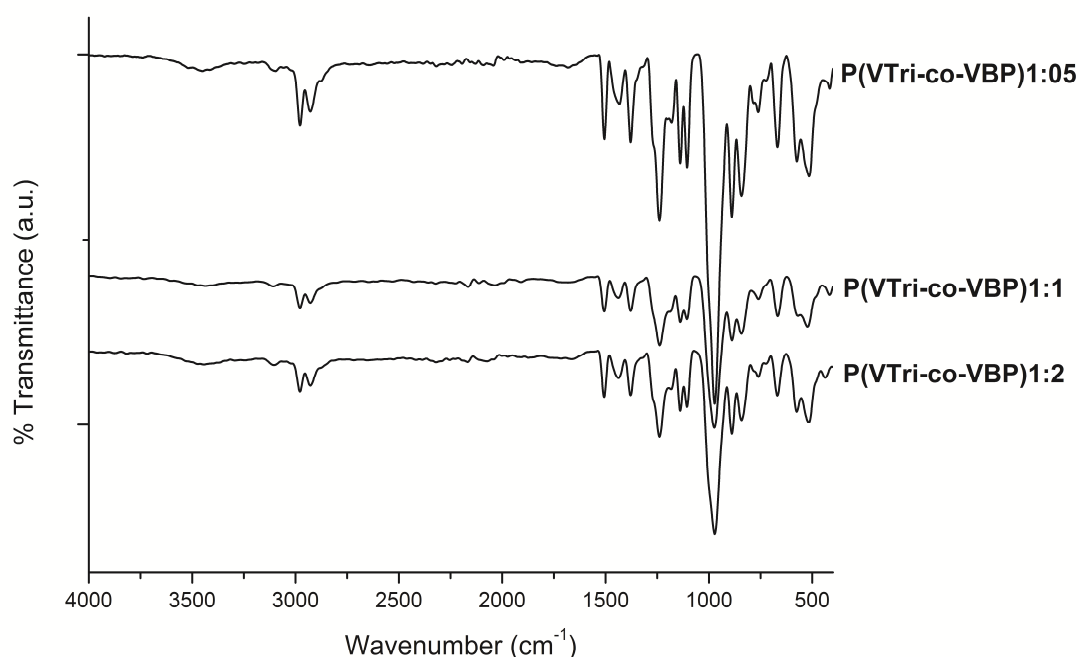


Figure 3.35. FTIR spectra of P(VTri-co-VBP) copolymers.

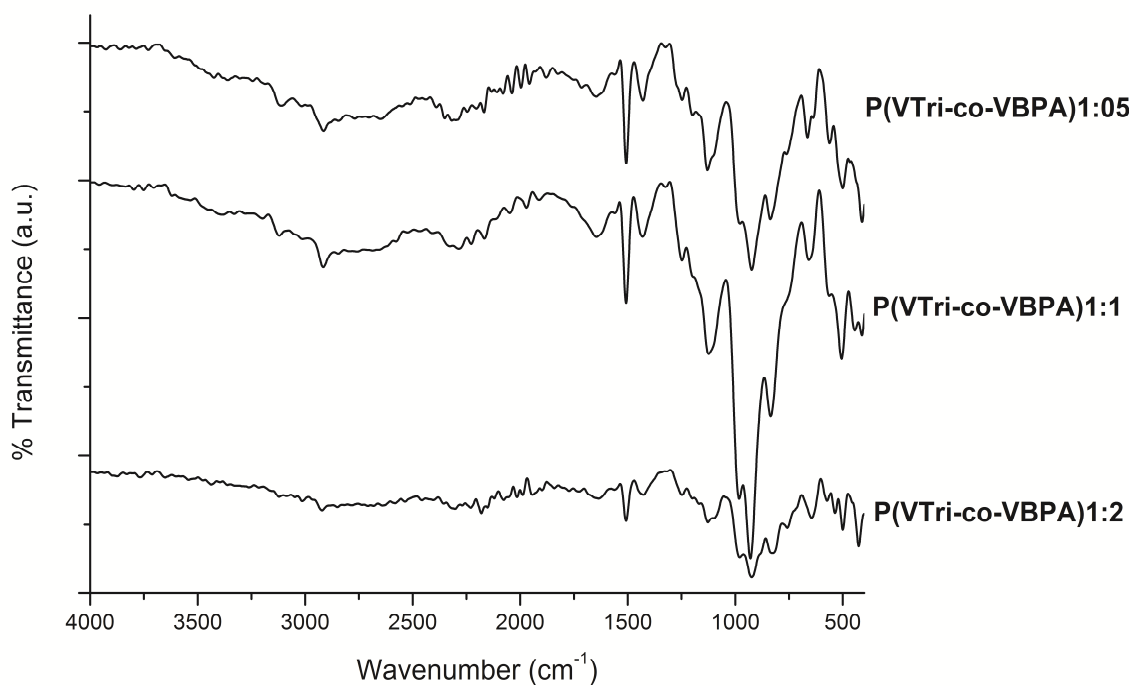


Figure 3.36. FTIR spectra of P(VTri-co-VBPA) copolymers.

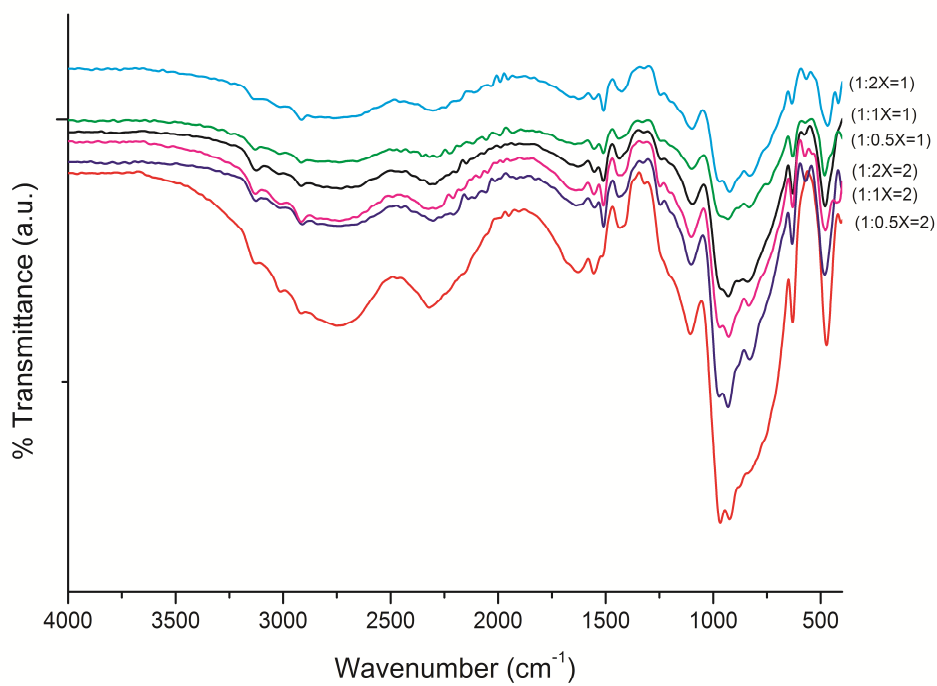


Figure 3.37. FTIR spectra of H_3PO_4 doped P(VTri-co-VBPA) copolymers.

3.6.2 Thermal properties

The thermal properties of the copolymers were analyzed with TGA and DSC. Pure PVBPA and PVTri are thermally stable up to 450 and 350 °C, respectively. In the copolymers there are two major decomposition regions between 300-350 °C and 450-500 °C due to VTri and VBPA decompositions, respectively (Fig. 3.38). The doping has little effect on the thermal stability of the copolymers. In Fig. 3.38 the two steps of degradation is more clear but they are not clear in Fig. 3.39 due to the loss of phosphoric acid also. The doped polymer electrolytes are also thermally stable up to at least 250 °C (Fig. 3.39).

The Tg of pure PVTri is reported as 165 °C (Celik et al., 2008a). Pure PVBPA shows no Tg which may be due to anhydride formation and crosslink during drying process (Kim et al., 2007). In DSC analysis of the copolymers and the doped samples no Tg was measured at -50 to 250 °C measurement range.

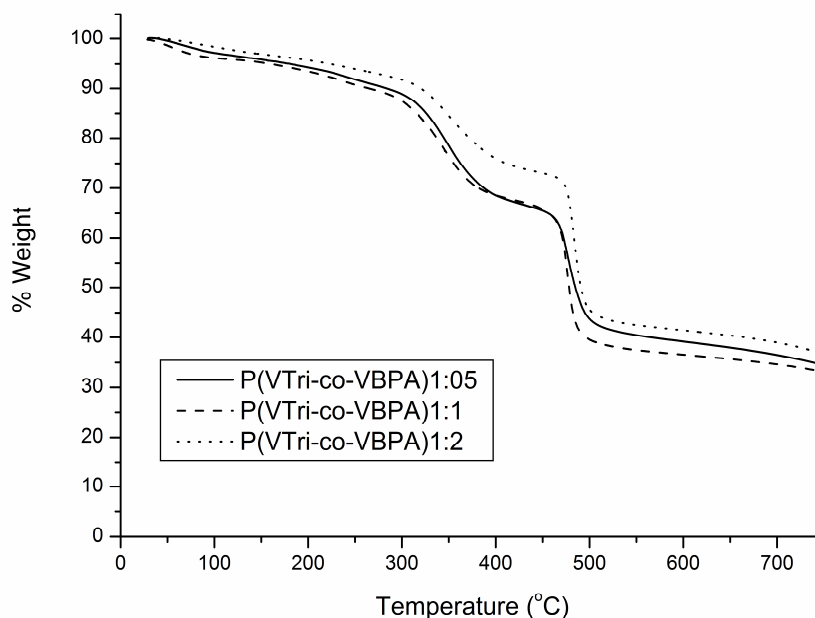


Figure 3.38. TG thermograms of P(VTri-co-VBPA) copolymers at a heating rate of 10 °C/min in inert atmosphere.

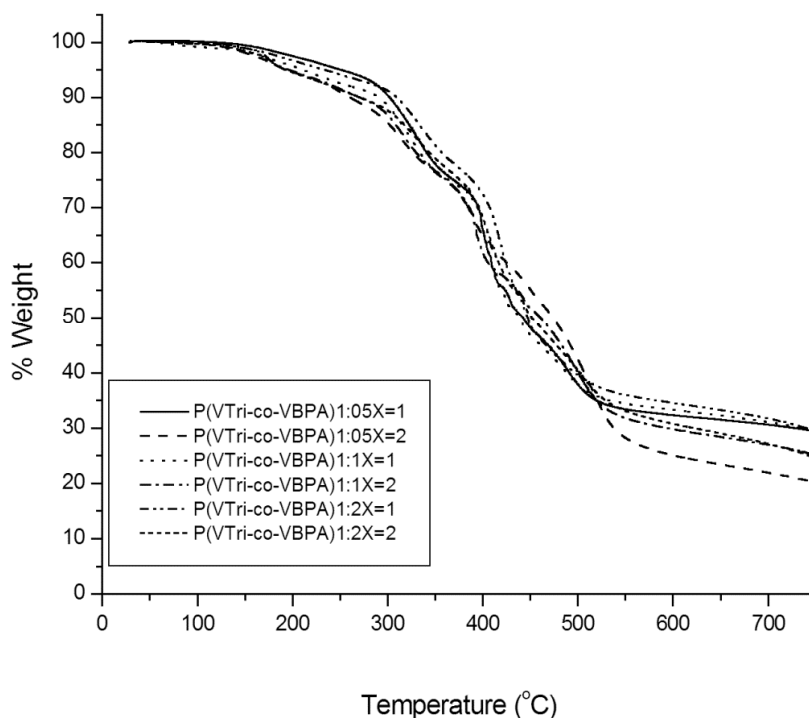


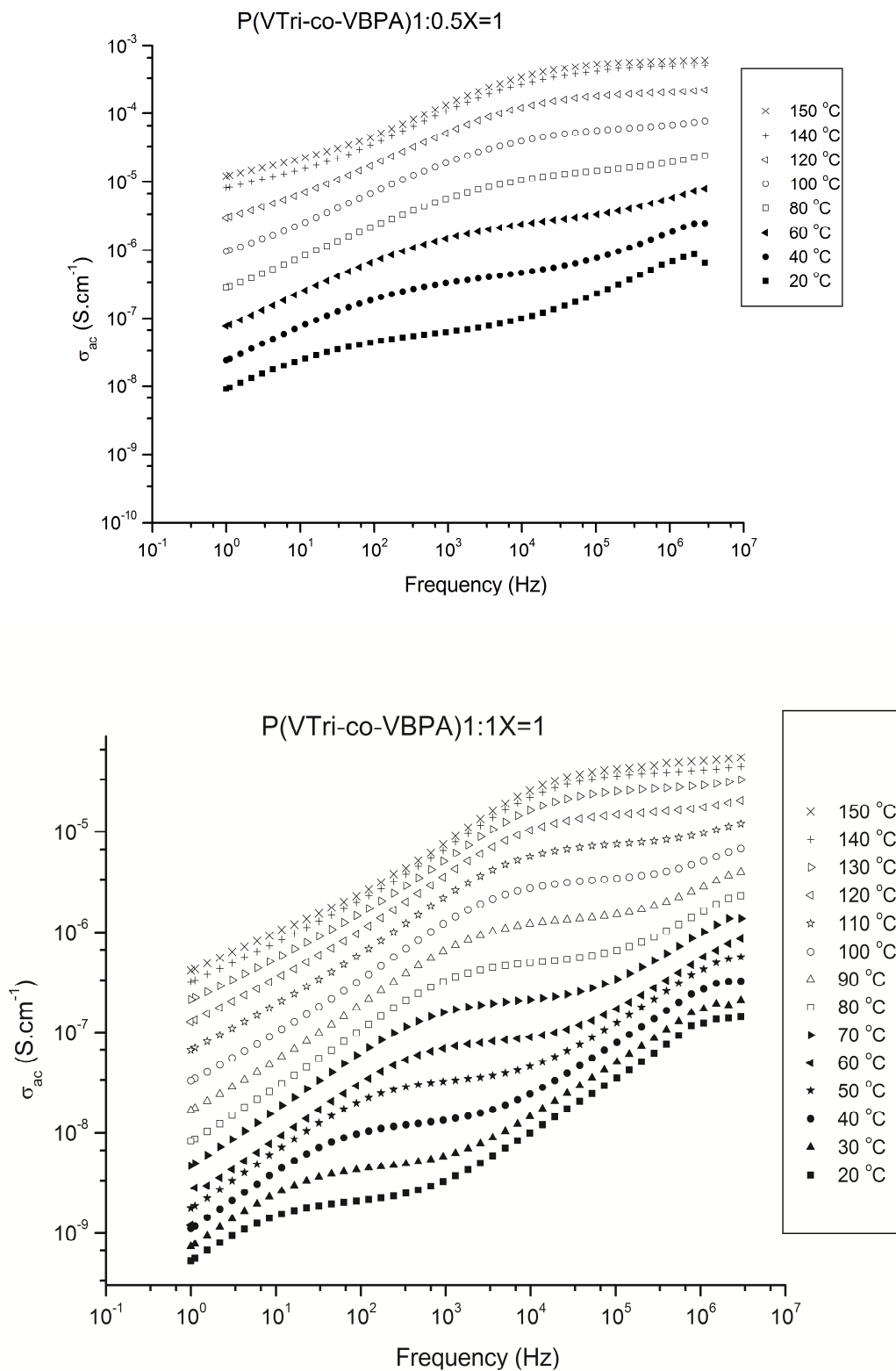
Figure 3.39. TG thermograms of H_3PO_4 doped P(VTri-co-VBPA) copolymers at a heating rate of $10\text{ }^\circ\text{C}/\text{min}$ in inert atmosphere.

3.6.3 Proton Conductivity

Fig. 3.40 shows the AC conductivity of the doped copolymers versus frequency at several temperatures. The σ_{ac} versus frequency curves change with the frequency where in the low frequency region, the reduction in the conductivity is due to polarization of the blocking electrodes. The conductivity increase at low temperature and high frequencies results from the regular dispersion in polymer electrolytes. The proton conductivity increases as temperature increases.

The DC conductivity (σ_{dc}) of the samples was derived from the plateaus of $\log \sigma_{ac}$ versus $\log F$ by linear fitting of the data. The DC conductivities of the samples were compared in Fig. 3.41. The conductivity isotherm illustrates that the DC conductivity depends on the temperature, VTri and acid content. Pure copolymers have low proton conductivity ($<10^{-7}\text{ S/cm}$) and after doping them with phosphoric acid the proton conductivity values increases to 0.005 S/cm at $150\text{ }^\circ\text{C}$ for P(VTri-co-VBPA)1:0.5X=2

which has the highest amount of VTri and H₃PO₄. In that system proton conduction occurs through protonated triazole units and acidic units via Grotthuss mechanism. 100% humidified membranes resulted proton conductivities around 10⁻³ - 10⁻² S/cm at 20 °C.



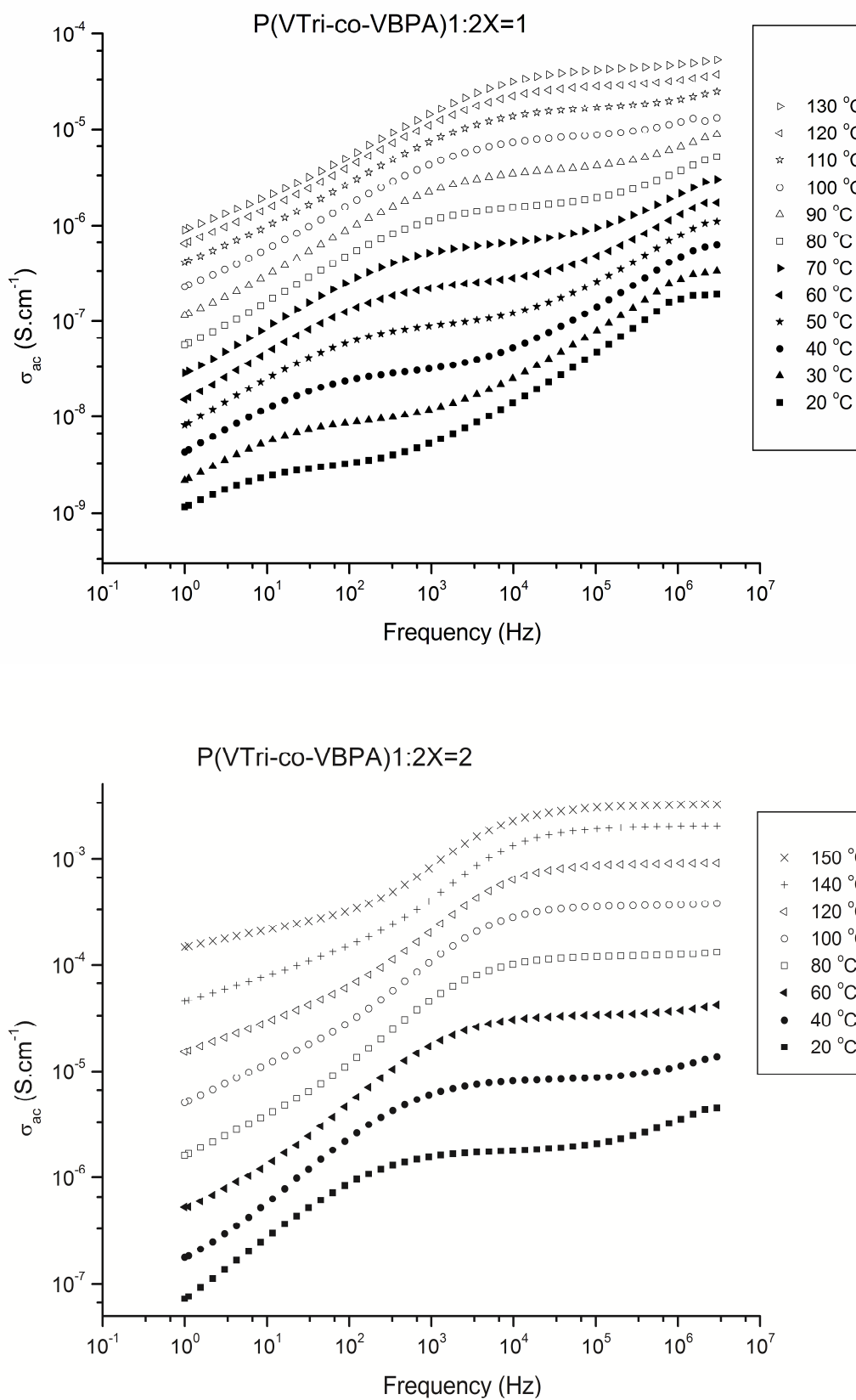


Figure 3.40. AC conductivity versus frequency for H_3PO_4 doped P(VTri-co-VBPA) copolymer electrolytes.

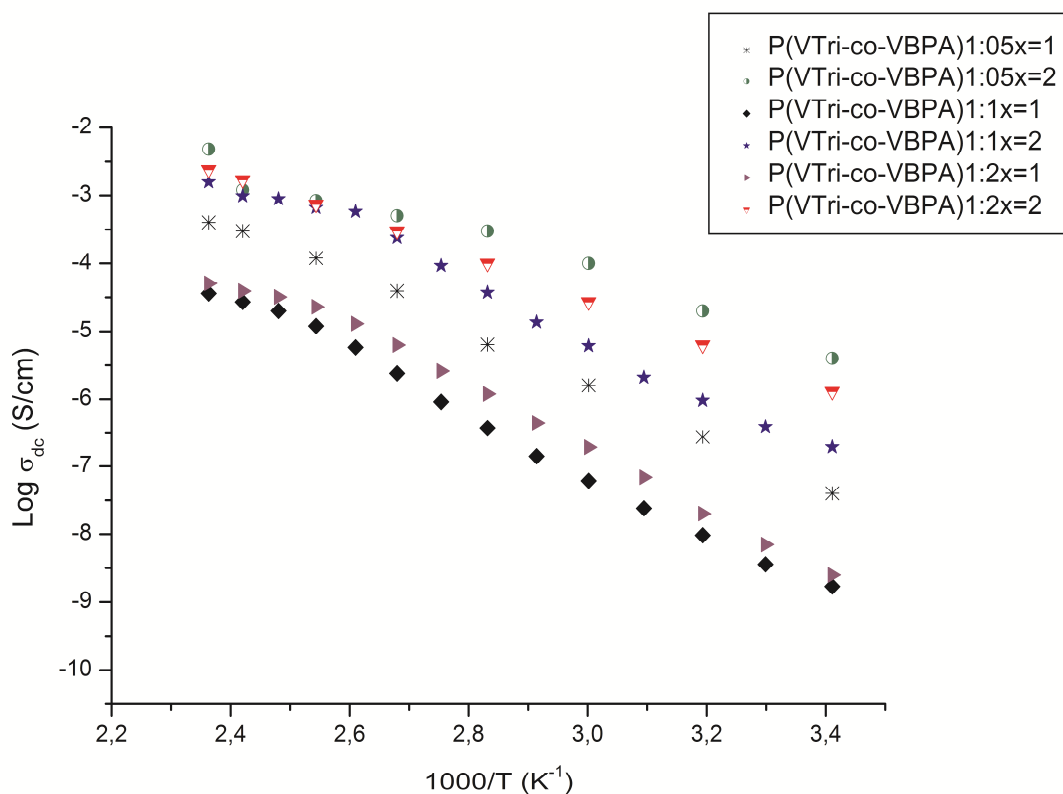


Figure 3.41. DC conductivity of H_3PO_4 doped P(VTri-co-VBPA) copolymer electrolytes at different temperatures.

3.6.4 Cyclic Voltammetry

Cyclic voltammogram of P(VTri-co-VBPA)1:0.5x=2 was shown in Fig. 3.42. The measurement was performed in a typical three electrode cell containing 0.1 mol dm^{-3} CH_3CN solution of tetrabutylammonium hexafluorophosphate (TBAPF6) using a platinum work electrode, a platinum auxiliary electrode, and an Ag/Ag⁺ reference electrode. The figure shows that the CV of the copolymer comprises no peak within in the anodic and cathodic sweep (-2.0 – 2.0 V potential range). Thus the electrochemical stability window is about 4 V. These results imply that the copolymer has adequate electrochemical stability under fuel cell conditions.

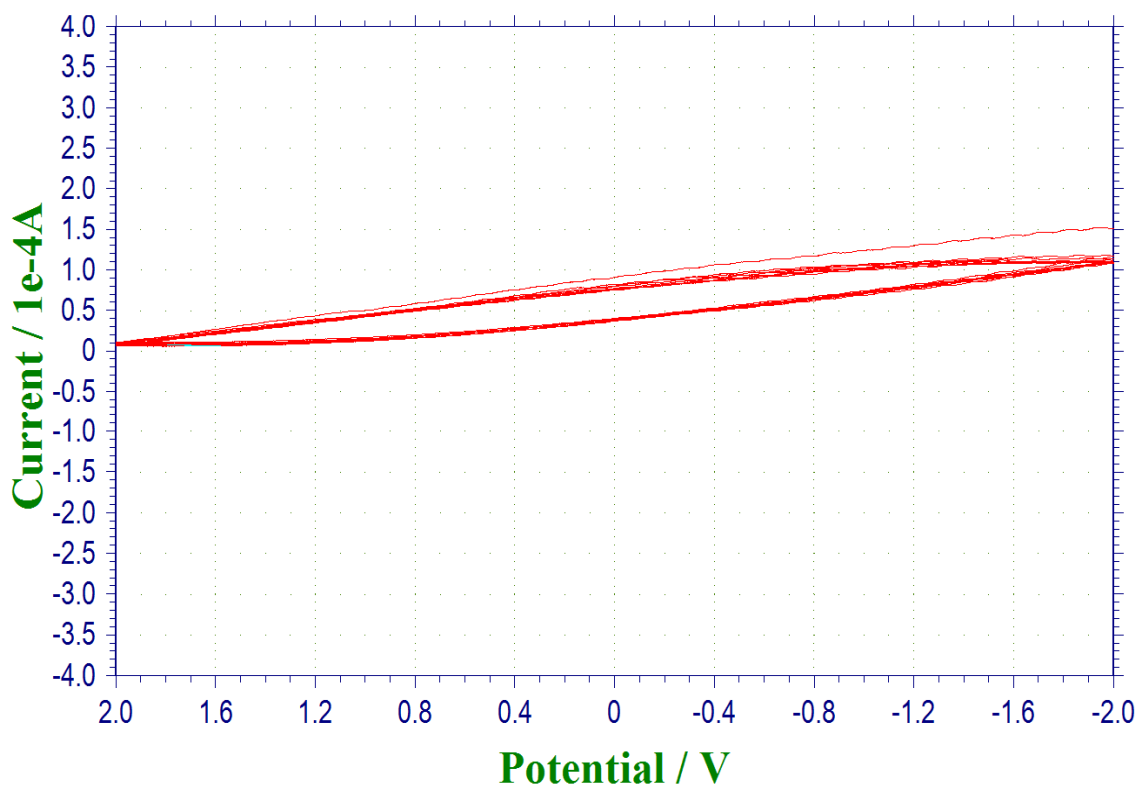


Figure 3.42. Cyclic voltammograms of P(VTri-co-VBPA)1:0.5x=2 in 0.1 M TBATFB/acetonitrile. Curves with a scan rate of 50 mV/s.

3.7 POLY(VINYL BENZENE BORONIC ACID-CO-VINYL BENZYL PHOSPHONIC ACID), P(VBBA-CO-VBPA) COPOLYMER

3.7.1 Characterizations

The FT-IR spectra of copolymers are shown in Fig. 3.43 and 44. Aliphatic C-H bond gives symmetric and asymmetric vibrations near 2981 cm^{-1} and 2820 cm^{-1} . C=C bond of benzene ring shows absorption at 1606 cm^{-1} . =C-H out-of-plane bending vibration of p-disubstituted benzene ring is seen at 835 cm^{-1} . The band at 1343 cm^{-1} is attributed to B-O bond. P-O-alkyl bonds have vibrations between $900\text{--}1150\text{ cm}^{-1}$ (Fig. 3.43a). In Fig. 3.43b the symmetric and asymmetric vibrations of P-OH bond in VPA are seen between $1040\text{--}910\text{ cm}^{-1}$ (Brown et al., 1999). The peak at 1176 cm^{-1} belongs to P-OH bond. After grafting the copolymers there is a strong peak at 1100 cm^{-1} due to C-O-C bond in PEGME (Fig. 3.44).

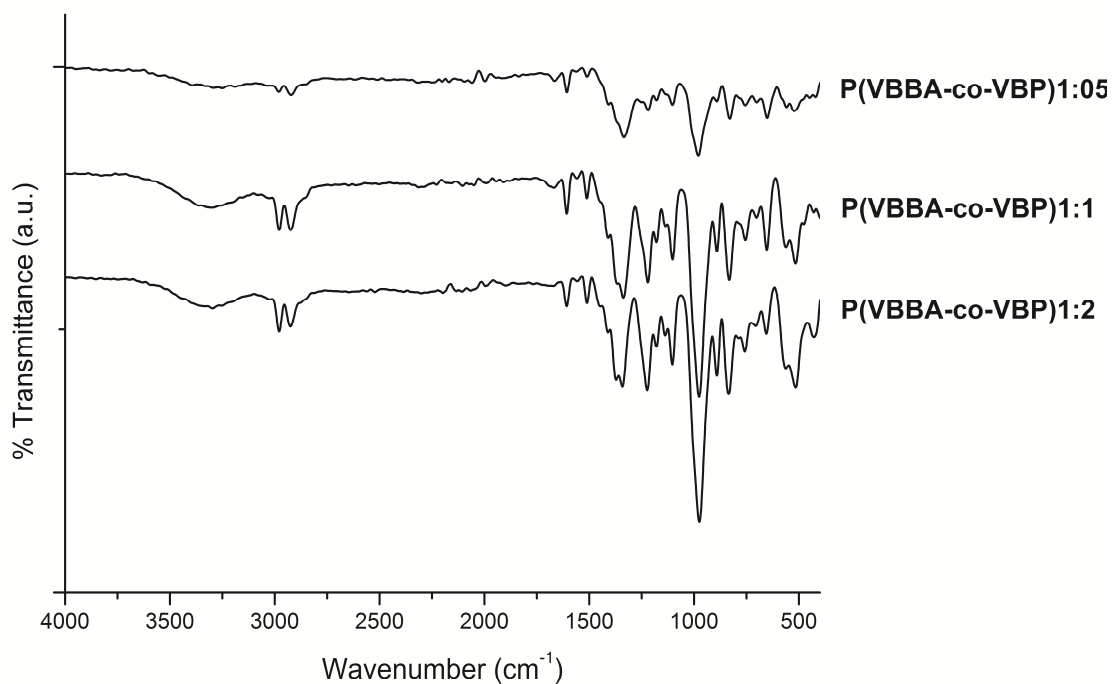


Figure 3.43a. FTIR spectra of P(VBBA-co-VBP) copolymers.

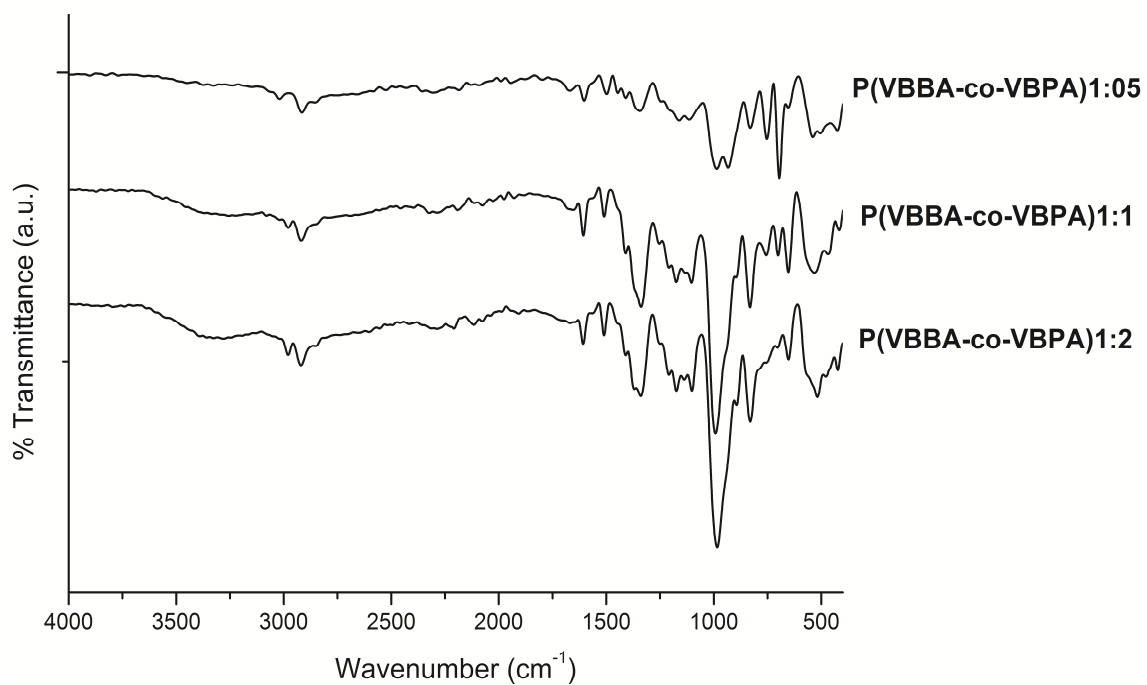


Figure 3.43b. FTIR spectra of P(VBBA-co-VBPA) copolymers.

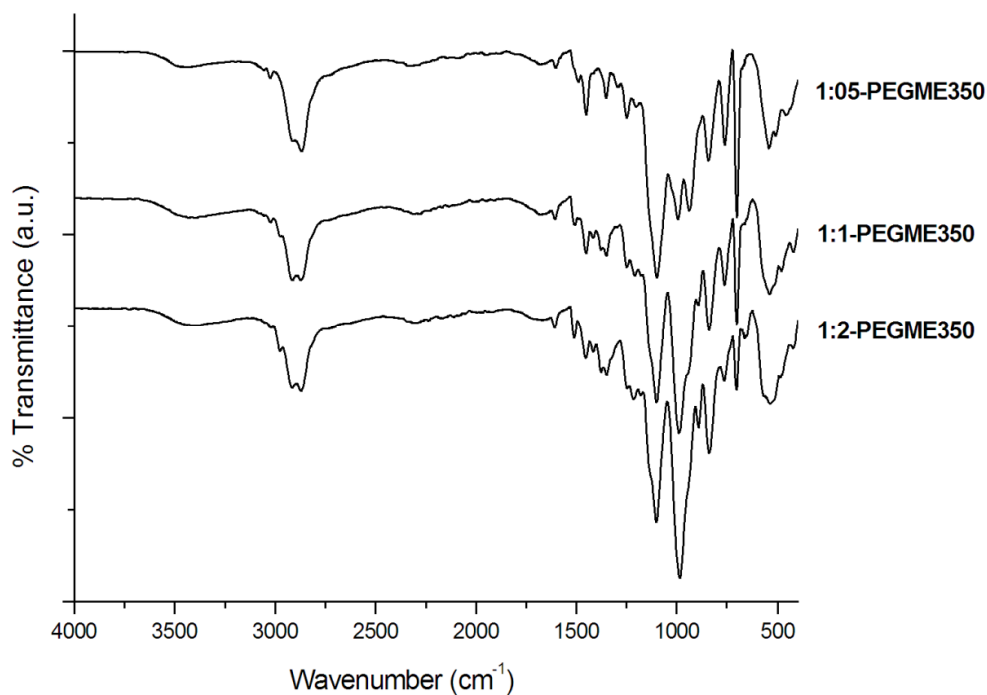


Figure 3.44. FTIR spectra of P(VBBA-co-VBPA)-PEGME copolymers.

3.7.2 Thermal Analysis

The thermal properties of the copolymers were investigated with TGA and DSC. PVBBA and PVBPA homopolymers are thermally stable up to 400 °C (Celik and Bozkurt, 2010b). As seen in Fig. 3.45 there is a little weight loss between 150-250 °C due to condensation of boronic and phosphonic acid units but the copolymers can be said to be thermally stable up to 400 °C. When the copolymers were grafted with PEGME the condensation was limited but the thermal stability decreased to 200 °C (Fig. 3.46). This thermal stability is enough for fuel cell application.

The glass transition temperatures of the copolymers were investigated with DSC. The T_g points of the copolymers were evaluated as 95, 110 and 110 °C for 1:0.5, 1:1 and 1:2 copolymers, respectively. When the copolymers were grafted with PEGME there is a melting behavior at -10 to 0 °C (Fig. 3.47).

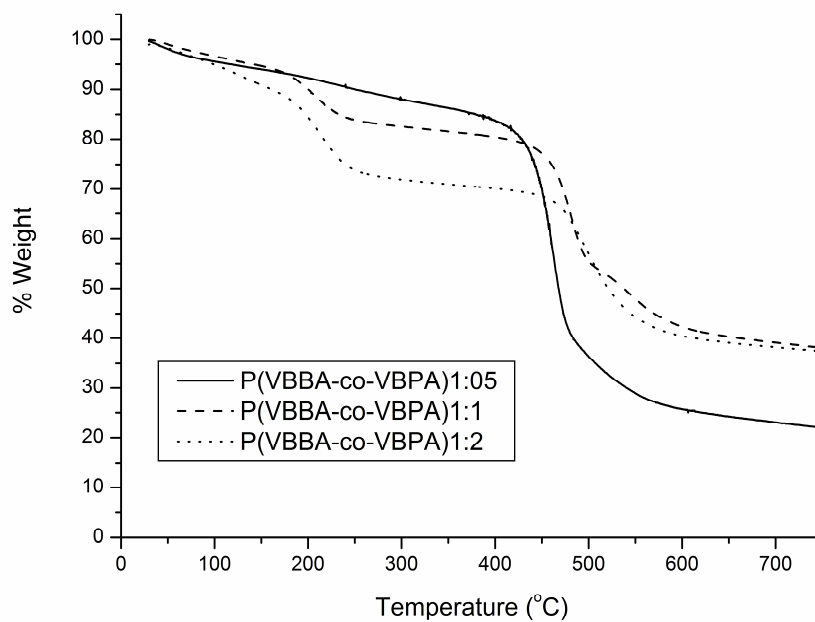


Figure 3.45. TG thermograms of P(VBBA-co-VBPA) copolymers at a heating rate of 10 °C/min in inert atmosphere.

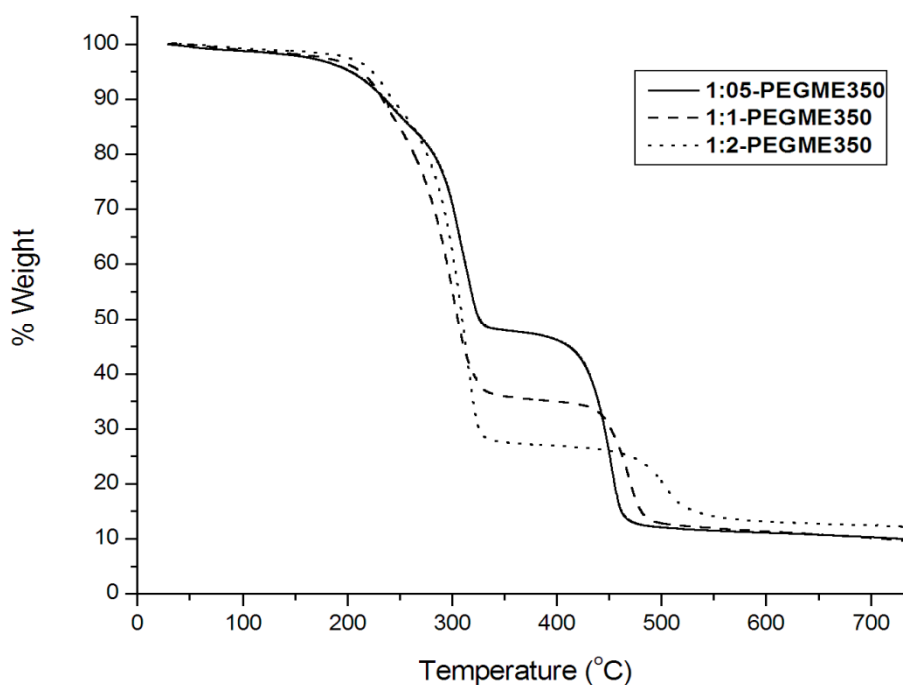


Figure 3.46. TG thermograms of P(VBBA-co-VBPA)-PEGME copolymers at a heating rate of 10 °C/min in inert atmosphere.

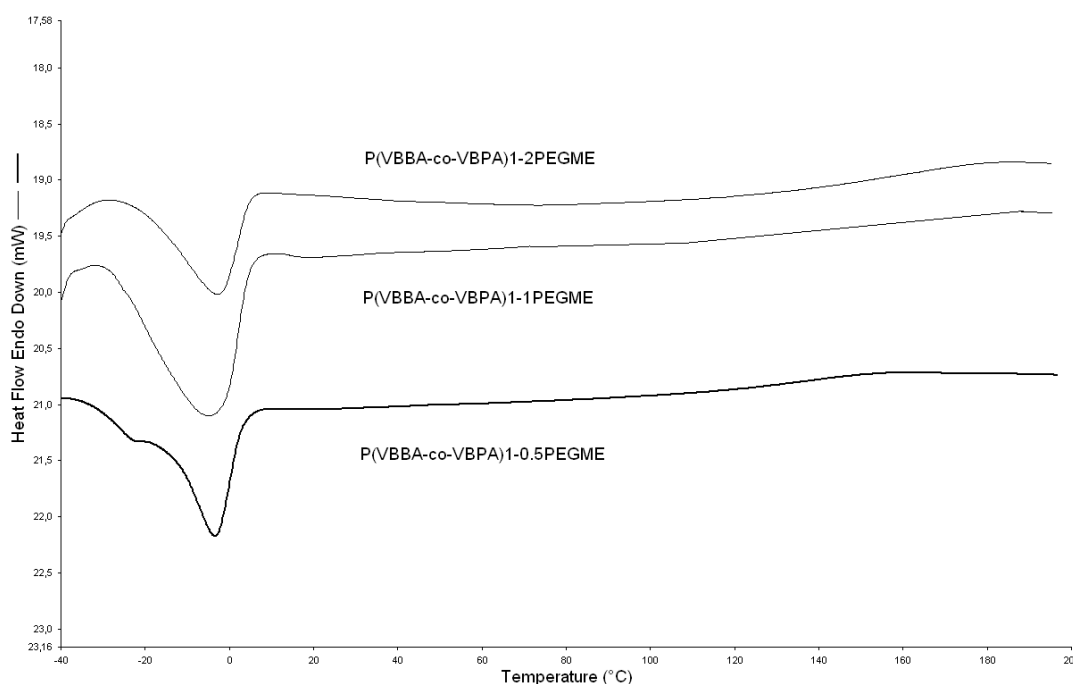


Figure 3.47. DSC curves of P(VBBA-co-VBPA)-PEGME copolymers at a heating rate of 10 °C/min in inert atmosphere.

3.7.3 Ion Exchange Capacity (IEC)

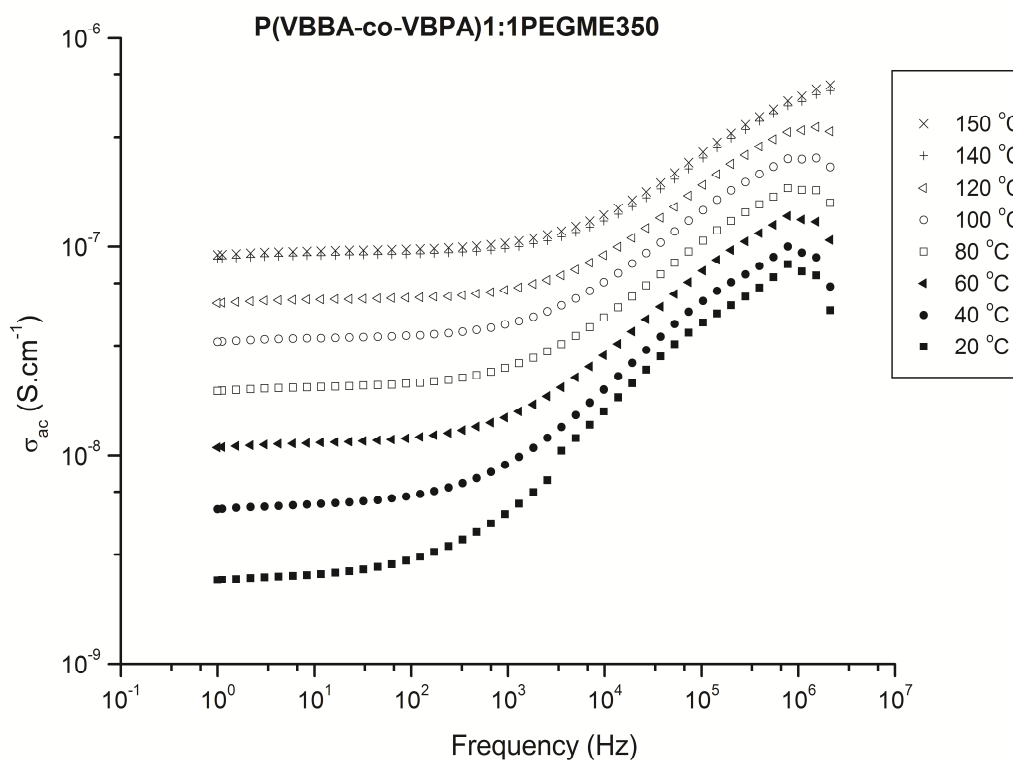
IEC of the copolymers were calculated using Eq. 2.1 and the values are 6.55, 7.05 and 7.55 mmol/g for 1:0.5, 1:1 and 1:2 copolymers, respectively. The ion exchange capacity of pure PVBPA and PVBBA were also determined with the same method and obtained as 9.7 mmol/g and 5.5 mmol/g, respectively. As expected IEC values increase with VPBA content. In these copolymers there may be little crosslink or anhydride formation due to condensation of both VBBA and VPBA units during drying process. The insoluble behavior of the materials verifies this consideration. In this IEC determination method the samples were put in alkaline salt solution for 24 h to provide complete salt formation and cleavage of anhydrides. This is also important for the efficiency of back titration (Kim et al., 2007).

3.7.4 Proton Conductivity

Fig. 3.48 shows the AC conductivity of the grafted copolymers versus frequency at several temperatures. The σ_{ac} versus frequency curves change with the frequency where in the low frequency region, the reduction in the conductivity is due to

polarization of the blocking electrodes. The conductivity increase at low temperature and high frequencies results from the regular dispersion in polymer electrolytes. The proton conductivity increases as temperature increases.

The DC conductivity (σ_{dc}) of the samples was derived from the plateaus of $\log \sigma_{ac}$ versus $\log F$ by linear fitting of the data. The DC conductivities of the samples were compared in Fig. 3.49. The conductivity isotherm illustrates that the DC conductivity depends on the temperature, PEGME and VBPA content. Pure copolymers have low proton conductivity ($<10^{-10}$ S/cm) and after grafting them with PEGME the proton conductivity values reaches to considerable values in anhydrous condition. In that system proton conduction occurs through acidic units via Grotthuss mechanism. The DC curves show VTF behavior which indicates contribution of segmental motions on proton conductivity. The membrane has very low water uptake, therefore proton conductivity was not measured in humidified condition.



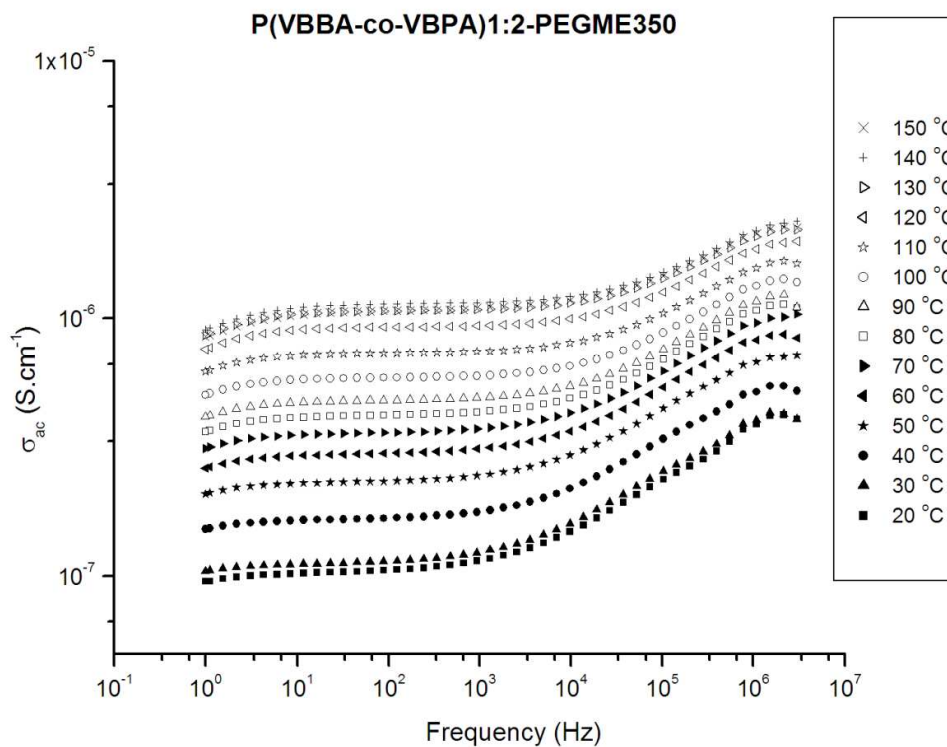


Figure 3.48. AC conductivity vs frequency for P(VBBA-co-VBPA)-PEGME copolymers at different temperatures.

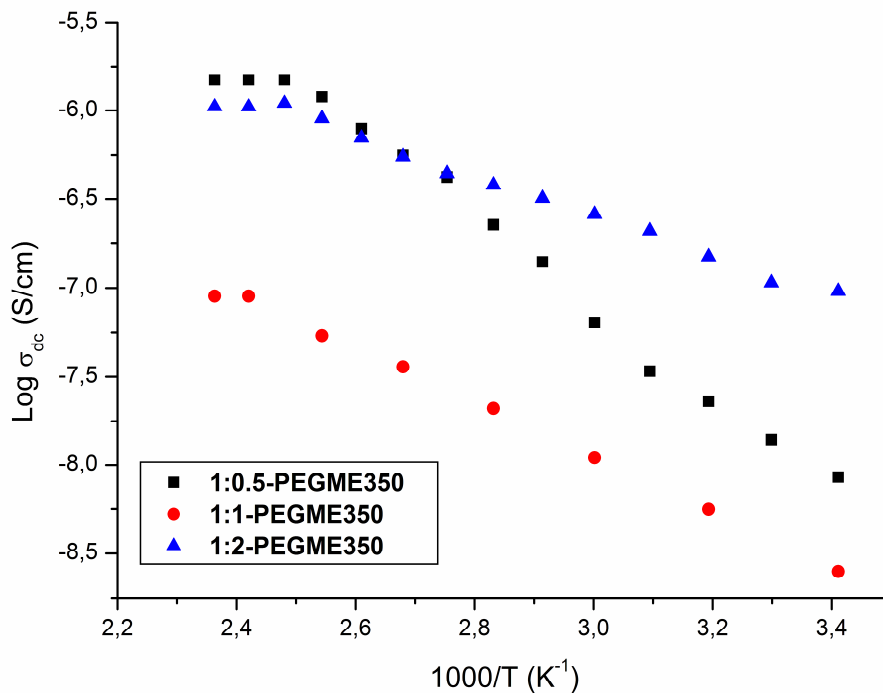


Figure 3.49. DC conductivity of P(VBBA-co-VBPA)-PEGME copolymers at different temperatures.

3.7.5 Cyclic Voltammetry

Fig. 3.50 shows cyclic voltammogram of P(VBBA-co-VBPA)1:0.5-PEGME in CH₃CN solution. The cyclic voltammetric measurements were performed in a typical three electrode cell containing 0.1 mol dm⁻³ CH₃CN solution of tetrabutylammonium hexafluorophosphate (TBAPF6) using a platinum work electrode, a platinum auxiliary electrode, and an Ag/Ag⁺ reference electrode. It is clearly observed that the CV of the copolymer comprises no peak within in the anodic and cathodic sweep (-2.0 – 2.0 V potential range). Thus the electrochemical stability window is about 4 V. These results imply that the copolymer has adequate electrochemical stability under fuel cell conditions.

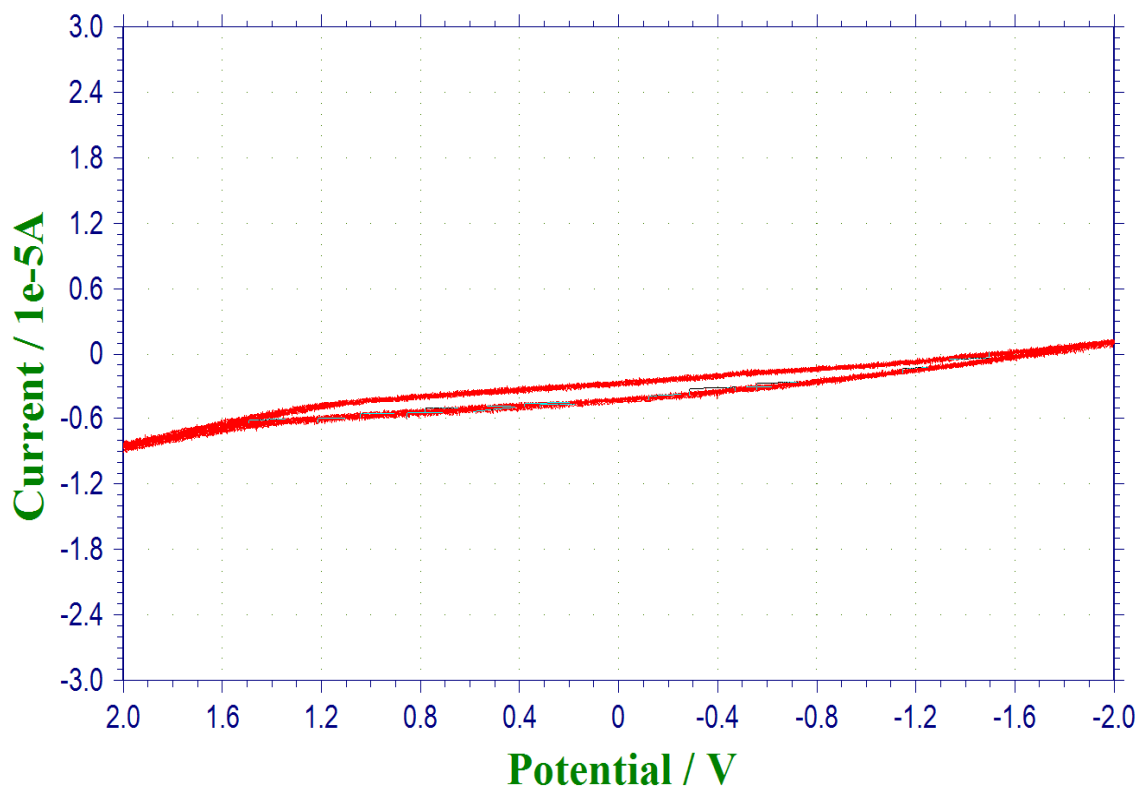


Figure 3.50. Cyclic voltammograms of P(VBBA-co-VBPA)1:0.5-PEGME in 0.1 M TBATFB/acetonitrile. Curves with a scan rate of 50 mV/s.

3.8 FUEL CELL TEST

Current-power density curve is the characteristic result for fuel cell test. The analysis of fuel cell performance, the determination of size of necessary system and control of fuel cell are done according to this curve. Power density (Wcm^{-2}) is obtained with multiplication of potential (V) with current density (i):

$$W = V \cdot i$$

As seen in the following figure fuel cell power density reaches to maximum in certain current density.

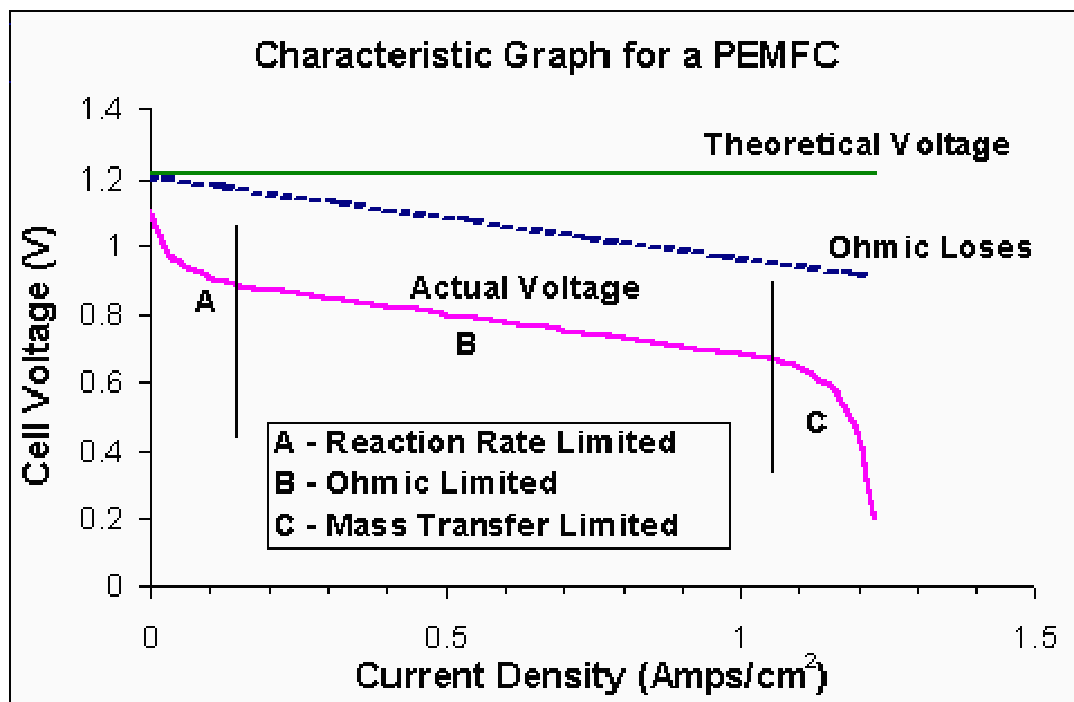


Figure 3.51. Characteristic graph for a PEMFC.

The theoretically voltage have not yet been reached, not even in open circuit (OC), but when running in OC the voltage tells the user about the state and health of the fuel cell. The reaction rate limited part of the curve are not commonly used, but the efficiency of each cell are best in this part of the curve, which normally can reach 80-90%. Most commercial system runs the fuel cell in the Ohmic limited part, which then to work like a battery and are easier to find applications for. The mass transfer limited

part can be reached even earlier if the fuel cell do not get enough hydrogen or oxygen supplied or the humidity of the cell is wrong.

In this study Si-TriTA1 and P(VBBA-co-VTri)1:2X=2 membranes were used for fuel cell test. Firstly mebrane electrode assembly (MEA) was prepared. Fig. 3.52 shows a typical PEMFC with its components. Here membrane, gas diffusion layer (GDL) and catalysts are called as MEA and it is obtained by hot pressing of catalyst covered GDL on each sides of the membrane.

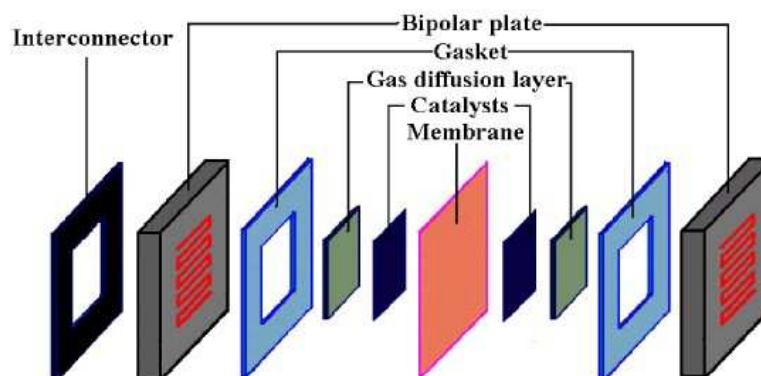


Figure 3.52. Components of a PEMFC.

Carbon paper, carbon textile and carbon fiber are used as GDL. These materials should be mechanically stable, high electrical conductive, high gas permeable, hydrophobically compatible and have high surface area. In this study carbon paper (5 cm²) was used as GDL and Pt catalyst (~7 mg) was covered on GDL with simple serigraphy machine.

Between an anode GDL and cathode GDL the membrane with a thickness of 0.3 mm was sandwiched just before the test. The performance was tested both in anhydrous state and also in 30-80 % humidified states. The starting voltages were high enough however we could not obtain a current in the testing system. The reason may be high thickness of the membranes which results high resistance. When we used membranes with lower thickness we faced problem of shrinkage of the membranes.

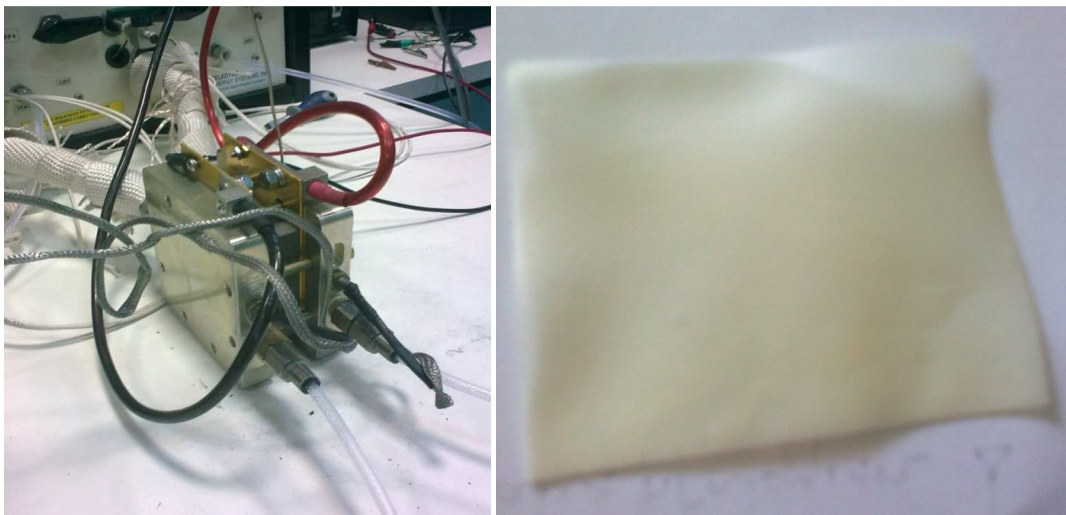


Figure 3.53. Single PEMFC test unit and tested membrane, P(VBBA-co-VTri)1:2X=2.

CHAPTER 4

CONCLUSIONS

Novel inorganic-organic hybrid membranes comprising triazole functional units have been successfully prepared via sol-gel process. Simply prepared, low costed membranes contain both an azole unit attached to a flexible side group and acid units interacting with the azole (Fig. 4.1). The interaction of triflic acid units with azole groups was confirmed by FT-IR. Thermogravimetry analysis (TGA) showed that the membranes are thermally stable up to 200 °C. Differential scanning calorimeter (DSC) verified the softening effect of the dopant. The proton conductivity of these inorganic-organic hybrid membranes were studied by dielectric-impedance spectroscopy in anhydrous state. The proton conductivity of these membrane electrolytes depends on the temperature and the acid ratio. Low T_g of the materials and Vogel–Tamman–Fulcher (VTF) behavior of the conductivity implies the coupling of the charge carriers with the segmental motion of the polymer chains. The maximum proton conductivity was obtained for the sample Si-TriTA1 as 8.9×10^{-4} S/cm at 150 °C in anhydrous condition.

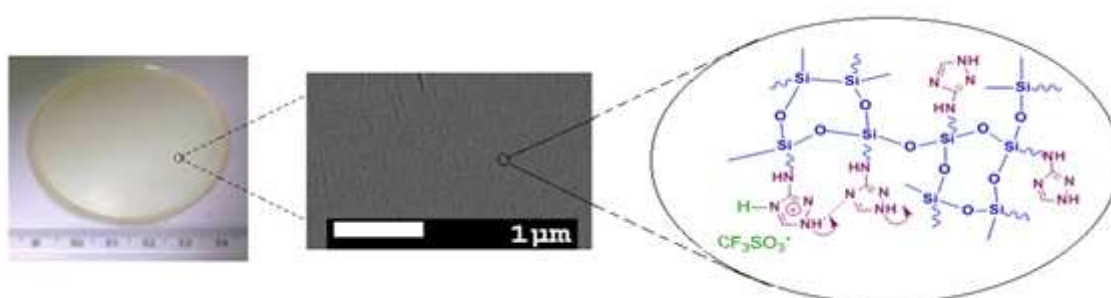


Figure 4.1. The images and chemical structure of Si-ATriTA0.5.

Tetrazole functional siloxane membranes have been successfully prepared via sol-gel process. The attachment of the ATet into the silane compound and the sol-gel reaction were confirmed by FT-IR. Thermogravimetry analysis (TGA) showed that the membranes are thermally stable up to 180 °C. Differential scanning calorimeter (DSC)

verified the softening effect of the dopant and the homogeneity of the samples. The proton conductivity of these inorganic-organic hybrid membranes were studied by dielectric-impedance spectroscopy in anhydrous state. The proton conductivity of these membrane electrolytes depends on the temperature and the acid content. Low T_g of the materials and Vogel–Tamman–Fulcher (VTF) behavior of the conductivity implies the coupling of the charge carriers with the segmental motion of the polymer chains. The maximum proton conductivity was obtained for the sample Si-ATetTA1 as 1.8×10^{-3} S/cm at 150 °C in anhydrous condition.

Novel copolymers of 4-vinyl benzene boronic acid (VBBA) and 1-vinyl-1,2,4-triazole (VTri) were successfully synthesized using free radical polymerization with high yield. Here, the presence of VBBA units prevented the solubility of the membrane as expected. The resulting copolymers were doped with H_3PO_4 at several molar ratios. Homogeneous and flexible membranes were obtained. The proton conductivity increases with VTri content and the maximum value was obtained as 1.5×10^{-3} S/cm at 150 °C (Table 4.1).

Table 4.1. Composition, T_d and maximum proton conductivities of the copolymers.

Sample	Copolymer mol ratio, (VBBA:VTri)	T_d (°C) (for x=2)	Max. proton Conductivity, S/cm (at 150 °C, x=2)
P(VBBA-co-VTri) 1:0.5	1:0.46	200	5.0×10^{-6}
P(VBBA-co-VTri) 1:1	1:0.83	200	5.0×10^{-4}
P(VBBA-co-VTri) 1:2	1:1.61	200	1.5×10^{-3}

Copolymers of 4-vinyl benzene boronic acid (VBBA) and vinyl phosphonic acid (VPA) were successfully synthesized using free radical polymerization. Poly(vinyl phosphonic acid) homopolymer is a high water soluble polymer and copolymerization with VBBA resulted insoluble membranes which is necessary for fuel cell applications. IEC of the copolymers were measured and it increases with VPA content as expected. 50 % humidified copolymers reached a proton conductivity of 4.3×10^{-3} S/cm at 30 °C. The resulting copolymers were grafted with polyethylene glycol methyl ether and homogeneous and soft materials were obtained. Grafted copolymers resulted a proton conductivity of 3×10^{-5} S/cm at 150 °C (Table 4.2).

Table 4.2. T_d, IEC and maximum proton conductivities of the copolymers.

Sample	T _d (°C) (S-PEGME)	IEC	Max. Proton Cond. (at 30 °C, 50 % RH)	Max. Proton Cond. (at 150 °C, S-PEGME)
S1	200	6.70 mmol/g	1.8x10 ⁻⁴ S/cm	1.0x10 ⁻⁵ S/cm
S2	250	7.05 mmol/g	3.7x10 ⁻⁴ S/cm	1.2x10 ⁻⁵ S/cm
S3	250	7.55 mmol/g	4.3x10 ⁻³ S/cm	2.5x10 ⁻⁵ S/cm

Diisopropyl-p-vinyl benzyl phosphonate monomer was successfully synthesized from vinyl benzyl chloride monomer. The purity and structure of the monomer was verified with NMR and FTIR methods. Using this monomer polyvinyl benzyl phosphonic acid homopolymer was obtained. The TGA of the homopolymer indicated that the sample is thermally stable up to 430 °C.

Novel copolymers of diisopropyl-p-vinyl benzyl phosphonate (VBP) and 1-vinyl-1,2,4-triazole (VTri) were successfully synthesized using free radical polymerization with high yield. The resulting copolymers were hydrolyzed to get P(VTri-co-VBPA) copolymers. The copolymers were doped with H₃PO₄ at several molar ratios. Homogeneous and flexible membranes were obtained. Maximum proton conductivity was obtained as 5x10⁻³ S/cm at 150 °C (Table 4.3).

Table 4.3. Composition, T_d and maximum proton conductivities of the copolymers.

Sample	Copolymer mol ratio, (VTri:VBPA)	T _d (°C) (for x=2)	Max. proton Conductivity, S/cm (at 150 °C, x=2)
P(VTri-co-VBPA) 1:0.5	1: 1.16	250	5.0x10 ⁻³
P(VTri-co-VBPA) 1:1	1: 1.39	250	1.6x10 ⁻³
P(VTri-co-VBPA) 1:1	1: 1.82	250	2.4x10 ⁻³

Copolymers of 4-vinyl benzoic acid (VBBA) and diisopropyl-p-vinyl benzyl phosphonate (VBP) were successfully synthesized. After hydrolysis, IEC of the copolymers were measured and it increases with VBPA content as expected. The resulting copolymers were grafted with polyethylene glycol methyl ether and homogeneous and soft materials were obtained. Grafted copolymers resulted a proton conductivity of 1.5×10^{-6} S/cm at 150 °C (Table 4.4).

Table 4.4. T_d, IEC and maximum proton conductivities of the copolymers.

Sample	T _d (°C) (X-PEGME)	IEC	Max. Proton Cond. (at 150 °C, X-PEGME)
P(VBBA-co-VBPA)1:0.5	200	6.55 mmol/g	1.5×10^{-6} S/cm
P(VBBA-co-VBPA)1:1	200	7.05 mmol/g	1.0×10^{-7} S/cm
P(VBBA-co-VBPA)1:2	200	7.55 mmol/g	1.1×10^{-6} S/cm

In this thesis proton conductive polymer matrices were synthesized with sol-gel and free radical polymerization methods. In most of these matrices azole molecules were used as proton transfer agent together with acidic units. As expected high proton conductivities were obtained in these studies. The proton transport is explained with Grotthuss mechanism and presence of flexible side groups also contributes the proton conduction which was clearly observed in PEGME grafted systems. Although pure copolymers have low proton conductivity, it increases with PEGME grafting due to the increase in segmental motions. Membrane formability and mechanical stability is very important in fuel cell application and we faced shrinkage problem when we used thin membranes. Therefore these matrices should be converted into thin and nonporous films with more efficient methods and also may be blended with more mechanically stable polymers.

REFERENCES

- Acheson, R.M. *An introduction to the chemistry of heterocyclic compounds*. 3rd ed. New York: Wiley-Interscience. 1976. p. 501.
- Adamson, K-A and W. Clint "Fuel Cell Annual Report 2011". 2Q 2011, Pike Research, 2011.
- Agmon, N., *J. Chim. Phys.*, Vol. 93, pp. 1714-1736, 1996.
- Agmon, N., *Chem. Phys. Lett.*, Vol. 244, pp. 456-462, 1995.
- Alberti, G., Casciola, M., *Solid State Ionics*, Vol. 145, pp. 3-16, 2001.
- Allcock, H. R., M. A. Hofmann, C. M. Ambler, S. N Lvov, X. Y, Zhou, E. Chalkova, J. Weston, *J. Membrane Science*, Vol. 201(1-2), pp. 47-54, 2002.
- Bermudez, V.D.Z., M. Armand, C. Poinsignon, L. Abello, J.Y. Sanchez, *Electrochimica Acta*, Vol. 37, pp. 1603-1609, 1992.
- Bischoff, M., *J. Power Sources*, Vol. 160, pp. 842, 2006.
- Bolufer, P., *Energia.*, Vol. 204, pp. 72, 2008.
- Bozkurt, A, W.H. Meyer, J. Gutmann, G. Wegner, *Solid State Ionics*, Vol. 164, pp. 169-176, 2003.
- Bozkurt, A., W.H. Meyer, *J. Polymer Science Part B Polymer Physics*, Vol. 39, pp. 1987-1994, 2001.
- Bozkurt, A., *Turk J. Chemistry*, Vol. 29, pp. 117, 2005.
- Brinker, C. J.; S. P. Mukherjee, *J. Materials Science*, Vol. 16 (7), pp. 1980, 1981.
- Brinker, C. J., K. D. Keefer, D. W. Schaefer, and C. S. Ashley, *J. Non-Crystalline Solids*, Vol. 48, pp. 47, 1982.
- Brookman, P. J., J. W. Nicholson, *Applied Developments in Ionic Polymers*, Vol. 2. London: Elsevier Science Publishers; p. 269-283, 1986.
- Brown, S. P, I. Schnell, J. D. Brand, K. Mullen, H. W. Spiess, *J. Am. Chem. Soc.*, Vol. 121, pp. 6712, 1999.
- Casciola, M., S. Chieli, U. Costantino, A. Peraio, *Solid State Ionics*, Vol. 46, pp. 53-59, 1991.
- Çelik, S.Ü, A. Bozkurt, *Solid State Ionics*, Vol. 181, pp. 525-530, 2010a.

- Celik, S. U., A. Bozkurt, *Solid State Ionics*, Vol. 181, pp. 987–993, 2010b.
- Çelik, S. Ü., A. Aslan, A. Bozkurt, *Solid State Ionics*, Vol. 179, pp. 683–688, 2008a.
- Çelik, S. Ü., U. Akbey, R. Graf, A. Bozkurt, *Phys. Chem. Chem. Phys.*, Vol. 10, pp. 6058–6066, 2008b.
- Chen, J., M. Asano, Y. Maekawa, M. Yoshida, *J. Membrane Science*, Vol. 296, pp. 77, 2007.
- Dippel, T, K.D. Kreuer, J.C. Lassègues, D. Rodriguez, *Solid State Ionics*, Vol. 61, pp. 41–46, 1993.
- Eigen, M., *Angew. Chem. Int. Edit.*, Vol. 3, pp. 1–19, 1964.
- Faur-Ghenciu, A., *Fuel Processing Catalysts for Hydrogen Reformate Generation for PEM Fuel Cells*, FuelCell Magazine, April/May 2003.
- Gierke, T.D., G.E. Munn, F. C. J. Wilson, *J. Polym. Sci: Polym. Phys. Edition*, Vol. 19, pp. 1687–1704, 1981.
- Goktepe, F., A. Bozkurt, S. T. Günday, *Polym. International*, Vol. 57, pp. 133–138, 2008.
- Granados-Focil, S., R. C. Woudenberg, O. Yavuzcetin, M. T. Tuominen, E. B. Coughlin, *Macromolecules*, Vol. 40, pp. 8708–8713, 2007.
- Grotthuss, C.J.D., *Ann. Chim.*, Vol. 58, pp. 54–73, 1806.
- Günday, S. T., A. Bozkurt, W.H Meyer, G. Wegner, *J. Polym. Sci. Part B Polym. Phys.*, Vol. 44, pp. 3315–3322, 2006.
- Guo, R., C. Hu, F. Pan, H. Wu, Z. Jiang, *J. Membrane Science*, Vol. 281, pp. 454–462, 2006.
- He, R., Q. Li, G. Xiao, N. J. Bjerrum, *J. Membrane Science*, Vol. 226, pp. 169–184, 2003.
- Heitner-Wirguin, C., *J. Membrane Science*, Vol. 120, pp. 1–33, 1996.
- Herz, H. G., K. D. Kreuer, J. Maier, G. Scharfenberger, M. F. H. Schuster, W. H. Meyer, *Electrochim. Acta*, Vol. 48, pp. 2165–2171, 2003.
- Iannuzzi, M., M. Parrinello, *Phys. Rev. Lett.*, Vol. 93, pp. 025901–025905, 2004.
- Jannasch, P., *Curr. Opin. Coll. Int. Sci.*, Vol. 8, pp. 96–102, 2003.
- Jiang, D.D., Q. Yao, M.A. McKinney, C.A. Wilkie, *Polym. Degrad. Stabil.*, Vol. 63, pp. 423, 1999.
- Jiang, F., *Proton-Conducting Copolymers, Blends and Composites with Phosphonic Acid as Protogenic Group*, PhD Thesis, Johannes Gutenberg-Universität Mainz, 2009.

- Kahraman, G., O. Beşkardeş, Z. M. O. Rzaev, E. Pişkin, *Polymer*, Vol. 45, pp. 5813, 2004.
- Kato, M., W. Sakamoto, T. Yogo, *J. Membrane Science*, Vol. 303, pp. 43-53, 2007.
- Kim, S. H., Y. C. Park, G. H. Jung, C. G. Cho, *Macromolecular Research*, Vol. 15, pp. 587-594, 2007.
- Klein, L. C., G. J. Garvey, *J. Non-Crystalline Solids*, Vol. 38, pp. 45, 1980.
- Kreuer, K. D., T. Dippel, W. Meyer, J. Maier, *Solid State Ionics III*, Mat. Res. Soc. Symp. Proc. Vol. 293. Pittsburgh: MRS; 1993. p. 273–282.
- Kreuer, K. D., A. Fuchs, M. Ise, M. Spaeth, J. Maier, *Electrochim. Acta*, Vol. 43, pp. 1281-1288, 1998.
- Kreuer, K. D., A. Rabenau, W. Weppner, *Angew. Chem. Int. Edit.*, Vol. 21, pp. 208-209, 1982.
- Kreuer, K. D., *Chem. Phys. Chem.*, Vol. 3, pp. 771-775, 2002.
- Kreuer, K. D., *Solid State Ionics*, Vol. 97, pp. 1-15, 1997.
- Kreuer, K. D., *J. Membrane Science*, Vol. 185, pp. 29-39, 2001.
- Kreuer, K. D., *Proton Conduction in Fuel Cells*, Germany: Wiley-VCH Verlag GmbH & Co. KGaA; 2007. p. 709-736.
- Kreuer, K. D., *Chem. Mater.*, Vol. 8, pp. 610-641, 1996.
- Krishnakumar, V., R. J. Xavier, *Spectrochim. Acta A*, Vol. 60, pp. 709, 2004.
- Kumura, M., *Materials Integration*, Vol. 17, pp. 17, 2004.
- Lecolley, F., C. Waterson, A. J. Carmichael, G. Mantovani, S. Harrisson, H. Chappell, A. Limer, P. Williams, K. Ohno, D. M. Haddleton, *J. Mater. Chem.*, Vol. 13, pp. 2689-2695, 2003.
- Lee, C. H., H. B. Park, Y. S. Chung, Y. M. Lee, B. D. Freeman, *Macromolecules*, Vol. 39, pp. 755-764, 2006.
- Lee, S-Y., G. Scharfenberger, W.H. Meyer, G. Wegner, *J. Power Sources*, Vol. 163, pp. 27–33, 2006.
- Lesnikovich, A. I., O. A. Ivashkevich, S. V. Levchik, A. I. Balabanovich, P. N. Gaponik, A. A. Kulak, *Thermochim. Acta*, Vol. 388, pp. 233-251, 2002.
- Levchik, S. V., G. A. Ivashkevich, A. I. Balabanovich, A. I. Lesnikovich, P. N. Gaponik, L. Costa, *Thermochim. Acta*, Vol. 207, 115-130, 1992.
- Li, Q., R. He, J. O. Jensen, N. J. Bjerrum, *Chem. Mater.*, Vol. 15, pp. 4896-4915, 2003.
- Li, Q., R. He, J. O. Jensen, N. J. Bjerrum, *Fuel Cells*, Vol. 4, pp. 147-159, 2004.

- Li, Q., J. O. Jensen, R. F. Savinell, N. J. Bjerrum, *Prog. Polym. Sci.*, Vol. 34, pp. 449-477, 2009.
- Li, S., Z. Zhou, Y. Zhang, M. Liu, *Chem. Mater.*, Vol. 17, pp. 5884-5886, 2005.
- Lufrano, F., V. Baglio, P. Staiti, A. S. Arico, V. Antonucci, *J. Power Sources*, Vol. 179, pp. 34, 2008.
- Martwiset, S., R. C. Woudenberg, S. Granados-Focil, O. Yavuzcetin, M. T. Tuominen, E. B. Coughlin, *Solid State Ionics*, Vol. 178, 1398-1403, 2007.
- Matijevic, E., *Langmuir*, Vol. 2, pp. 12, 1986.
- Mauritz, K. A., R. B. Moore, *Chem. Rev.*, Vol. 104, pp. 4535-4585, 2004.
- Mihina, J. S., R. M. Herbst, *J. Org. Chem.*, Vol. 15, pp. 1082-1092, 1950.
- Minkin, V., A. Garnovsk, J. Elguero, A. Katritzky, O. Denisko, *Adv. Heterocycl. Chem.*, Vol. 76, pp. 157-323, 2000.
- Münch, W., K. D. Kreuer, W. Silvestri, J. Maier, G. Seifert, *Solid State Ionics*, Vol. 145, pp. 437-443, 2001.
- Noda, A., M. H. Susan, K. Kudo, S. Mitsushima, K. Hayamizu, M. B. Watanabe, *J. Phys. Chem. B*, Vol. 107, pp. 4024-4033, 2003.
- Perrin, J. C., S. Lyonnard, A. Guillermo, P. Levitz, *Fuel Cell*, Vol. 6, pp. 5-9, 2006.
- Pezzin, S. H., N. Stock, S. Shishatskiy, S.P. Nunes, *J. Membrane Science*, Vol. 325, pp. 559, 2008.
- Pu, H., L. Qiao, Q. Liu, Z. Yang, *Eur. Polym. J.*, Vol. 41, pp. 2505-2510, 2005.
- Pu, H, S. Ye, D. Wan, *Electrochim. Acta.*, Vol. 52, pp. 5879-5883, 2007.
- Pu, H., Y. Qin, D. Wan, Z. Yang, *Macromolecules*, Vol. 42, pp. 3000-3004, 2009.
- Rauhut, G., *Phys. Chem. Chem. Phys.*, Vol. 5, pp. 791-800, 2003.
- Rikukawa, M., K. Sanui, *Prog. Polym. Sci.*, Vol. 25, pp. 1463-1502, 2000.
- Russell, D. G., J. B. Senior. *Can. J. Chem.*, Vol. 58, pp. 22, 1980.
- Sakka, S., K. Kamiya, *J. Non-Crystalline Solids*, Vol. 48, pp. 31, 1982.
- Sakka, S., K. Kamiya, *J. Non-Crystalline Solids*, Vol. 42, pp. 403, 1980.
- Sanghi, S., M. Tuominen, E. B. Coughlin, *Solid State Ionics*, Vol. 181, pp. 1183-1188, 2010.
- Satchell, J. F., B. J. Smith, *Phys. Chem. Chem. Phys.*, Vol. 4, pp. 4314-4318, 2002.
- Scharfenberger, G., W. H. Meyer, G. Wegner, M. Schuster, K. D. Kreuer, J. Maier, *Fuel*

- Cells*, Vol. 6, pp. 237-250, 2006.
- Schechter, A., R. F. Savinell, *Solid State Ionics*, Vol. 147, pp. 181-187, 2002.
- Schmidt-Rohr, K., Q. Chen, *Nat. Mater.*, Vol. 7, pp. 75-83, 2008.
- Schuster, M., W. H. Meyer, G. Wegner, H. G. Herz, M. Ise, M. Schuster, K. D. Kreuer, J. Maier, *Solid State Ionics*, Vol. 145, pp. 85-92, 2001.
- Schuster, M., T. Rager, A. Noda, K. D. Kreuer, J. Maier, *Fuel Cells*, Vol. 5, pp. 355-365, 2005.
- Sen, Ü., S. Ü. Çelik, A. Bozkurt, A. Ata, *Int. J. Hydrogen Energy*, Vol. 33, pp. 2808–2815, 2008.
- Sevil, F., A. Bozkurt, *J. Phys. Chem. Solids*, Vol. 65, pp. 1659-1662, 2004.
- Sezgin, A., Ü. Akbey, R. Graf, A. Bozkurt, A. Baykal, *J. Polym. Sci.: Part B: Polym. Phys.*, Vol. 47, pp. 1267–1274, 2009.
- Singhal, S. C., *Industrial Ceramics*, Vol. 28, pp. 53, 2008.
- Starz, K. A., E. Auer, T. Lehmann, R. Zuber, *J. Power Sources*, Vol. 84, pp. 167, 1999.
- Steininger, H., M. Schuster, K. D. Kreuer, A. Kaltbeitzel, B. Bingöl, W. H. Meyer, S. Schauff, G. Brunklaus, J. Maier, H. W. Spiess, *Phys. Chem. Chem. Phys.*, Vol. 9, pp. 1764-1773, 2007.
- Subbaraman, R., H. Ghassemi, T. Zawodzinski Jr, *Solid State Ionics*, Vol. 180, pp. 1143-1150, 2009.
- Sun, J., L. R. Jordan, M. Forsyth, D. R. MacFarlane, *Electrochim. Acta*, Vol. 46, pp. 1703-1708, 2001.
- Tripathi, B. P., A. Saxena, V. K. Shahi, *J. Membrane Science*, Vol. 318, pp. 288–297, 2008.
- Van den Broeck, H., *Fuel Cell Syst*, 245, 1993.
- Wei, J., C. Stone, A. E. Steck, *Trifluorostyrene and substituted trifluorostyrene copolymeric compositions and ion-exchange membranes formed therefrom*. US 5422411. 1995.
- Wesoff, E., *Year-End Reflections on the Fuel Cell Industry in 2010*, Greentech Media, Jan 5, 2011.
- Woudenberg, R. C., O. Yavuzcetin, M. T. Tuominen, E. B. Coughlin, *Solid State Ionics*, Vol. 178, pp. 1135-1141, 2007.
- Yamada, M., I. Honma, *Polymer*, Vol. 46, pp. 2986-2992, 2005.
- Yang, C., P. Costamagna, S. Srinivasan, J. Benziger, A. B. Bocarsly, *J. Power Sources*, Vol. 103, pp. 1-9, 2001.

- Yang, S-J., W. Jang, C. Lee, Y. G. Shul, H. Han, *J. Polym. Sci. Part B Polym. Phys.*, Vol. 43, pp. 1455-1464, 2005.
- Yazawa, T., T. Shojo, A. Mineshige, S. Yusa, M. Kobune, K. Kuraoka, *Solid State Ionics*, Vol. 178, pp. 1958, 2008.
- Yeager, H. J., A. Eisenberg, *Perfluorinated Ionomer Membranes*. ACS Symp. Ser. No.180. Washington DC: American Chemical Society; 1982. p. 41-63.
- Yen, C-Y., C-H. Lee, Y-F. Lin, H-L. Lin, Y-H. Hsiao, S-H. Liao, C-Y. Chuang, C-C Ma, *J. Power Sources*, Vol. 173, pp. 36-44, 2007.
- Zhou, Z., S. Li, Y. Zhang, M. Liu, W. Li, *J. Am. Chem. Soc.*, Vol. 127, pp. 10824-10825, 2005.
- Zhou, Z., R. Liu, J. Wang, S. Li, M. Liu, J. L. Brédas, *J. Phys. Chem. A*, Vol. 110, pp. 2322-2324, 2006.

APPENDIX A

Curriculum Vitae

Name&Surname: Sevim ÜNÜGÜR ÇELİK

E-mail: sunugur@fatih.edu.tr, sevimu@yahoo.com

Address: Fatih Univesity, Chemistry Department
Büyükçekmece, İstanbul

Education

- PhD, Fatih University, Chemistry, İstanbul
- MS, Fatih University, Chemistry-2008, İstanbul
- BS, Bilkent University, Chemistry-2005, Ankara

Experience

- Lecturer, Fatih University, Sept. 2011-...
- Research/Teaching Assistant, Fatih University, Sept. 2005- Sept. 2011

Research Interests

- Anhydrous Proton Conducting Polymer Membranes
- Li-polymer Batteries

Research Projects

- Polimer Elektrolit Membran Yakıt Hücrelerinde (PEMFC) Kullanım Amaçlı Vinil Fosfonik Asit ve Vinil Benzen Boronik Asit İçerikli Farklı Proton İletken Kopolimerlerin Üretilmesi, BOREN, Apr 2011- Apr 2013, Araştırmacı, 45.00 TL.
- Polimer Elektrolit Membran Yakıt Hücrelerinde (PEMFC) Kullanım Amaçlı Siloksan Bazlı Proton İletken Membranların Üretilmesi, Üniversite Araştırma Proje Fonu, Jun 2010-Jun 2011, Araştırmacı, 15.000 TL
- Polimer Elektrolit Membran Yakıt Hücrelerinde (PEMFC) Kullanım Amaçlı Proton İletken Nemsiz Membranların Üretilmesi, TUBITAK, May 2008-May 2010, Araştırmacı, 201.220 TL

Publications

Academic Journals

- M.Ş. Boroğlu, S.Ü. Çelik, A. Bozkurt, İ. Boz, "PROTON-CONDUCTING BLEND MEMBRANES OF CROSS-LINKED POLY(VINYL ALCOHOL)-SULFOSUCCINIC ACID ESTER AND POLY(1-VINYL-1,2,4-TRIAZOLE) FOR HIGH TEMPERATURE FUEL CELLS", *Polymer Engineering & Science*, May. 2012, pp. in press
- M.Ş. Boroğlu, S.Ü. Çelik, A. Bozkurt, İ. Boz, "Fabrication and characterization of anhydrous polymer electrolyte membranes based on sulfonated poly(vinyl alcohol) and benzimidazole", *Polymer Science Series*, Vol. 54, No. 3, Apr. 2012, pp. 231-239
- Sevim Ünügür Çelik, Sedat Coşgun, Ümit Akbey, Ayhan Bozkurt, "Synthesis and proton conductivity studies of azole functional organic electrolytes", *IONICS*, Vol. 18, No. 1, Jan. 2012, pp. 101-107
- S.U.Celik, A.Bozkurt, S.S. Hosseini, "Alternatives toward proton conductive anhydrous membranes for fuel cells: Heterocyclic protogenic solvents comprising polymer electrolytes", *Progress in Polymer Science*, Jan. 2012, pp. in press
- M.Ş. Boroğlu, S.Ü. Çelik, İ. Boz, A. Bozkurt, "Synthesis and proton conductivity studies of 5-aminotetrazole-doped sulfonated polymer electrolyte membranes", *Polymer Composites*, Vol. 32, No. 10, Oct. 2011, pp. 1625-1632
- Sevim Ünügür Çelik, Ayhan Bozkurt, "Novel triazole functional sol-gel derived inorganic-organic hybrid networks as anhydrous proton conducting membranes", *Polymer*, Vol. 52, No. 21, Sep. 2011, pp. 4670-4675
- Sevim Ünügür Çelik, Ayhan Bozkurt, "Sol-gel synthesis of proton conductive tetrazole functional silane networks", *Solid State Ionics*, Vol. 199-200, Sep. 2011, pp. 1-5
- Irfan Gustian, Sevim Ünügür Çelik, Wawang Suratno, Ayhan Bozkurt, "Proton conducting composite membranes based on poly(1-vinyl-1,2,4-triazole) and nitrilotri(methyl triphosphonic acid)", *Journal of Physics and Chemistry of Solids*, Vol. 72, No. 11, Sep. 2011, pp. 1377-1380
- Sevim Ünügür Çelik, Ayhan Bozkurt, "Proton conduction promoted by 1H-1,2,3-benzotriazole in non-humidified polymer membranes", *Electrochimica Acta*, Vol. 56, No. 17, Jul. 2011, pp. 5961-5965
- M.Ş. Boroğlu, S.Ü. Çelik, A. Bozkurt, İ.Boz, "The synthesis and characterization of anhydrous proton conducting membranes based on sulfonated poly(vinyl alcohol) and imidazole", *Journal of Membrane Science*, Vol. 375, No. 1-2, Jun. 2011, pp. 157-164
- Melike Türk, Sedat Coşgun, Sevim Ünügür Çelik, Hamit Erdemi, C. Gérardin-Charbonnier, Ayhan Bozkurt, "New type of anhydrous organic electrolyte based on carboxylic acid functional triazole as model system ", *Synthetic Metals*, Vol. 161, No. 9-10, May. 2011, pp. 665-669
- Z. Durmus, H. Kavas, A. Baykal, H. Sozeri, L. Alpsoy, S.Ü. Çelik, M.S. Toprak, "Synthesis and characterization of L-carnosine coated iron oxide nanoparticles", *Journal of Alloys and Compounds*, Vol. 509, No. 5, Feb. 2011, pp. 2555 - 2561
- F. Hacivelioglu, Ş. Özden, S.Ü. Çelik, S. Yeşilot, A. Kılıç, A. Bozkurt, "Azole substituted polyphosphazenes as nonhumidified proton conducting membranes", *Journal of Materials Chemistry*, Vol. 21, No. 4, Jan. 2011, pp. 1020 - 1027
- Sehmus Özden, Sevim Ünügür Çelik, Ayhan Bozkurt, "Synthesis and Proton Conductivity Studies of Polystyrene-Based Triazole Functional Polymer Membranes",

- Journal of Polymer Science Part A: Polymer Chemistry, Vol. 48, No. 22, Nov. 2010, pp. 4974-4980
- Şehmus Özden, Sevim Ünügür Çelik, Ayhan Bozkurt, "Synthesis and proton conductivity studies of doped azole functional polymer electrolyte membranes ", *Electrochimica Acta*, Vol. 55, No. 28, Nov. 2010, pp. 8498-8503
 - Sevim Ünügür Çelik, Ayhan Bozkurt, "Polymer electrolytes based on the doped comb-branched copolymers for Li-ion batteries", *Solid State Ionics*, Vol. 181, No. 21-22, Jul. 2010, pp. 987-993
 - Sedat Coşgun, Sevim Ünügür Çelik, Şehmus Özden, Suat Tüysüz, Ayhan Bozkurt, C. Gérardin-Charbonnier , "Proton conductivity properties of acid doped fluoroalkylated 1,2,3-triazole ", *Journal of Fluorine Chemistry*, Vol. 131, No. 7, Jul. 2010, pp. 776-779
 - Şehmus Özden, Sevim Ünügür Çelik, Ayhan Bozkurt, "Polymer electrolyte membranes based on p-toluenesulfonic acid doped poly(1-vinyl-1,2,4-triazole): synthesis, thermal and proton conductivity properties", *Journal of Polymer Science Part B: Polymer Physics*, Vol. 48, No. 10, May. 2010, pp. 1016-1021
 - Sevim Ünügür Çelik, Ayhan Bozkurt, "The synthesis and proton conducting properties of the copolymers based on 1-vinyl-1,2,4-triazole and 2-acrylamido-2-methyl-1-propanesulfonic acid", *Solid State Ionics*, Vol. 181, No. 11-12, Jan. 2010, pp. 525-530
 - Sedat Coşgun, Sevim Ünügür Çelik, Abdulhadi Baykal, Ayhan Bozkurt, "Dielectric and proton conductivity studies in organic electrolytes based on 2-perfluoroalkyl-ethyl-azides", *Current Applied Physics*, Vol. 10, No. 1, Jan. 2010, pp. 133-137
 - Ayşe Aslan, Sevim Ünügür Çelik, Ayhan Bozkurt, "Proton-conducting properties of the membranes based on poly(vinyl phosphonic acid) grafted poly(glycidyl methacrylate)", *Solid State Ionics*, Vol. 180, No. 23-25, Dec. 2009, pp. 1240-1245
 - Ayşe Aslan, Sevim Ü. Çelik, Ünal Şen, Resul Haser, Ayhan Bozkurt, "Intrinsically proton-conducting poly(1-vinyl-1,2,4-triazole)/triflic acid blends", *Electrochimica Acta*, Vol. 54, No. 11, Apr. 2009, pp. 2957-2961
 - Sevim Ünügür Çelik, Ümit Akbey, Robert Graf, Ayhan Bozkurt, Hans W. Spiess, "Anhydrous proton-conducting properties of triazole-phosphonic acid copolymers: a combined study with MAS NMR", *Physical Chemistry Chemical Physics*, Vol. 10, Nov. 2008, pp. 6058 - 6066
 - Sevim Ü. Çelik, Ayşe Aslan, Ayhan Bozkurt , "Phosphoric acid-doped poly(1-vinyl-1,2,4-triazole) as water-free proton conducting polymer electrolytes", *Solid State Ionics*, Vol. 179, No. 19-20, Aug. 2008, pp. 683-688
 - Unal Sen, Sevim Ünügür Çelik, Ali Ata, Ayhan Bozkurt, "Anhydrous proton conducting membranes for PEM fuel cells based on Nafion/Azole composites", *INTERNATIONAL JOURNAL OF HYDROGEN ENERGY*, Vol. 33, No. 11, Jun. 2008, pp. 2808 – 2815
 - Fadime Göktepe, Sevim Ünügür Çelik, Ayhan Bozkurt, "Preparation and the proton conductivity of chitosan/poly(vinyl phosphonic acid) complex polymer electrolytes", *Journal of Non-Crystalline Solids*, Vol. 354, No. 30, Apr. 2008, pp. 3637-3642
 - Sevim Ünügür Çelik, Ümit Akbey, Ayhan Bozkurt, Robert Graf, Hans W. Spiess, "Proton-Conducting Properties of Acid-Doped Poly(glycidyl methacrylate)-1,2,4-Triazole Systems", *MACROMOLECULAR CHEMISTRY AND PHYSICS*, Vol. 209, No. 6, Mar. 2008, pp. 593-603
 - Sevim Ünügür Çelik, Ayhan Bozkurt, "Preparation and proton conductivity of acid-doped 5-aminotetrazole functional poly(glycidyl methacrylate)", *European Polymer Journal*, Vol. 44, No. 1, Jan. 2008, pp. 213-218

- T.Shahwan, H.N.Erten, S.Unugur, "A characterization study of some aspects of the adsorption of aqueous Co^{+2} ions on a natural bentonite clay", Journal of Colloid and Interface Science, Vol. 300, No. 2, Aug. 2006, pp. 447-452

Proceedings

- S.U.Celik, A.Bozkurt, "Novel Azole Functional Sol-Gel Derived Inorganic-Organic Hybrid Networks as Anhydrous Proton Conducting Membranes", 2011 MRS Fall Meeting, Boston/ ABD, Dec. 2011, 2011 MRS Fall Meeting,
- Sevim Ünügür Çelik, Hamit Erdemi, Ayhan Bozkurt, "PEG crosslinked poly(vinylbenzene boronic acid) polymer electrolytes for Li-ion batteries", International Symposium on 17th Boron, Borides and Related Materials, İstanbul, Sep. 2011, International Symposium on 17th Boron, Borides and Related Materials Oral Presentations,
- Sevim Ünügür Çelik, Ayhan Bozkurt, "Nemsiz proton iletken membran olarak azol fonksiyonlu yeni anorganik-organik hibrit membranların sol-jel yöntemiyle sentezlenmesi", 25. Uluslararası Katılımlı Ulusal Kimya Kongresi , Erzurum/ Türkiye, Jul. 2011, 25. Uluslararası Katılımlı Ulusal Kimya Kongresi Sözlü Sunumlar Özet Kitabı, pp. 153
- Şehmus Özden, Sevim Ünügür Çelik, Ayhan Bozkurt, "Azol Fonksiyonlu polisteren/Triflik Asit Esaslı Polimer Elektrolitlerin Sentez ve Proton iletkenliklerinin İncelenmesi", 24. Ulusal Kimya Kongresi, Zonguldak, Türkiye, Jun. 2010,
- Sevim Ünügür Çelik, Ayhan Bozkurt, "Li-iyon Pillerinde Kullanım Amaçlı Poli(vinilbenzenboronikasit)-PEG Graft Kopolimer Elektrolit Sentezi ve İyon İletkenlik Özelliklerinin İncelenmesi", 24. Ulusal Kimya Kongresi, Zonguldak/Türkiye, Jun. 2010,
- Şehmus Özden, Sevim Ünügür Çelik, Ayhan Bozkurt, "Azol fonksiyonlu polistiren esaslı polimer elektrolit membranların sentez ve proton iletkenliklerinin incelenmesi", III. Polimer Kongresi ve Sergisi, Kocaeli Üniversitesi, May. 2010, III. Polimer Kongresi ve Sergisi, pp. 83
- Sevim Ünügür Çelik, Ayşe Aslan, Ayhan Bozkurt, Ümit Akbey, Robert Graf, Hans W. Spiess, "Proton conducting polymer electrolytes based on 1-vinyl-1,2,4-triazole and vinylphosphonic acid", 10 th European Symposium on Polymer Blends, Dresden/Almanya, Mar. 2010,
- Sevim Ünügür Çelik, Ayşe Aslan, Ayhan Bozkurt, "POLİ(GLİSİDİL METAKRİLAT-g-VİNİLFOSFONİK ASİT) KOPOLİMERİNİN SENTEZLENMESİ VE PROTON İLETKENLİK ÖZELLİKLERİNİN İNCELENMESİ", IV. ULUSAL HİDROJEN ENERJİSİ KONGRESİ (UHK 2009) veSERGİSİ, KOCAELİ/TÜRKİYE, Oct. 2009, IV. ULUSAL HİDROJEN ENERJİSİ KONGRESİ (UHK 2009) veSERGİSİ,
- Hamza Kocatürk, Ş. inceoğlu, B. Birkan, Sevim Ü. Çelik, Ayhan Bozkurt, Y.Z. Menceloğlu, M.H. Acar, "PVDF Bazlı Proton İletken Kopolimerlerin Sentezi ve Karakterizasyonları", IV. Ulusal Hidrojen Enerjisi Kongresi ve Sergisi, Kocaeli/Türkiye, Oct. 2009, pp. 81
- Sevim Ünügür Çelik, Ayhan Bozkurt, Ümit Akbey, Robert Graf, Hans W. Spiess, "A comparative study on proton conducting blends of poly(1-vinyl-1,2,4-triazole)/H₃PO₄ and copolymers of vinylphosphonic acid/1-vinyl-1,2,4-triazole) ", E-MRS Spring

Meeting 2009 SYMPOSIUM C Materials for Polymer Electrolyte, Strasbourg/Fransa, Jun. 2009, E-MRS Spring Meeting 2009, pp. 3

- Sevim Ünügür Çelik, Ayhan Bozkurt, "Preparation and Proton Conductivity of Acid-doped Azole Functional Poly (glycidyl methacrylate)", II. International Hydrogen Energy Congress and Exhibition, İstanbul/Türkiye, Jul. 2007, Proceedings ,

Posters

- Sevim Ünügür Çelik, Ayhan Bozkurt, "2011 MRS Fall Meeting", Boston/ ABD, Dec. 2011,
- Sevim Ünügür Çelik, Ayhan Bozkurt, "17th International Symposium on Boron, Borides and Related Materials", İstanbul, Sep. 2011,
- Ferda Hacıvelioğlu, Şehmus Özden, Sevim Ünügür Çelik, Serkan Yeşilot, Adem Kılıç, Ayhan Bozkurt, Glasgow, UK, Aug. 2011,
- Irfan Gustian, Sevim Ünügür Çelik, Wawang Suratno, Ayhan Bozkurt, "25. Uluslararası Katılımlı Ulusal Kimya Kongresi Fizikokimya-Polimer Kimyası Poster Sunumları Kitabı", Erzurum/ Türkiye, Jul. 2011, 238,
- Acar, M. H., Kocaturk, H., Inceoglu, S., Celik, S. U., Bozkurt, A., Menciloglu, Y., "MACRO2010, 43rd IUPAC World Polymer Congress", Glasgow, UK, Jul. 2010,
- Hamide Aydın, Mehmet Şenel, Hamit Erdemi, Sevim Ü. Çelik, A. Baykal, M. Tülü, Ali Ata, Ayhan Bozkurt, Zonguldak/Türkiye, Jun. 2010,
- Sedat Coşgun, Sevim Ü. Çelik, Şehmus Özden, Suat Tüysüz, Ayhan Bozkurt, C. Gérardin-Charbonnier, Zonguldak/Türkiye, Jun. 2010,
- Sevim Ünügür Çelik, Ayhan Bozkurt, Kocaeli/Türkiye, May. 2010, 131,
- Hamide Aydın, Şehmus Özden, Sevim Ünügür Çelik, Ayhan Bozkurt, Kocaeli/Türkiye, May. 2010, 168,
- Ayşe Aslan, Sevim Ünügür Çelik, Ünal Şen, Ayhan Bozkurt, "10 th European Symposium on Polymer Blends", Dresden/ Almanya, Mar. 2010,
- Sevim Ünügür Çelik, Şehmus Özden, Ayhan Bozkurt, "IV. ULUSAL HİDROJEN ENERJİSİ KONGRESİ (UHK 2009) ve SERGİSİ", KOCAELİ/TÜRKİYE, Oct. 2009,
- Sevim Ünügür Çelik, Ünal Şen, Ayhan Bozkurt, Şanlıurfa/Türkiye, Apr. 2008,
- Fadime Göktepe, Sevim Ünügür Çelik, Ayhan Bozkurt, "Anhydrous Proton Conductive Membrane Consisting of Chitosan and Poly(vinyl phosphonic acid)", II. International Hydrogen Energy Congress & Exhibition, İstanbul/Türkiye, Jul. 2007, Abstracts,
- S.Unugur,H.N.Erten, "Cs-137 nin Doğal Zeolitler Tarafından Adsorpsiyonunun İncelenmesi", IX.Ulusal Nükleer Bilimler ve Teknoloji Kongresi, İzmir/Türkiye, Sep.